

**EFFECT OF MOISTURE ON FATIGUE
CHARACTERISTICS OF ASPHALT CONCRETE
MIXTURES**

A THESIS

submitted by

MOHIT CHAUHAN

for the award of the degree

of

MASTER OF SCIENCE

(by Research)



**DEPARTMENT OF CIVIL ENGINEERING
INDIAN INSTITUTE OF TECHNOLOGY MADRAS**

DECEMBER 2020

THESIS CERTIFICATE

This is to certify that the thesis titled "**Effect of Moisture on Fatigue Characteristics of Asphalt Concrete Mixtures**", submitted by **Mohit Chauhan**, CE15S010, to the **Indian Institute of Technology Madras**, for the award of the degree of **Master of Science in Civil Engineering** is a bonafide record of the research work done by him under our supervision. The contents of this thesis, in full or in parts, have not been submitted to any other Institute or University for the award of any degree or diploma to the best of our knowledge.

Place: Chennai

Date: 09th December 2020

Dr. Atul Narayan
Research Guide
Assistant Professor
Department of Civil Engineering
IIT Madras, 600 036

ACKNOWLEDGEMENTS

I wish to convey my sincere gratitude to my adviser, **Dr. Atul Narayan** for the motivation and support to pursue this research work. I am grateful for his kind advice whenever I needed them the most. I would like to thank him for his sincere corrections to every research document, that helped me in improving my writing skills. He has spent substantial time during my seminar and synopsis presentations.

I express sincere thanks to **Dr. Manu Santhanam**, Head of Department of Civil Engineering for their valuable administrative support for the successful submission of my thesis.

I also express sincere thanks to **Dr. K. Ramamurthy**, former Head of Department of Civil Engineering for their administrative support and facilities rendered by them for completing the research work.

I like to acknowledge **Dr. J. Murali Krishnan**, Head of Laboratory, Transportation Engineering Division for all the support rendered during the research work. Sincere thanks to him for constantly guiding with new ideas for research.

Special thanks to all the faculty members of Transportation Engineering Division, Department of Civil Engineering for their encouragement and good wishes.

My sincere thanks to my General Test Committee members, **Dr. Subhadeep Banerjee** and **Dr. Abhijit P. Deshpande** for their critical comments and continuous support for the successful completion of this work.

I wish to thank **Mr. Pugazhenti**, Senior technical superintendent of Pavement and Asphalt laboratory and the project assistants, **Devika** and **Arbin** for their assistance in doing experiments in Pavement and Asphalt laboratory. I also thank project assistants, **Prasath**, **David**, **Krishna** and **Anusha** for preparing samples in Asphalt and Pavement laboratory. I also thank project officer **Divya** for help in conducting the experiments. I would like to thank **Mr. Elangovan** for his help related to administrative aspects.

I would also like to thank **Mr. R. Murali** and all assistants in the Engineering Workshop

and all the office staff of Civil Engineering Department for rendering their help during this research.

Many thanks to all my fellow research scholars and friends of IITM specially **Abhijit, Amit, Aravind, Tirthankar,** and **Uma** for their valuable support, suggestions during the course of this work and making my whole journey joyful.

I am grateful to my **family** who have supported and cared for me in the most needed times. Above all I thank the **God** for showering his blessing and giving me good health to complete my research work.

ABSTRACT

KEYWORDS: Asphalt concrete, Contact angle, Fatigue life, Moisture-induced damage, Surface energy.

Moisture does not only cause distresses like potholes, ravelling, etc., in asphalt concrete (AC) pavements but also exacerbates distresses like fatigue and rutting. There is a need for a test procedure that can characterize the effect of moisture on the fatigue behavior of AC mixtures. In this study, changes in fatigue characteristics after moisture-conditioning were evaluated by conducting four-point beam (4PB) fatigue tests on dry and moisture-conditioned beam specimens. For this purpose, AC beam specimens were prepared with two different types of binders, a binder with viscosity grade VG10 and another with viscosity grade VG30. These specimens were subjected to vacuum saturation by submerging completely in water and applying vacuum pressure to the system. Fatigue tests were conducted at four different strain amplitudes of 200, 400, 600 and 800 micro-strains. The results were then compared with the fatigue tests results obtained with dry beam specimens. Test results show that the conditioning reduces both the fatigue life and initial flexural stiffness of the beam specimens. It was observed that the phase angle of the moisture-conditioned sample was similar to that of the dry sample in the initial cycles. However, the phase angle drops at a much earlier cycle for moisture-conditioned samples. Moreover, it was also observed that the binder type plays a significant role in the degree of saturation and the extent of decrease in the initial modulus and fatigue life from moisture-conditioning.

The surface free energy of asphalt and aggregate were also be used to evaluate the change in the cohesive bond energy of asphalt mastic and adhesive bond energy between asphalt mastic and aggregate in the presence of moisture. For this purpose, a Sessile Drop apparatus was used to measure the contact angles between five different probe liquids (whose surface free energies were known) and asphalt binder/aggregates surfaces. A ratio of work of adhesion under the wet condition to dry condition was used in this study to rank the mixtures.

Surface free energy measurement test results (i.e., the ratio of the work of adhesion under the wet condition to dry condition) are found to be consistent with the fatigue test results (i.e., the ratio of fatigue life in moisture-conditioned state to dry state). The higher values of fatigue life ratio and $(\Delta W_a^{wet} / \Delta W_a^{dry})$ for VG10 binder show that the mixtures with VG10 binder have good resistance to moisture-induced damage (MID) as compared to mixtures with VG30 binder.

TABLE OF CONTENTS

ACKNOWLEDGEMENTS	i
ABSTRACT	iii
LIST OF TABLES	ix
LIST OF FIGURES	xii
ABBREVIATIONS	xiii
1 INTRODUCTION	1
1.1 General	1
1.2 Moisture-induced Damage in AC Pavements	2
1.3 Need for the Study	3
1.4 Objectives	4
1.5 Scope	5
1.6 Organisation of the Thesis	5
2 LITERATURE REVIEW	7
2.1 Moisture-induced Damage	7
2.2 Distresses Related to Moisture-induced Damage	7
2.3 Mechanisms of Moisture-induced Damage	9
2.3.1 Cohesive Failure due to Molecular Diffusion	9
2.3.2 Adhesive Failure due to Molecular Diffusion	10
2.3.3 Failure due to Cyclic Pore pressure	10
2.3.4 Failure due to Dynamic Action of Tyres	11
2.4 Models for Moisture-induced Damage	12
2.4.1 Adhesion Model	12
2.4.2 Cohesion Model	14

2.5	Factors Influencing Moisture-induced Damage in Asphalt Concrete Mixtures	14
2.6	Experimental Characterization of Moisture-Susceptibility of AC Mixtures	15
2.6.1	Tests on Compacted Mixtures	15
2.6.2	Tests on Loose Mixtures and Asphalt Binders	15
2.7	Flexural Fatigue Beam Test with Moisture-Conditioning	16
2.8	Surface Free Energy Measurement	20
2.9	Summary	25
3	EXPERIMENTAL METHODOLOGY	27
3.1	Material Selection	27
3.1.1	Binder	27
3.1.2	Aggregate Gradation	28
3.2	Sample Fabrication for 4PB Fatigue Testing	29
3.2.1	Batching and Mixing	29
3.2.2	Theoretical Maximum Specific Gravity (G_{mm})	30
3.2.3	Compaction	33
3.2.4	Slicing	34
3.3	Sample Preparation for Surface Free Energy Measurement	36
3.3.1	Asphalt Binder	36
3.3.2	Aggregates	37
3.4	Preconditioning of Beam Specimens	37
3.5	Experimental Investigation	40
3.5.1	4PB Fatigue Test Equipment	40
3.5.2	Test Procedure for 4PB Fatigue Beam	41
3.5.3	Integrity of the Waveform	42
3.5.4	Sessile Drop Testing Equipment	42
4	ANALYSIS AND DISCUSSION	45
4.1	4PB Fatigue Test Methods	45
4.1.1	Post-Processing of Fatigue Test Data	46
4.2	Analysis of Fatigue Test Data	47
4.2.1	Initial Stiffness Modulus	47

4.2.2	Fatigue life using AASHTO T321-17 (2017)	52
4.2.3	Fatigue life using ASTM D7460-10 (2010)	55
4.2.4	Reduction in the Fatigue Life after Moisture-Conditioning	62
4.2.5	Total Dissipated Energy per Cycle	63
4.2.6	Lissajous Plots	67
4.2.7	Phase Angle	70
4.3	S-N Plot	73
4.3.1	Incorporation of of Moisture Effect in Pavement Design	76
4.4	Degree of Saturation	78
4.5	Analysis for Surface Free Energy Measurement	79
4.5.1	Contact Angle Measurement	79
4.5.2	Selection of Probe Liquids	80
4.5.3	Surface Energy Components	81
4.5.4	Work of Adhesion and Cohesion	83
4.6	Comparison of 4PB and SFE Test Results	83
5	SUMMARY AND CONCLUSION	85
5.1	Summary	85
5.2	Conclusions and Recommendations	85
5.3	Future Research	86

LIST OF TABLES

2.1	Literature on Fatigue of moisture influenced AC mixtures	19
2.2	Literature on Preconditioning parameters	20
3.1	Properties of VG 10 binder as per IS:73 (2013)	27
3.2	Properties of VG 30 binder as per IS:73-2013	28
3.3	Mixing and Compaction Temperature	30
3.4	Theoretical Maximum Specific Gravity G_{mm}	32
3.5	Test matrix	41
3.6	RMSE value of loading waveform for different strain levels and cycles	42
3.7	Surface Energy Components of Liquid Probes	44
3.8	Test matrix	44
4.1	Fatigue Test Parameters	45
4.2	Initial Stiffness Ratio (ISR)	52
4.3	Parameters obtained from exponential fit	55
4.4	Fatigue life as per AASHTO T321-17	55
4.5	Parameters obtained from linear fit	61
4.6	Fatigue life as per ASTM D7460-10	62
4.7	FLR AASHTO T321-17	62
4.8	FLR ASTM D7460-10	62
4.9	Effect of conditioning on the fatigue life	63
4.10	Estimated parameters as per AASHTO T321-07	76
4.11	Estimated parameters as per ASTM D7460-10	76
4.12	Average contact angle and COV for two binders and aggregate at 20°C	80
4.13	Condition number and Coefficient of determination (R^2)	81
4.14	Surface Energies Calculated from Contact Angle Data	82
4.15	Comparison of Surface Energy Components	82
4.16	Work of adhesion in dry and wet condition	83
4.17	Work of cohesion in dry and wet condition	83

4.18 Comparison between the test results	84
--	----

LIST OF FIGURES

1.1	Processes causing Moisture-induced Damage (Kringos <i>et al.</i> (2008))	2
2.1	Cohesive and adhesive failure due to molecular diffusion (Caro <i>et al.</i> (2008))	10
2.2	Failure due to pore pressure (Kringos <i>et al.</i> (2008))	11
2.3	Failure due to dynamic action of tires	11
2.4	Mechanical interlocking	12
2.5	Strain-fatigue life relation (Shatnawi <i>et al.</i> (1995))	17
2.6	Surface free energy (Bhasin <i>et al.</i> (2006))	23
3.1	Aggregate gradation curve (MoRTH, 2013)	28
3.2	Sieving, batching and mixing of asphalt concrete	30
3.3	Measurement of G_{mm} in CORELOK	31
3.4	UTS 16 software screenshot	33
3.5	Illustration of the compaction process as per ASTM:D7981 (2015)	34
3.6	Sample Cutter	35
3.7	Samples produced using shear box beam	35
3.8	Slicing process (Krishnan, J M and Veeraragavan, A, 2013)	35
3.9	36
3.10	37
3.11	Schematic drawing of saturation of beams	38
3.12	Setup for moisture-conditioning	38
3.13	Jig	40
3.14	Four point beam bending equipment	40
3.15	(a) Contact angle between a liquid drop and substrate; (b) Sessile drop method	43
3.16	Experimental setup of sessile drop	43
4.1	Variation of stiffness modulus for BC-VG30 samples at $800\mu\epsilon$	48
4.2	Variation of stiffness modulus for BC-VG30 samples at $600\mu\epsilon$	48

4.3	Variation of stiffness modulus for BC-VG30 samples at 400 $\mu\epsilon$	49
4.4	Variation of stiffness modulus for BC-VG10 samples at 800 $\mu\epsilon$	49
4.5	Variation of stiffness modulus for BC-VG10 samples at 600 $\mu\epsilon$	50
4.6	Variation of stiffness modulus for BC-VG10 samples at 400 $\mu\epsilon$	50
4.7	Initial Stiffness for BC-VG30 samples	51
4.8	Initial Stiffness for BC-VG10 samples	52
4.9	Exponential fit, BC-VG30 at 200 $\mu\epsilon$	53
4.10	Exponential fit, BC-VG10 at 200 $\mu\epsilon$	53
4.11	Exponential fit, BC-VG10 at 200 $\mu\epsilon$	54
4.12	Exponential fit, BC-VG10 at 200 $\mu\epsilon$	54
4.13	Normalized modulus curve for BC-VG30 samples at 800 $\mu\epsilon$	56
4.14	Normalized modulus curve for BC-VG30 samples at 600 $\mu\epsilon$	56
4.15	Normalized modulus curve for BC-VG30 at 400 $\mu\epsilon$	57
4.16	Normalized modulus curve for BC-VG30 at 200 $\mu\epsilon$	57
4.17	Normalized modulus curve for BC-VG10 at 800 $\mu\epsilon$	58
4.18	Normalized modulus curve for BC-VG10 at 600 $\mu\epsilon$	58
4.19	Normalized modulus curve for BC-VG10 at 400 $\mu\epsilon$	59
4.20	Weibull curve for BC-VG30 (dry) at 200 $\mu\epsilon$	59
4.21	Weibull curve for BC-VG10 (conditioned) at 200 $\mu\epsilon$	60
4.22	Weibull curve for BC-VG10 (dry) at 200 $\mu\epsilon$	60
4.23	Weibull curve for BC-VG10 (conditioned) at 200 $\mu\epsilon$	61
4.24	Dissipated energy per cycle for BC-VG30 at 800 $\mu\epsilon$	64
4.25	Dissipated energy per cycle for BC-VG30 at 600 $\mu\epsilon$	64
4.26	Dissipated energy per cycle for BC-VG30 at 400 $\mu\epsilon$	65
4.27	Dissipated energy per cycle for BC-VG10 at 800 $\mu\epsilon$	65
4.28	Dissipated energy per cycle for BC-VG10 at 600 $\mu\epsilon$	66
4.29	Dissipated energy per cycle for BC-VG10 at 400 $\mu\epsilon$	66
4.30	Variation of stress-strain curve with the loading cycles for BC-VG30 at 800 $\mu\epsilon$	67
4.31	Variation of stress-strain curve with the loading cycles for BC-VG30 at 600 $\mu\epsilon$	67
4.32	Variation of stress-strain curve with the loading cycles for BC-VG30 at 400 $\mu\epsilon$	68

4.33	Variation of stress-strain curve with the loading cycles for BC-VG30 at 200 $\mu\epsilon$	68
4.34	Variation of stress-strain curve with the loading cycles for BC-VG10 at 800 $\mu\epsilon$	68
4.35	Variation of stress-strain curve with the loading cycles for BC-VG10 at 600 $\mu\epsilon$	69
4.36	Variation of stress-strain curve with the loading cycles for BC-VG10 at 400 $\mu\epsilon$	69
4.37	Variation of stress-strain curve with the loading cycles for BC-VG10 at 200 $\mu\epsilon$	69
4.38	Variation of phase angle with the loading cycles for BC-VG30 at 800 $\mu\epsilon$	70
4.39	Variation of phase angle with the loading cycles for BC-VG30 at 600 $\mu\epsilon$	71
4.40	Variation of phase angle with the loading cycles for BC-VG30 at 400 $\mu\epsilon$	71
4.41	Variation of phase angle with the loading cycles for BC-VG10 at 800 $\mu\epsilon$	72
4.42	Variation of phase angle with the loading cycles for BC-VG10 at 600 $\mu\epsilon$	72
4.43	Variation of phase angle with the loading cycles for BC-VG10 at 400 $\mu\epsilon$	73
4.44	S-N plot for BC-VG30 samples using AASHTO T321-07	74
4.45	S-N plot for BC-VG10 samples using AASHTO T321-07	74
4.46	S-N plot for BC-VG30 samples using ASTM D7460-10	75
4.47	S-N plot for BC-VG10 samples using ASTM D7460-10	75
4.48	Degree of saturation for BC-VG10 and BC-VG30 moisture-conditioned samples	78
4.49	Procedure for measuring contact angles	79
4.50	Sessile drop on the surface of VG10 binder	79
4.51	Sessile drop on the surface of VG30 binder	80
4.52	Sessile drop on the surface of aggregate	80

ABBREVIATIONS

AASHTO	Association of State Highway and Transportation Officials
AC	Asphalt Concrete
ASTM	American Society for Testing and Materials
CR	Compatibility Ratio
FLR	Fatigue Life Ratio
ISR	Initial Flexural Stiffness Modulus Ratio
LVDT	Linear Variable Displacement Transducer
MID	Moisture-induced Damage
MoRTH	Ministry of Road Transport and Highways
SD	Sessile Drop
SFE	Surface Free Energy
4PB	Four-Point Beam

CHAPTER 1

INTRODUCTION

1.1 General

The Indian road network is the world's second-largest (5.5 million kilometers), comprising of Expressways, National Highways, State Highways, Major District Roads, Other District Roads and Village Roads. Road infrastructure projects in India are given high priority since they carry more than 65% of all goods and 80% cent of total passenger traffic. The majority of road construction throughout the country involves the use of AC mixtures. Thus, evaluating the performance of AC mixtures during the service life of the pavement is important.

Moisture in AC layers weakens the layer and makes it susceptible to damage. The damage associated with moisture in AC pavements is called moisture-induced damage (MID). Moisture causes various types of distress to develop in the AC pavement, such as stripping, potholes etc. But, in addition to them, its presence may exacerbate the other distresses, such as fatigue cracking, top-down cracking, rutting, ravelling, and bleeding ([Kanitpong and Bahia, 2008](#); [Hicks, 1991](#); [Kandhal, 1992](#); [Lytton, 2002](#)).

Amongst these distresses, fatigue cracking is a predominant form of distress in AC pavements and one of the key modes of failure considered during the design of AC pavement. The presence of moisture in the AC layer of pavements reduces the cohesion within the asphalt, and the adhesion at the asphalt-aggregate interface ([Majidzadeh and Brovold, 1968](#); [Fromm, 1974](#); [Taylor and Khosla, 1983](#); [Kringos and Scarpas, 2008](#)). Moreover, moisture increases pore pressure within the AC layer during vehicle loading, which, in turn, causes excessive stresses/strains in the pavement structure ([Lu, 2005](#)). Moisture in this way weakens the AC mixture and makes it more susceptible to fatigue cracking. This effect of moisture on the fatigue resistance of AC is the object of the current study.

1.2 Moisture-induced Damage in AC Pavements

The most prominent indication of MID in AC mixtures is that the asphalt mastic coating is separated from the aggregates surface, generally known as "stripping" (Taylor and Khosla, 1983; Lytton, 2002). If the stripping continues for a longer duration of time, it eventually leads to the formation of potholes (Kringos and Scarpas, 2008). Moreover, the AC mixture disintegrates in the presence of moisture, thereby reducing the load-bearing capacity of the AC layers, and the pavement may fail prematurely (Masad *et al.*, 2006; Bhasin *et al.*, 2007; Lu, 2005).

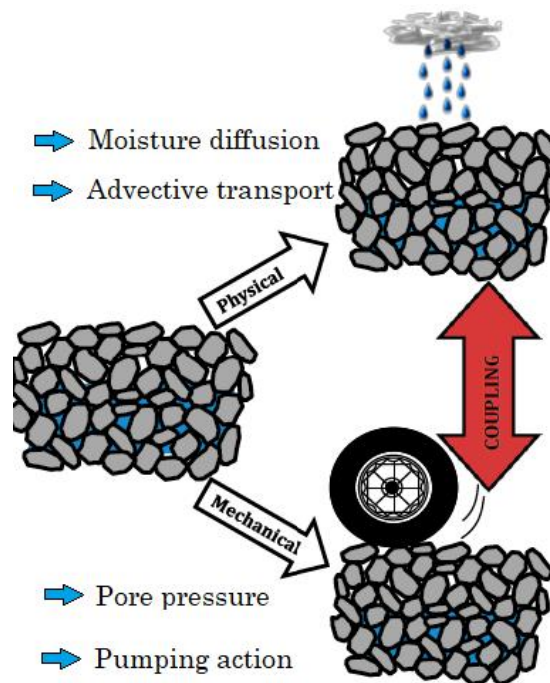


Figure 1.1: Processes causing Moisture-induced Damage (Kringos *et al.* (2008))

The processes that cause MID in AC mixtures are grouped into physical and mechanical processes. Physical processes include (i) cohesive failure (loss in the cohesive bond strength within the asphalt mastic) and an adhesive failure (loss in the adhesive bond strength between the asphalt-aggregate interface) due to molecular diffusion of moisture and (ii) weakening of asphalt mastic due to scouring process, caused by the flow of water through the connected pores. Mechanical processes include (i) the cyclic increase and decrease of pore pressure in the AC mixture and (ii) the dynamic action of tires in the presence of moisture during the movement of vehicles (Caro *et al.*, 2008; Kringos *et al.*, 2008). The mechanisms associated with physical processes are

detachment, displacement, and spontaneous emulsification while the mechanisms associated with mechanical processes are pore pressure and hydraulic scour (Little and Jones, 2003).

Fatigue cracking in AC pavements is caused by the fatigue failure of the AC layer under repeated vehicle loading. It is also known as "Bottom-up" cracking as it begins at the bottom of the AC layer where the tensile stress or strain along the horizontal direction is highest under a wheel load (Huang, 1993). As moisture is often retained for a relatively long duration at the bottom of the AC layer; the movement of vehicle loading in this wet condition of AC pavements would cause excess stresses or strains which weaken the AC mixture (due to loss of adhesion and cohesion). This would accelerate the development of fatigue or bottom-up or alligator cracking in AC pavements (Shatnawi *et al.*, 1995; Lu, 2005). On the other hand, rutting in the asphalt layers of the pavement occurs when the shear stress due to wheel loading is relatively high (Huang, 1993). The loss of cohesion within the asphalt mastic due to the presence of moisture in the surface layer reduces the stiffness of the AC mixture and accelerates the development of rutting, especially when the rainfall and traffic are heavy (Shatnawi *et al.*, 1995; Lytton, 2002; Lu, 2005).

1.3 Need for the Study

The Modified Lottman Test (AASHTO T283) is the most commonly used method for determining the sensitivity of AC mixtures to moisture. The Tensile Strength Ratio (TSR) obtained from the test is an empirical measurement which can not be used explicitly in performance models to predict pavement life. It also does not provide much insight on how moisture affects the fatigue characteristics of AC mixtures. Moreover, this test cannot be used to study the effect of moisture on the cohesive bonding within the asphalt mastic and the adhesive bond between asphalt-aggregate interface (Lytton *et al.*, 2005; Lu, 2005; Kringos *et al.*, 2009). Therefore, there is a need for a performance-based test to evaluate the effect of moisture on the fatigue life of pavements, a test that enables the consideration of the effect of moisture in the AC pavement design.

When characterizing the influence of moisture on the fatigue behavior of AC mixtures through laboratory experiments, the observed behavior may change markedly with

the type of test used to quantify fatigue resistance and the type of moisture-conditioning used to simulate MID. Typically, the effect of moisture on the fatigue resistance of AC mixtures has been quantified through three different types of tests - cyclic indirect tension test (IDT), dynamic mechanical analysis test (DMA) and flexural beam test (Chen and Huang, 2008; Mehrara and Khodaii, 2011, 2013). Among them, the flexural beam test with strain-controlled sinusoidal loading is possibly the most suitable test, since the fatigue behavior of mixtures in dry conditions has been extensively characterized using such tests (Shatnawi *et al.*, 1995; Lu, 2005). However, the effect of moisture on the variation of fatigue life with the amplitude of the applied loading has received relatively less attention from researchers. For incorporating the effect of moisture on fatigue behaviour in the pavement design procedures, the change in fatigue life due to moisture conditioning at various stress / strain levels needs to be examined.

Another approach for examining the influence of moisture on the fatigue behavior of asphalt mixtures is by calculating surface-free energy (SFE). The SFE of asphalts and aggregates in the presence of moisture can be used to evaluate the change in the cohesive bond energy within the asphalt mastic and the change in the adhesive bond energy between the asphalt-aggregate interface (Lytton *et al.*, 2005; Masad *et al.*, 2006; Bhasin *et al.*, 2007). The reduction in the cohesive strength within the asphalt mastic and the reduction in the adhesive strength between the asphalt-aggregate interface may lead to the formation and propagation of cracks under repeated loading (Cheng *et al.*, 2002; Bhasin *et al.*, 2007). Since SFE is a commonly used approach for characterizing damage caused by moisture, it can be related to the change in the fatigue characteristics of AC mixtures in the presence of moisture.

Therefore, it is necessary to examine the relationship between the SFE of asphalt binders and aggregates and the fatigue characteristics of AC mixtures in the presence of moisture. Such a relationship would help in choosing an appropriate combination of asphalt and aggregates during mix design.

1.4 Objectives

There are two objectives of the present work, which are listed below:

- To characterize the effect of moisture on fatigue behavior of asphalt concrete

mixtures through four-point beam fatigue tests.

- To examine the relationship between the change in the fatigue characteristics and the loss of the cohesive and the adhesive bond strength of AC mixtures in the presence of moisture.

1.5 Scope

- Two binders are used for the study and they are both unmodified binders. Polymer modification and its effect on moisture-induced damage is not considered in this study.
- Only one type of aggregates were used for the study. The aggregates used for the study is a type of locally available blue granite.
- All fatigue tests and surface free energy measurements were conducted at a temperature of 20° C.
- Moisture-conditioning of AC mixtures involved simply saturating the mixtures with moisture and holding them in saturated conditions for a certain period of time. The mixtures were not subjected to freeze-thaw cycles.
- For moisture-conditioning, AC specimens were submerged underwater and subjected to a vacuum pressure for a fixed period of time. The conditioning was not continued until complete saturation of the air voids of the mixture.

1.6 Organisation of the Thesis

This thesis is organized in five chapters. The background and motivation for the study, followed by the objectives, and the scope of the work.were covered in the present chapter.

Chapter 2 contains a review of the literature. The literature review includes a brief introduction of moisture-induced damage (MID) along with the various distresses associated with it, mechanisms, and models related to MID. The factors that can affect MID in AC and the test methods that can be use for characterization are also summarized.

Chapter 3 contains details of the experimental investigation carried out. Details of the material used, volumetric properties of the mix, sample fabrication, and testing are described in this chapter. The process of preconditioning of the beams is also described in this chapter.

Chapter 4 contains the post-processing of the experimental data. Analysis of fatigue tests was conducted as per prevailing AASHTO and ASTM protocols. The chapter also includes calculation of the SFE components from contact angle measurements.

Chapter 5 presents the summary and conclusion drawn from the study. The scope of further research work is also discussed.

CHAPTER 2

LITERATURE REVIEW

Since moisture has been known to either cause or exacerbate distresses in AC pavements, and thereby significantly reduce the functional capacity of pavements, MID has received much attention from researchers. In this chapter, a review of the literature on MID is presented. The chapter begins with a review of distresses that are associated with MID. This is followed by a review of the literature on the mechanisms, the factors affecting the same, and the models used to describe such behavior in separate sections. The chapter ends with a review of experimental procedures suggested in the literature to characterize MID of AC mixtures.

2.1 Moisture-induced Damage

While several definitions of MID exist in the literature, one of the most rigorous definition of the same can be found in the works of [Kiggundu and Roberts \(1988\)](#) as reduction in the cohesive bond strength within the asphalt mastic and reduction in the adhesive bond strength at the asphalt-aggregate interface of an AC mixture due to the effects of moisture.

2.2 Distresses Related to Moisture-induced Damage

The most prominent indication of MID is the dislodging of the aggregates from the AC mixture which is commonly referred to as "stripping" ([Taylor and Khosla, 1983](#); [Lytton, 2002](#)). If the stripping continues for a relatively long duration, it causes disintegration of the AC mixture, thereby reducing the load-carrying capacity of the AC layer, and eventually complete failure of the pavements ([Masad *et al.*, 2006](#); [Bhasin *et al.*, 2007](#); [Lu, 2005](#)). Moreover, once the stripping of wearing surface starts (raveling), it may progress into a more severe degradation of the wearing surface in the presence of repeated vehicle loading and eventually lead to the formation of potholes ([Kringos and Scarpas,](#)

2008). Moreover, the presence of moisture may exacerbate already existing distress, such as bottom-up (fatigue) cracking, top-down cracking, rutting, raveling, bleeding, etc (Kanitpong and Bahia, 2008; Hicks, 1991; Kandhal, 1992; Lytton, 2002). Below is the description of some distresses that can be related to moisture-damage mechanisms:

Fatigue Cracking: Fatigue cracking is a network of interconnected cracks caused by the fatigue failure of the AC layer under repeated vehicle loading. It is also known as "Bottom-up" cracking as it begins at the bottom of the AC layer where the tensile stress or strain along the horizontal direction is highest under a wheel load (Huang, 1993). As moisture is often retained for a relatively long duration at the bottom of the AC layer; the movement of vehicle loading in this wet condition of AC pavements would cause excess stresses or strains which weaken the AC mixture (due to loss of adhesion and cohesion). This would accelerate the development of fatigue or bottom-up or alligator cracking in AC pavements (Shatnawi *et al.*, 1995; Lu, 2005).

Rutting: Rutting in the asphalt layers of the pavement occurs when the shear stress due to wheel loading is relatively high (Huang, 1993). The loss of cohesion in the asphalt mastic due to the presence of moisture in the surface layer reduces the stiffness of the AC mixture and accelerates the development of rutting, especially when the rainfall and traffic are heavy (Shatnawi *et al.*, 1995; Lytton, 2002; Lu, 2005).

Raveling: Raveling is the dislodgement of aggregate particles from the surface of the pavement. Moisture may reduce the tensile strength of the mixture, resulting in increased disintegration of wearing surface under repeated vehicle loading (Kandhal, 1992; Lytton, 2002).

Potholes: When stripping continues in different AC layers, it eventually leads to the formation of potholes (Kandhal, 1992; Lytton, 2002). Freeze-thaw cycling and excessive or severe fatigue cracking, longitudinal cracking and raveling can also lead to the formation of potholes (Maher *et al.*, 2001).

Bleeding: The asphalt stripped from the aggregate surface due to the presence of moisture may often migrate to the road surface due to the pumping action of vehicle

loads. This reduces the friction between the vehicle tires and pavement (Kandhal, 1992; Lytton, 2002).

2.3 Mechanisms of Moisture-induced Damage

The processes that cause MID in AC mixtures are grouped into physical and mechanical processes. Physical processes include (i) cohesive failure (loss in the cohesive bond strength within the asphalt mastic) and an adhesive failure (loss in the adhesive bond strength between the asphalt-aggregate interface) due to molecular diffusion of moisture and (ii) weakening of asphalt mastic due to scouring process, caused by the flow of water through the connected pores. Mechanical processes include (i) the cyclic increase and decrease of pore pressure in the AC mixture and (ii) the dynamic action of tires in the presence of moisture during the movement of vehicles (Caro *et al.*, 2008; Kringos *et al.*, 2008).

2.3.1 Cohesive Failure due to Molecular Diffusion

Though the asphalt mastic is relatively impermeable, moisture can infiltrate through the phenomenon of molecular diffusion into it. (Kiggundu and Roberts, 1988; Cheng *et al.*, 2003; Kringos and Scarpas, 2005; Arambula *et al.*, 2009; Kassem *et al.*, 2009; Varveri *et al.*, 2016). However, the rate of diffusion depends on the type of asphalt binder, type and content of filler and surrounding temperature (Shatnawi *et al.*, 1995; Cheng *et al.*, 2003). Molecular diffusion is a long-term process, in which moisture infiltrates gradually into the asphalt mastic, due to the difference in moisture concentration gradient (Kringos *et al.*, 2008). This would result in reducing the cohesive strength of the mastic. Moreover, the cyclic pore pressure may cause the movement of water through the connecting pores of the AC mixture which is likely to cause degradation of mastic by the abrasion action of water. Kringos *et al.* (2008) state this loss of asphalt mastic particles as ‘scouring’ and referred this damage process as ‘advective transport’. This degradation of the mastic reduced the density of the mastic and, thus, affects the mechanical properties of the mastic (Varveri *et al.*, 2016). Birgisson *et al.* (2003) notes that the loss of cohesion in this manner results in a weakened AC mixture that is more susceptible to premature cracking. Moisture can also reduce cohesion by - spontaneous

emulsification.

2.3.2 Adhesive Failure due to Molecular Diffusion

As mentioned in the previous section, moisture can infiltrate through molecular diffusion into the asphalt mastic. Subsequently, moisture would reach the asphalt-aggregate interface depending on the moisture diffusion coefficients and the thickness of asphalt mastic coating. This would result in the separation of the asphalt mastic from the surface of the aggregate (Kringos *et al.*, 2008; Caro *et al.*, 2008). The loss of adhesion results in stripping and raveling of AC mixtures (Birgisson *et al.*, 2003). Moisture can reduce adhesion by two mechanisms: detachment and displacement. Detachment is the separation of asphalt mastic from the surface of aggregates by a thin film of water without a noticeable crack in the asphalt mastic film, while displacement is the separation of asphalt mastic from the surface of aggregates by a thin film of water through a crack in the asphalt mastic. (Little and Jones, 2003).

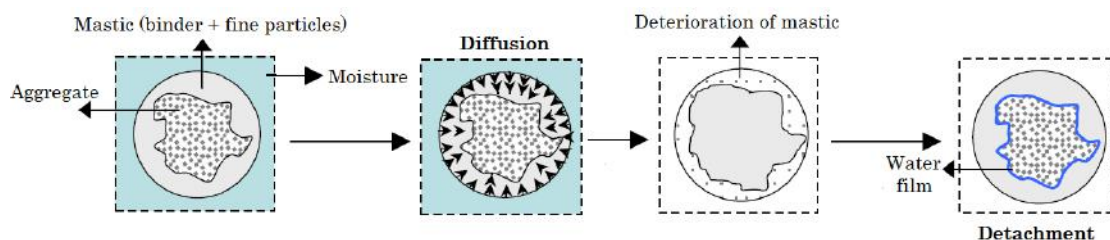


Figure 2.1: Cohesive and adhesive failure due to molecular diffusion (Caro *et al.* (2008))

2.3.3 Failure due to Cyclic Pore pressure

Pore pressure may develop in the AC mixture due to the entrapped moisture in the pores (Little and Jones, 2003). When the pavement is saturated, moisture entrapped in the pores resists the densification of the mixture under wheel loads. This would lead to building up of cyclic pore pressure in the mixture (Kringos and Scarpas, 2008). If an AC pavement is highly permeable, then moisture can easily drain off through the connected voids of the pavement. However, if it is impermeable or the permeability is relatively low, the cyclic pore pressure would induce extra stresses which may exceed the tensile strength of the AC mixture and separate asphalt mastic film from the aggregate surface (Little and Jones, 2003). Moreover, cyclic pore pressure would create a movement of

water through the connecting pores of the mixture which contribute to the scouring of mastic from the surface of aggregate (Kringos *et al.*, 2008).

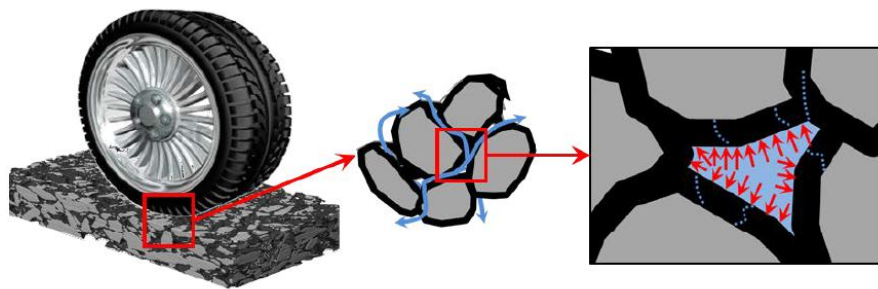


Figure 2.2: Failure due to pore pressure (Kringos *et al.* (2008))

2.3.4 Failure due to Dynamic Action of Tyres

When the vehicles are moving on a saturated pavement surface, tires of moving vehicles first apply a compression (positive pressure) to the moisture present in the pores in front of the tires than a suction or tension (negative pressure) behind the tires. This dynamic action of tires may cause movement of water within the mixture, and thereby separate asphalt mastic film from the aggregate surface (Caro *et al.*, 2008). This process is termed as 'pumping action' (Kiggundu and Roberts, 1988; Kandhal, 1992). Hicks (1991) defines pumping action as a short-term process as it happens only when the vehicles pass over the saturated AC pavement. The distress manifested by this process can be in the form of surface raveling (Little and Jones, 2003).

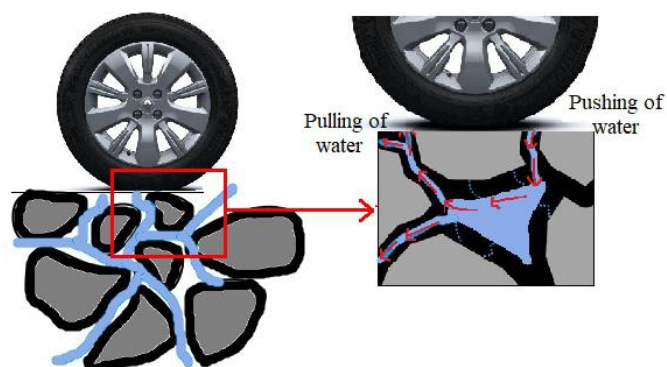


Figure 2.3: Failure due to dynamic action of tires

2.4 Models for Moisture-induced Damage

2.4.1 Adhesion Model

Most researchers consider that MID in AC mixtures is only due to the failure of adhesion between asphalt-aggregates interface. The adhesion of asphalt mastic to aggregate depends on both the asphalt and the aggregate's physical and chemical properties (Hicks, 1991; Hefer, 2005). A number of models have been suggested to describe the asphalt mastic and the aggregate adhesion characteristics. Terrel and Al-Swailmi (1994) broadly classified four different models of adhesion as discussed below:

Mechanical Interlocking Model

Mechanical adhesion can be achieved between the asphalt mastic and the aggregate by penetrating asphalt mastic into surface defects such as pores and cavities on the aggregate surface. Mechanical adhesion thus depends on the "mechanical interlocking" of the aggregate with the asphalt mastic, as shown in Fig.2.4. However, various physical properties of aggregates can also affect mechanical adhesion, including surface texture, surface area, surface coating, particle size and absorption capacity (Terrel and Al-Swailmi, 1994; Little and Jones, 2003). Aggregates having a comparatively rough surface texture and a large number of surface pores appear to be firmly interlocked with the asphalt binder and thus provide higher resistance to moisture damage (Hicks, 1991).

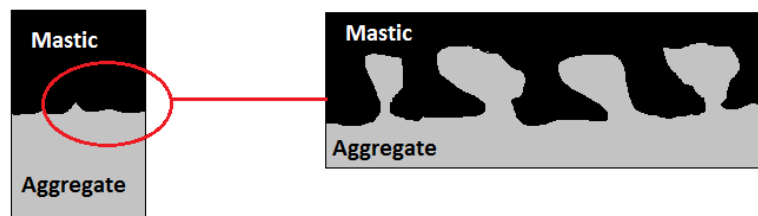


Figure 2.4: Mechanical interlocking

Chemical Reaction Model

Asphalt binder adhesion to the aggregate may be attributed to the presence of acidic and basic asphalt and aggregate components. These components result in a chemical reaction between asphalt and aggregate surface to form water-insoluble compounds that can withstand stripping (Kiggundu and Roberts, 1988). Terrel and Al-Swailmi (1994) found that basic aggregates can lead to better adhesion of asphalt to aggregates. They also found that the extent of acidic and basic nature of aggregates is based on the percentage of silicon dioxide (SiO_2) present in the aggregates. In another study, Bhasin *et al.* (2006) found that the portion of the bond strength resulting from the interaction between the acid components of the asphalt binder and the basic components of the aggregates contributes most to the mixture's total adhesive bond strength.

Molecular Orientation Model

Hicks (1991) suggested that, when the asphalt comes into contact with the aggregate surface, the molecules in the asphalt may align in the direction of polarization of the aggregate ions in order to minimize the repulsion energy that has developed between them. In general, asphalt molecules are non-polar although they have some polar components (Hicks, 1991). Water molecules are, on the other hand, di-polar. As a result, the surface of the aggregate tends to prefer water rather than asphalt, due to the high polarity of the water molecules which tend to displace the asphalt at the asphalt-aggregate interface (Hicks, 1991; Hefer, 2005).

Surface Energy Model

Surface energy can be characterized as "how well asphalt or water coats aggregate particle" (Terrel and Al-Swailmi, 1994). The wetting ability of any liquid is related to its surface tension than viscosity (Hicks, 1991). As asphalt spreads over an aggregate surface, there has been a change in surface energy. This energy change is related to the adhesion-tension. The adhesion-tension of the water-aggregate interface is higher than that of the asphalt-aggregate interface. Water will therefore tend to displace the asphalt at the asphalt-aggregate interface. (Hicks, 1991; Cheng *et al.*, 2002; Bhasin *et al.*, 2006; Masad *et al.*, 2006; Little and Bhasin, 2006).

The surface energy components of both asphalt and aggregates can be evaluated by measuring the contact angle of drops formed using standard probe liquids deposited on the asphalt or aggregate (Wei and Zhang, 2012; Koc and Bulut, 2013). These surface energy components of asphalt and aggregate can be used to evaluate the adhesive strength between asphalt-aggregate interface and the cohesive strength within the asphalt mastic in presence or absence of moisture (Cheng *et al.*, 2002; Bhasin *et al.*, 2006, 2007; Hefer *et al.*, 2006; Wei and Zhang, 2012; Hamed and Nejad, 2015)

2.4.2 Cohesion Model

The infiltration of moisture into the mastic would cause swelling or expansion of voids, which results in the loss of cohesive strength of mastic (Little and Jones, 2003). In their study, Cheng *et al.* (2002) observed that due to the infiltration of moisture into the asphalt mastic, the cohesive strength of various AC mixtures decreased.

Although the cohesive failure mechanism eventually leads to an adhesive failure (Kringos *et al.*, 2008), it is difficult to distinguish between these two failure modes unless the surface of the AC mixtures is visually inspected (Terrel and Al-Swailmi, 1994).

2.5 Factors Influencing Moisture-induced Damage in Asphalt Concrete Mixtures

Over the years several researchers have identified many factors, including the type of mixture, asphalt characteristics, aggregate characteristics, environmental conditions during and after construction and the use of anti-stripping additives which makes MID a complex phenomenon. The following are some desirable characteristics of aggregates in order to produce a moisture-resistant AC mixture: aggregates should be dry and basic in nature (absence of clay particles) with a rough surface texture. Several desirable characteristics of the binders are higher viscosity with low diffusivity, presence of phenol and nitrogen, and a thicker asphalt film to provide a moisture-resistant AC mixture. In addition to that, AC mixture should also have a higher bitumen content and a very dense or very open gradation such that air voids are below 7% and above 13%.

Moreover, construction in warm weather condition is favourable.

2.6 Experimental Characterization of Moisture-Susceptibility of AC Mixtures

Over the years comprehensive laboratory studies have been developed to describe the sensitivity to moisture in AC mixtures. Hicks (1991) indicated that AC mixtures failure due to the MID occurs in two stages. The failure in the first stage is due to the loss of cohesive and adhesive strength, while in the second stage it is due to the pavement's mechanical failure under repeated traffic loading in practice. Therefore, there are many tests available for asphalt binders and AC mixtures. The AC mixture tests are further divided into loose asphalt mixture tests and compacted asphalt mixture tests.

2.6.1 Tests on Compacted Mixtures

These tests are conducted on laboratory-compacted specimens, beams and field cores. Moisture Vapour Susceptibility Test, Immersion-Compression Test (ASTM D1075), Marshall Immersion Test, Freeze/Thaw Pedestal Test, Original Lottman Indirect Tension Test (NCHRP Report 246), Modified Lottman Indirect Tension Test (AASHTO T283), Hamburg Wheel Tracking Test, and Beam Fatigue Test with Moisture-Conditioning were some commonly used test methods (Solaimanian *et al.*, 2003).

A major advantage of these tests is that it can take into account the physical and mechanical properties of the mixture, the moisture effect, the application of repeated traffic loading and the effect of pore pressure. There are also some drawbacks of performing tests on compacted mixtures such as expensive testing facilities, longer test time and more complicated test procedures.

2.6.2 Tests on Loose Mixtures and Asphalt Binders

Such tests are carried out in the presence of water on aggregates coated with asphalt to determine the moisture-susceptibility of loose mixtures. Methylene Blue Test, Film Stripping Test, Static Immersion Test (AASHTO T182), Chemical Immersion Test,

Boiling Test (ASTM D3625), Surface Energy Measurement and Pneumatic Pull-Off Test were some commonly used test methods (Solaimanian *et al.*, 2003).

The two main advantages of these tests are that these tests are easy to perform and are more efficient than tests on compacted specimens. Such tests are primarily used in terms of compatibility, adhesion strength, and stripping for comparison of different mixtures.

In particular following test methods were selected for review:

- Flexural Fatigue Beam Test with Moisture-Conditioning
- Sessile Drop Test

2.7 Flexural Fatigue Beam Test with Moisture-Conditioning

Within the context of fatigue behavior, there is a necessity to investigate the effect of moisture-conditioning. The four-point beam (4PB) fatigue test is a popular method for characterizing the fatigue behavior of AC mixtures. However, very limited test data is available in the literature as far as the effect of moisture on the fatigue behavior of AC mixtures is concerned.

In the following, some of the recent literature corresponding to the effects of moisture-conditioning on fatigue characteristics of AC mixtures are reviewed. The detailed experimental investigation carried out to quantify the effect of moisture-conditioning on fatigue characteristics is presented followed by the analysis of the results.

Fatigue behavior of AC mixtures under moisture-conditioning has been investigated in three different types of loading conditions. This includes cyclic indirect tension test (IDT), dynamic mechanical analysis test (DMA) and flexural beam test (Chen and Huang, 2008; Mehrara and Khodaii, 2011, 2013). Among them, the flexural beam test with strain-controlled sinusoidal loading is possibly the most suitable test for characterization of the effect of moisture on fatigue, since the test is most widely used for characterizing fatigue. This test measures the engineering properties which are used in pavement design i.e. the stiffness and fatigue life under repeated traffic loading (Shatnawi *et al.*, 1995; Lu, 2005). Using this test, one can predict the performance life an AC pavement in a saturated condition.

Shatnawi *et al.* (1995) used beam fatigue tests to characterize the effect of moisture on the fatigue behavior of AC mixtures samples. In fact, it was one of the first investigations in which the effect of moisture on the fatigue behavior of AC mixtures was studied. Three-point flexural fatigue test in controlled-strain mode was conducted at 20 °C and 10 Hz frequency with sinusoidal loading. Specimens were tested at two different strain amplitudes - 200 and 300 $\mu\epsilon$, with a termination criterion of 50% reduction in the stiffness. They reported that conditioning reduced both the fatigue life and the flexural stiffness. They also reported that the reduction in binder content from optimum binder content (OBC) by 0.5% adversely affects the resistance to MID. They introduced an initial stiffness ratio (ISR) defined as the ratio of the initial flexural stiffness before and after moisture-conditioning and a fatigue life ratio (FLR) defined as the ratio of the fatigue life before and after moisture-conditioning and suggested that such parameters can be used for determining the sensitivity of AC mixtures to moisture.

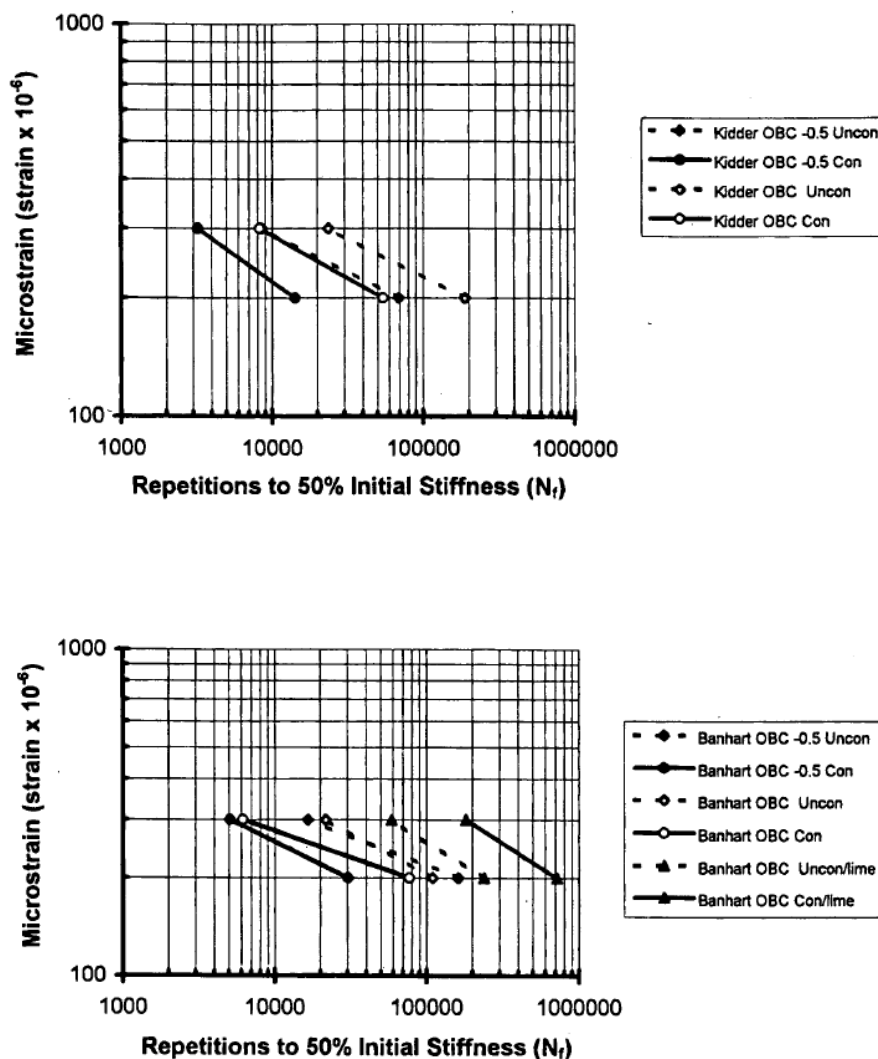


Figure 2.5: Strain-fatigue life relation (Shatnawi *et al.* (1995))

The study conducted by Lu (2005) is another example of using the controlled-strain fatigue beam test to measure the effect of moisture on fatigue behavior of AC mixtures. Fatigue tests were carried out at two different strain amplitude 200 and 400 $\mu\epsilon$. All tests were conducted at a temperature of 20 °C with a frequency of 10 Hz. They also reported that conditioning reduced both the fatigue life and the flexural stiffness. Researchers also measured the long-term effectiveness of both hydrated lime and liquid anti-strip agents by conducting both the Tensile Strength Ratio (TSR) test and the 4PB fatigue test. Results indicated that both treatment methods are effective in preventing moisture-damage. Table 2.1 summarizes the relevant literature related to fatigue of moisture influenced AC mixtures.

Table 2.1: Literature on Fatigue of moisture influenced AC mixtures

Author	Mode of test	Controlling variable	Test details	Fatigue life criteria	Fatigue life
Shatnawi et al. (1995)	Three point beam test with sinusoidal loading	Strain	200 and 300 $\mu\epsilon$, 10 Hz, 20 °C	50% reduction in initial stiffness	$N_f^{dry} > N_f^{wet}$
Lu (2005)	Four point beam test with sinusoidal loading	Strain	200 and 400 $\mu\epsilon$, 10 Hz, 20 °C	50% reduction in initial stiffness	$N_f^{dry} > N_f^{wet}$

Preconditioning of beam specimens:

Shatnawi *et al.* (1995) and Lu (2005) determined three parameters for the preconditioning process: saturation level, conditioning temperature, and conditioning duration. In their research, Lu (2005) revealed that the degree of saturation and the duration of the conditioning does not significantly affect the extent of moisture damage, however the conditioning temperature significantly increases the extent of moisture damage.

Shatnawi *et al.* (1995) conditioned the beam specimens in a procedure similar to that established as part of the SHRP A-003A project (Harvey and Monismith, 1993). Half of the beams were vacuum-saturated with water to about 60-80 percent degree of saturation during this conditioning cycle. These conditioned beams were then subjected to repeated loading as mentioned in Table 2.2. The beams were kept saturated by wrapping them with a moisture-resistant, thermoplastic flexible sheet. In their study, Lu (2005) conditioned the beams by partially saturating for 30 minutes under a vacuum of 16 kPa absolute pressure (635 mm-Hg vacuum), and then submerged for 24 hours in a 60°C water bath.

Table 2.2: Literature on Preconditioning parameters

Author	Saturation level	Preconditioning temperature	Preconditioning duration
		60 °C	5 hours
Shatnawi et al., 1995	60 - 80 %	25 °C	4 hours
		-18 °C	5 hours
Lu and Harvey, 2008	50 - 80 %	60 °C	24 hours

2.8 Surface Free Energy Measurement

Surface free energy (SFE) is an important parameter for evaluating the cohesive bond strength within asphalt binder and the adhesive bond strength between the asphalt-aggregate interface. In addition, water can be used in combination with asphalt binders

and aggregates SFE values to predict the sensitivity of AC mixtures to moisture (Cheng *et al.*, 2001, 2002; Lytton *et al.*, 2005; Bhasin *et al.*, 2006; Masad *et al.*, 2006; Little and Bhasin, 2006; Hefer *et al.*, 2006; Bhasin *et al.*, 2007; Hamed and Nejad, 2015). To assess the moisture-susceptibility of any given combination of asphalt aggregates, the strength of adhesive bond energy under dry conditions is compared to the strength of adhesive bond energy under wet conditions (Bhasin *et al.*, 2006; Masad *et al.*, 2006).

The Van Oss theory states that the total surface-free energy of any material is divided into two components based on the surface forces (Van Oss *et al.*, 1988). These are the non-polar component Lifshitz – van der Waals (LW) and the polar Lewis acid-base (AB) component, as represented using Equation 2.1.

$$\gamma = \gamma^{LW} + \gamma^{AB}, \quad (2.1)$$

where γ = surface energy of an asphalt or aggregate; γ^{LW} = Lifshitz-van der Waals component; and γ^{AB} = acid-base component. The γ^{AB} can be further represented using Equation 2.2

$$\gamma^{AB} = 2\sqrt{\gamma^+\gamma^-}, \quad (2.2)$$

where γ^+ is Lewis acid component; γ^- is Lewis base component.

From a thermodynamic point of view, the work of cohesion (ΔW_i^c) is the energy needed to create a crack of the unit area under the vacuum within the binder. The relation between work of cohesion and the surface energy is shown in Equation 2.3

$$\Delta W_i^c = 2\gamma_i, \quad (2.3)$$

The surface energy of cohesion can be rewrite in the form of Equation 2.1. as shown in Equation 2.4

$$\Delta W_i^c = \Delta W_i^{cLW} + \Delta W_i^{cAB}, \quad (2.4)$$

Similarly, the surface energy of adhesion can be rewrite as Equations 2.5 and 2.6

$$\Delta W_{ij}^a = \Delta W_{ij}^{aLW} + \Delta W_{ij}^{aAB}, \quad (2.5)$$

$$\Delta W_{ij}^a = \gamma_i + \gamma_j - \gamma_{ij}, \quad (2.6)$$

where γ_{ij} is the interfacial surface energy between i and j. Furthermore, interfacial surface energy has two components as described in Equation 2.7

$$\gamma_{ij} = \gamma_{ij}^{AB} + \gamma_{ij}^{LW}, \quad (2.7)$$

Lifshitz–van der Waals component of surface energy can be represented as, ((van Oss, 2002)):

$$\gamma_{ij}^{LW} = \left(\sqrt{\gamma_i^{LW}} - \sqrt{\gamma_j^{LW}} \right)^2, \quad (2.8)$$

$$\Delta W_{ij}^{aAB} = 2\sqrt{\gamma_i^{LW}\gamma_j^{LW}} = \sqrt{\Delta W_i^{cLW}\Delta W_j^{cLW}}, \quad (2.9)$$

Similarly, the acid–base component of surface energy can be represented as:

$$\gamma_{ij}^{AB} = 2\left(\sqrt{\gamma_i^+} - \sqrt{\gamma_j^+}\right)\left(\sqrt{\gamma_i^-} - \sqrt{\gamma_j^-}\right), \quad (2.10)$$

$$\Delta W_{ij}^{aAB} = 2\sqrt{\gamma_i^+\gamma_j^-} + 2\sqrt{\gamma_i^-\gamma_j^+}, \quad (2.11)$$

Thus the surface energy of adhesion between asphalt(i) and aggregate (j) is given by:

$$\Delta W_{ij}^a = 2\left[\sqrt{\gamma_i^{LW}\gamma_j^{LW}} + \sqrt{\gamma_i^+\gamma_j^-} + \sqrt{\gamma_i^-\gamma_j^+}\right], \quad (2.12)$$

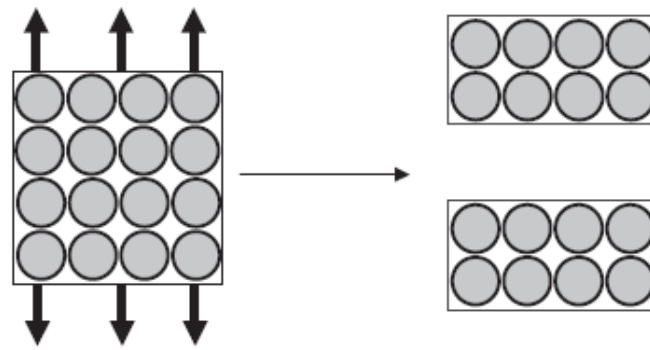
Similarly, the surface energy of adhesion between asphalt (i) and aggregate (j) in presence of water or moisture (k) is given as:

$$\Delta W_{ijk}^{aW} = \gamma_{ik} + \gamma_{jk} - \gamma_{ij}, \quad (2.13)$$

or,

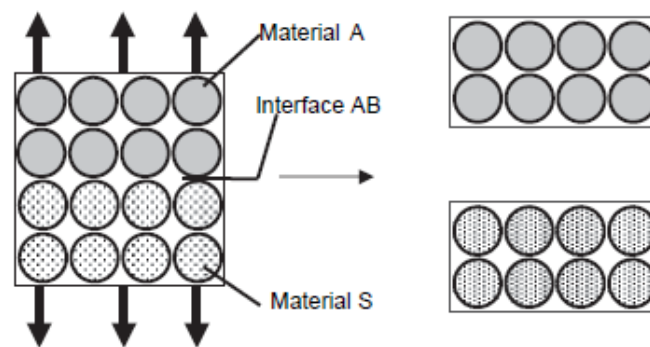
$$\begin{aligned} \Delta W_{ijk}^{aW} = & 2\gamma_k^{LW} + 2\sqrt{\gamma_i^{LW}\gamma_j^{LW}} - 2\sqrt{\gamma_i^{LW}\gamma_k^{LW}} - 2\sqrt{\gamma_j^{LW}\gamma_k^{LW}} + 4\sqrt{\gamma_k^+\gamma_k^-} \\ & - 2\sqrt{\gamma_k^+}\left(\sqrt{\gamma_i^-} + \sqrt{\gamma_j^-}\right) - 2\sqrt{\gamma_k^-}\left(\sqrt{\gamma_i^+} + \sqrt{\gamma_j^+}\right) + 2\sqrt{\gamma_i^+\gamma_j^-} + 2\sqrt{\gamma_i^-\gamma_j^+}, \end{aligned} \quad (2.14)$$

If the above value comes to be positive it means that the two phases of the material prefer to bond together.



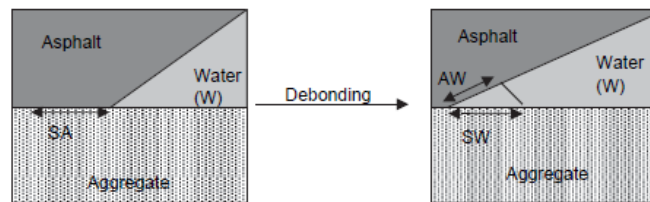
Work done for each side of new unit area created = γ
 Cohesive bond energy = Total work done = 2γ

(a)



Work done to create new unit area of A = γ_A
 Work done to create new unit area of S = γ_S
 Work due to loss of interface AS = $-\gamma_{AS}$
 Adhesive bond energy = Total work done = $\gamma_A + \gamma_S - \gamma_{AS}$

(b)



SA = Removal of Aggregate-Asphalt Interface; Work done = $-\gamma_{SA}$
 SW = Formation of Aggregate-Water Interface; Work done = γ_{SW}
 AW = Formation of Asphalt-Water Interface; Work done = γ_{AW}
 Total Work Done = $\gamma_{AW} + \gamma_{SW} - \gamma_{SA}$

(c)

Figure 2.6: Surface free energy (Bhasin et al. (2006))

The Wilhelmy plate (WP) and the sessile drop (SD) methods have been used in recent studies to measure the surface energy components of the asphalt by determining the dynamic and static contact angle between the asphalt and the various probe liquids (Solaimanian *et al.*, 2003; Cheng *et al.*, 2003; Koc and Bulut, 2013; Wei and Zhang, 2012; Hefer *et al.*, 2006) and the Universal Sorption System (USD) test to measure the

surface energy components of the aggregates (Solaimanian *et al.*, 2003; Cheng *et al.*, 2003; Bhasin *et al.*, 2007). Another recent research also uses the SD method to calculate the surface energy components of an aggregate (Wei and Zhang, 2012; Koc and Bulut, 2013). The determined surface energy components were then used in the presence or absence of moisture to determine the adhesive bond between the asphalt and aggregates. To assess the moisture-sensitivity of any given mixture of asphalt-aggregates, the adhesive bond energy under dry condition is compared with the adhesive bond energy under the wet condition.

In WP method, a small plate-shaped sample of the solid, attached to the arm of a force meter, is vertically dipped into a pool of the probe liquid (in actuality, the design of a stationary force meter would have the liquid being brought up, rather than the sample being brought down), and the force exerted on the sample by the liquid is measured by the force meter.

The SD approach is ideally suited for surfaces such as asphalts which have low energy (Bhasin *et al.*, 2007). The static contact angle of probe liquids dispensing on any solid surface are directly determined by capturing a photographic image of the dispensing drop. The captured image is then analyzed using a image processing software (Wei and Zhang, 2012; Koc and Bulut, 2013).

van Oss (2002) strongly suggests that two of the liquids in three probes should be polar and one of them should be apolar. It is also stated that the two polar liquids must be considerably different in terms of their polarity. Lytton *et al.* (2005) and Bhasin *et al.* (2006) found that the measured surface energy components would differ significantly with minor changes in the contact angle measurements unless a suitable combination of the probe liquids is chosen.

A drawback of this method is that the probe liquids used for measuring the contact angle must be pure (more than 99%) and solid surface roughness should be minimal, ideally to radius of roughness curvature below 1 micrometer as it will affect the sensitivity of measuring the contact angles (van Oss, 2002).

In earlier studies, Cheng *et al.* (2001) identified a relationship between the reduction in the magnitude of SFE due to the debonding in the presence of moisture and the moisture-sensitivity of several AC mixtures. The reduction in the magnitude of SFE due

to debonding in the presence of moisture is a function of the SFE components of asphalt binder, aggregate and water. In the literature several energy parameters were proposed to measure the sensitivity of the moisture for any combination of asphalt binders and aggregates. The ratio of adhesive bond energy under wet condition to dry condition ($\Delta W a^W / \Delta W a^D$) was used to classify best combinations of aggregates and binders (Lytton *et al.*, 2005). In another study, Bhasin *et al.* (2007) compared the various energy parameters with the fatigue life ratio and the dynamic modulus ratio in tension. They found that the correlation between the fatigue life ratio and the energy parameters was significant than the correlation between the dynamic modulus ratio in tension and the energy parameters. Four energy parameters were also used by Hamed and Nejad (2015) to select mixtures which offer better resistance to moisture damage. They observed that the tensile strength measured as per AASHTO T283 is well correlated with that. They also noticed that the component Lifshitz – van der Waals (LW) formed a significant part of asphalt's total SFE. Moreover, they also found that the introduction of anti-stripping agents resulted in a greater adherence between asphalt and acidic aggregates due to an increase in basic components and a decrease in surface energy acid components. In another research, Bhasin *et al.* (2006) found that the fraction of the bond energy resulting from the interaction of the asphalt acid component and the aggregate basic component contributes the most to a mixture's overall adhesive bond strength. They also found that asphalt with the same performance grade from different sources can have substantially different bond energies with any given aggregate.

2.9 Summary

Moisture in asphalt concrete (AC) pavement does not only cause distresses like stripping, potholes, etc. but also increases the extent and severity of other distresses like fatigue cracking, which is a predominant form of distress in AC pavements and one of the key modes of failure considered during AC pavement design. The effect of moisture on AC mixtures is usually characterized using the Modified Lottman Test (AASHTO T283) adopted in Superpave mix design. This test does not provide much insight on how moisture affects the fatigue characteristics of AC mixtures. Moreover, being an empirical measure, the results from the test cannot be used directly in performance models to predict the pavement life in the presence of moisture. The flexural beam test has been

used in the past studies to quantify the fatigue resistance of AC mixtures in the presence of moisture. The effect of moisture on the fatigue life of mixtures and its dependence on the type of binder, mixture volumetric, etc. has been extensively investigated in the literature. However, the effect of moisture on the variation of fatigue life with the amplitude of applied loading has received relatively less attention from researchers. Since the surface energy concept is also widely used to characterize the moisture-induced damage in terms of the change in the cohesive bond energy within the asphalt mastic and the adhesive bond energy between an asphalt-aggregate interface in the presence of moisture. Hence, it is necessary to examine the relationship between the change in the cohesive and the adhesive bond energy with the change in the fatigue characteristics of AC mixtures in the presence of moisture. To summarize, it is necessary to evaluate the effect of moisture on the fatigue characteristics of AC mixtures taking account of the influence of binder type and different strain amplitude level through experimental investigations and to examine its relationship with the change in the cohesive and the adhesive bond energy in the presence of moisture.

CHAPTER 3

EXPERIMENTAL METHODOLOGY

3.1 Material Selection

3.1.1 Binder

Two unmodified binders were used in this study, a binder of Viscosity Grade 10 (VG 10) and another with Viscosity Grade 30 (VG 30) as per [IS:73 \(2013\)](#) of the Indian Standards. The binders were supplied by M/s Hindustan Petroleum Corporation Limited (HPCL), India. The physical properties of VG 10 and VG 30 binders are shown in [Tables 3.1](#) and [3.2](#) respectively.

Table 3.1: Properties of VG 10 binder as per IS:73 (2013)

Characteristics	Measured Value	IS 73 (2013) Recommendation	Test Method
Absolute viscosity at 60°C (Poises)	1432	800-1200	IS 1206 (Part 2)
Kinematic viscosity at 135°C (cSt), Min.	412	250	IS 1206 (Part 3)
Penetration at 25°C (0.1mm), Min.	104	80	IS 1203
Softening point, R&B (°C), Min.	46	40	IS 1205
Tests on residue from rolling thin-film oven tests/ RTFOT			
1) Viscosity ratio at 60°C, Max	3.5	4.0	IS 1206 (Part 2)
2) Ductility at 25 °C after rolling thin- film oven test, Min (cm)	100 +	75	IS 1208

Table 3.2: Properties of VG 30 binder as per IS:73-2013

Characteristics	Measured Value	IS 73 (2013) Recommendation	Test Method
Absolute viscosity at 60°C (Poises)	3335	2400-3600	IS 1206 (Part 2)
Kinematic viscosity at 135°C (cSt), Min.	534	350	IS 1206 (Part 3)
Penetration at 25°C (0.1mm), Min.	43	45	IS 1203
Softening point, R&B (°C), Min.	52	47	IS 1205
Tests on residue from rolling thin film oven tests/ RTFOT			
1) Viscosity ratio at 60°C, Max	2.93	4.0	IS 1206 (Part 2)
2) Ductility at 25 °C after rolling thin-film oven test, Min (cm)	100 +	40	IS 1208

3.1.2 Aggregate Gradation

Blue granite aggregates from a quarry near Chennai were used for fabricating the AC mixtures. The gradation chosen for the study is the mid-gradation of Bituminous Concrete Grade II (BC - II) mixture with a nominal maximum aggregate size of 13.2 mm, as per [MoRTH \(2013\)](#) specification. The aggregate gradation curve is shown in Figure 3.1.

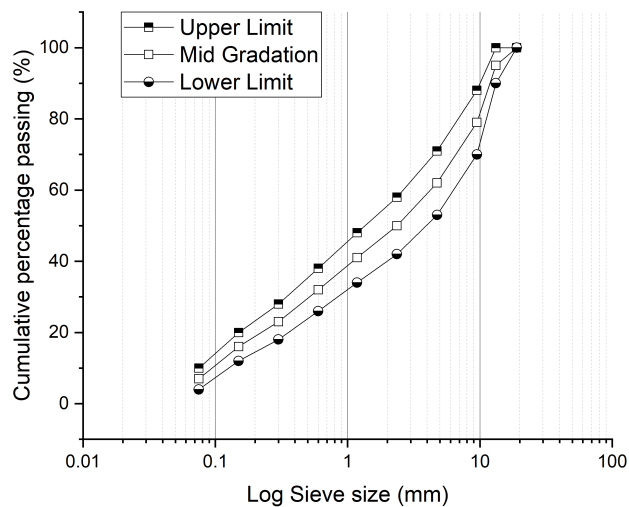


Figure 3.1: Aggregate gradation curve (MoRTH, 2013)

3.2 Sample Fabrication for 4PB Fatigue Testing

The different stages of sample preparation include batching, mixing, compaction and slicing of casted sample are discussed below.

3.2.1 Batching and Mixing

The aggregates were sieved into different standard sizes with an automatic sieving machine as shown in Figure 3.2. The sieved aggregates were batched (Figure 3.2b) to meet the mid-gradation in accordance with the MoRTH (2013). The corresponding details are given in Annexure A. Batched aggregates were kept in an oven for drying at $110 \pm 5^\circ\text{C}$ for 24 hours. The oven-dried aggregates were then preheated for 1 hour at a temperature of $170 \pm 5^\circ\text{C}$ and binder was preheated to its mixing temperature prior to mixing MoRTH (2013). The mixing and compaction temperature range of the AC mixture is defined as the temperature range where the unaged binder has a kinematic viscosity of approximately $0.17 \pm 0.02\text{Pa}\cdot\text{s}$ and $0.28 \pm 0.03\text{Pa}\cdot\text{s}$, respectively, calculated in accordance with ASTM:D4402/D4402M (2015). Table 3.3 shows the mixing and compaction temperature range for the VG 10 and VG 30 binders. According to MoRTH (2013) specifications, if the specific gravity of the aggregate is 2.7, BC-II mixture requires a minimum bitumen content of 5.4% by mass of the total mixture. However, the minimum binder content can be decreased proportionately in the case of aggregates with specific gravity greater than 2.7. For this study, however, no mix design was performed and a 5% binder content by mass of the total mix was selected. The preheated aggregates along with the binder content of 5% by mass of the total mixture were transferred to the automatic mixer (Figure 3.2c) and mixed at the mixing temperature of the binder. The AC mixture is then aged at $135 \pm 3^\circ\text{C}$ for $4\text{h} \pm 5$ minutes and then placed at a compaction temperature of 150°C for 30 minutes in accordance to AASHTO:R30 (2002) in order to account for the ageing that occurs in the field during mixing and compaction.

Table 3.3: Mixing and Compaction Temperature

Bitumen Viscosity Grade	Mixing Temperature (°C)	Compaction Temperature (°C)
VG-10	150 - 156	140 - 145
VG-30	155 - 160	145 - 150



(a) Sieving



(b) Batched Samples



(c) Mixing

Figure 3.2: Sieving, batching and mixing of asphalt concrete

3.2.2 Theoretical Maximum Specific Gravity (G_{mm})

The theoretical maximum specific gravity of the AC mixture was determined according to [ASTM:D6857/D6857M \(2011\)](#) specification. 2000 grams of batched aggregates were mixed with a binder content of 5% by mass of the total mixture at temperatures specified in Table 3.3 for preparing AC mixtures. After mixing, the AC mixtures were loosened and allowed to cool to room temperature. A CoreLok device was used to measure G_{mm} . The batching details for G_{mm} samples are given in Table 3.4.

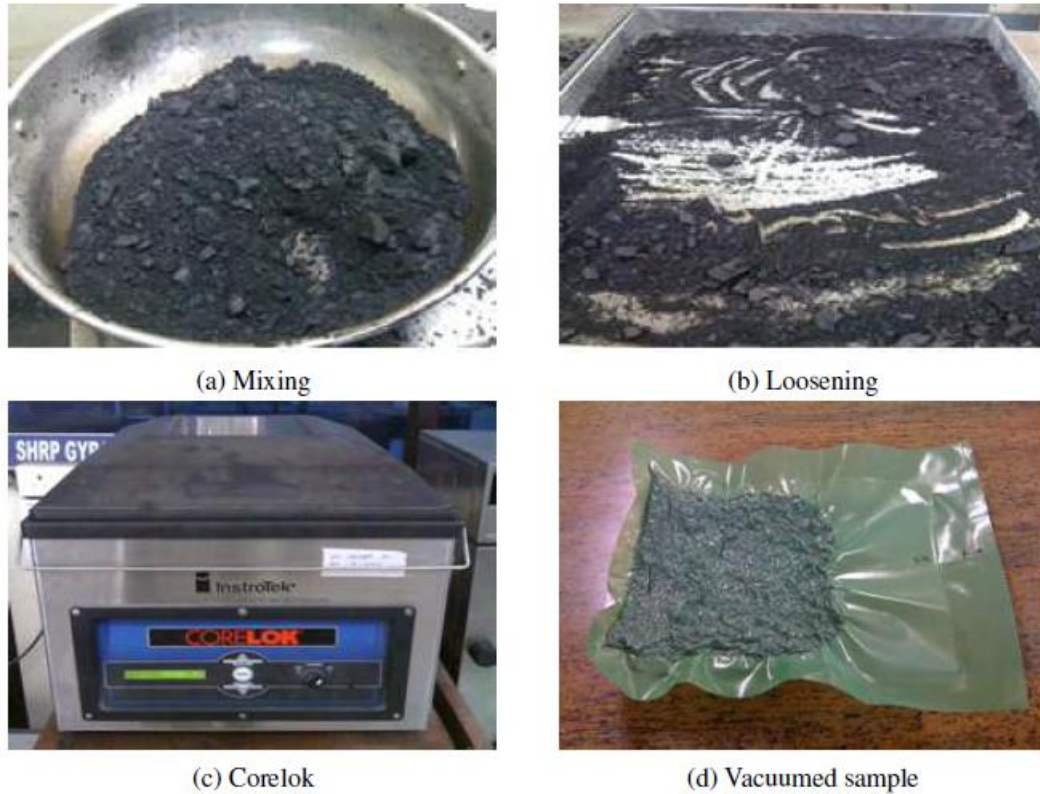


Figure 3.3: Measurement of G_{mm} in CORELOK

The weight of the sample and polymer bags were noted. The samples were placed inside the polymer bags and then sealed inside the CoreLok device such that the air voids in the sample were removed. The sealed samples were then immersed in water, the polymer bag was cut open 5 cm below the water surface inside the water bath and the water was allowed to infiltrate the sample. The sample along with the polymer bags was weighed by keeping below the water surface and the volume was determined. The theoretical maximum specific gravity was then calculated from the sample weight by dividing it by its volume. The measured G_{mm} values for the two mixtures are given in Table 3.4.

Table 3.4: Theoretical Maximum Specific Gravity G_{mm}

Mixture	Green + White Bags Weight (gms)	Sample + Bags Weight (gms)	Sample Weight in air (gms)	Sample Weight in water (gms)	G_{mm}	Average G_{mm}
AC - VG30						
1	69.30	2145.07	2075.77	1278.50	2.628	2.616
2	69.85	2168.90	2099.05	1288.20	2.614	
3	69.69	2170.88	2101.19	1291.06	2.618	
4	69.46	2171.28	2101.82	1290.93	2.616	
5	69.19	2153.24	2084.05	1279.62	2.615	
6	69.69	2170.21	2100.52	1290.53	2.617	
AC - VG10						
1	70.15	2168.90	2098.75	1284.90	2.603	2.606
2	70.06	2164.32	2094.26	1283.28	2.607	
3	70.14	2161.65	2091.51	1282.45	2.609	
4	69.19	2158.76	2089.57	1279.88	2.605	
5	69.64	2145.82	2076.19	1272.76	2.608	
6	69.55	2143.77	2074.22	1270.05	2.604	

3.2.3 Compaction

The loose asphalt mixture was compacted using a PReSBOX Shear Compactor - IPC Global. The compaction temperature was taken as $150 \pm 5^\circ\text{C}$ for both VG 10 and VG 30 in accordance with [ASTM:D4402/D4402M \(2015\)](#). The input parameters required for software as shown in Figure 3.4 are sample weight, vertical stress and maximum density. The compaction termination criterion can be specified in terms of cycles, height, density or air voids. In this investigation, the air void was selected as the termination parameter and a target was set for the same. The uniformity of the target air voids within the samples was achieved by adjusting the number of cycles. The compaction was carried out by the combined effect of constant vertical force and cyclic shear force. As per [ASTM:D7981 \(2015\)](#), constant vertical stress of 600 kPa and a shear angle amplitude of 4 degrees are applied for the compaction. The compaction was stopped automatically once the sample reached the target air voids. The compaction process is illustrated in Figure 3.5. The sample was then ejected and allowed to cool down to room temperature. After the compaction, the sample of size 450 mm length, 150 mm width and 165 mm thickness was kept at room temperature for one day before slicing.

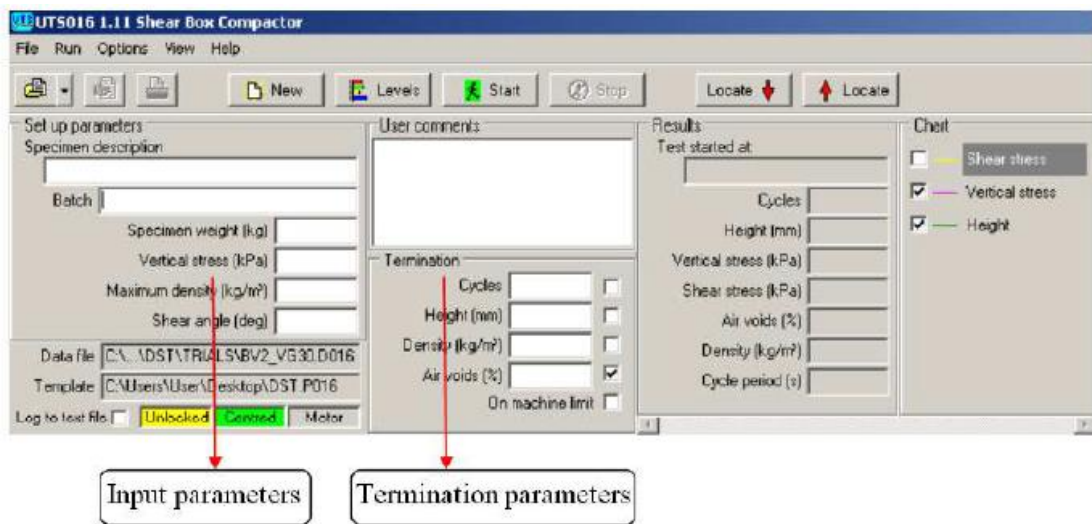


Figure 3.4: UTS 16 software screenshot

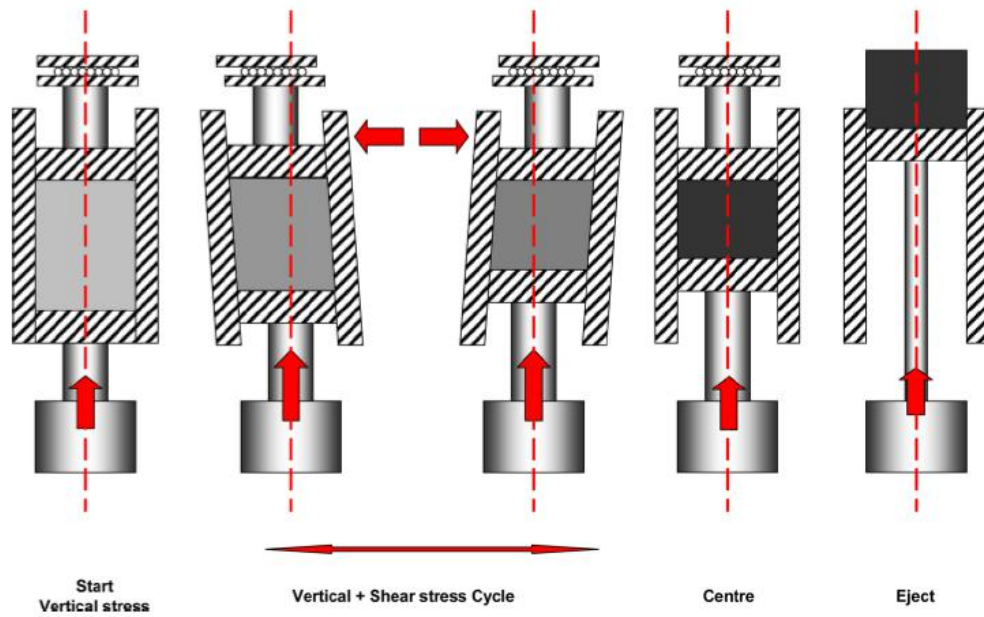


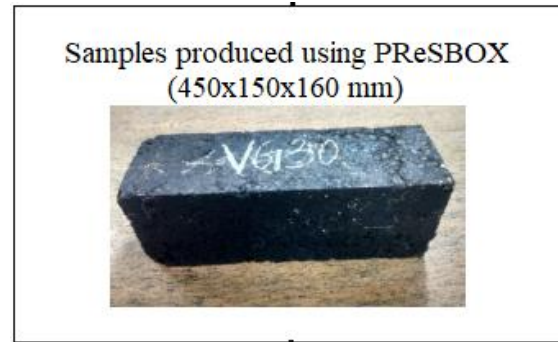
Figure 3.5: Illustration of the compaction process as per [ASTM:D7981 \(2015\)](#)

3.2.4 Slicing

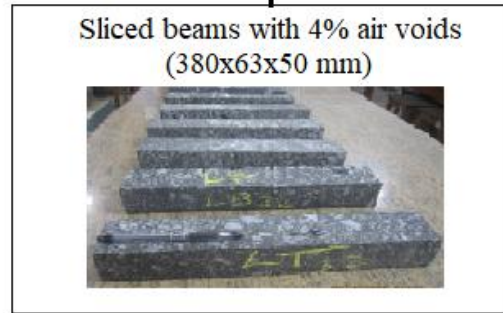
An asphalt mixture sawing machine was used for sawing and slicing the shear box compacted bituminous sample as shown in Figure 3.6. The slicing process is illustrated in Figure 3.8. From each shear box compacted sample, four beam specimens were obtained after slicing as shown in Figure 3.7. Sliced rectangular beams with 380 ± 6 mm length, 63 ± 2 mm width and 50 ± 2 mm height were used for the fatigue test.



Figure 3.6: Sample Cutter

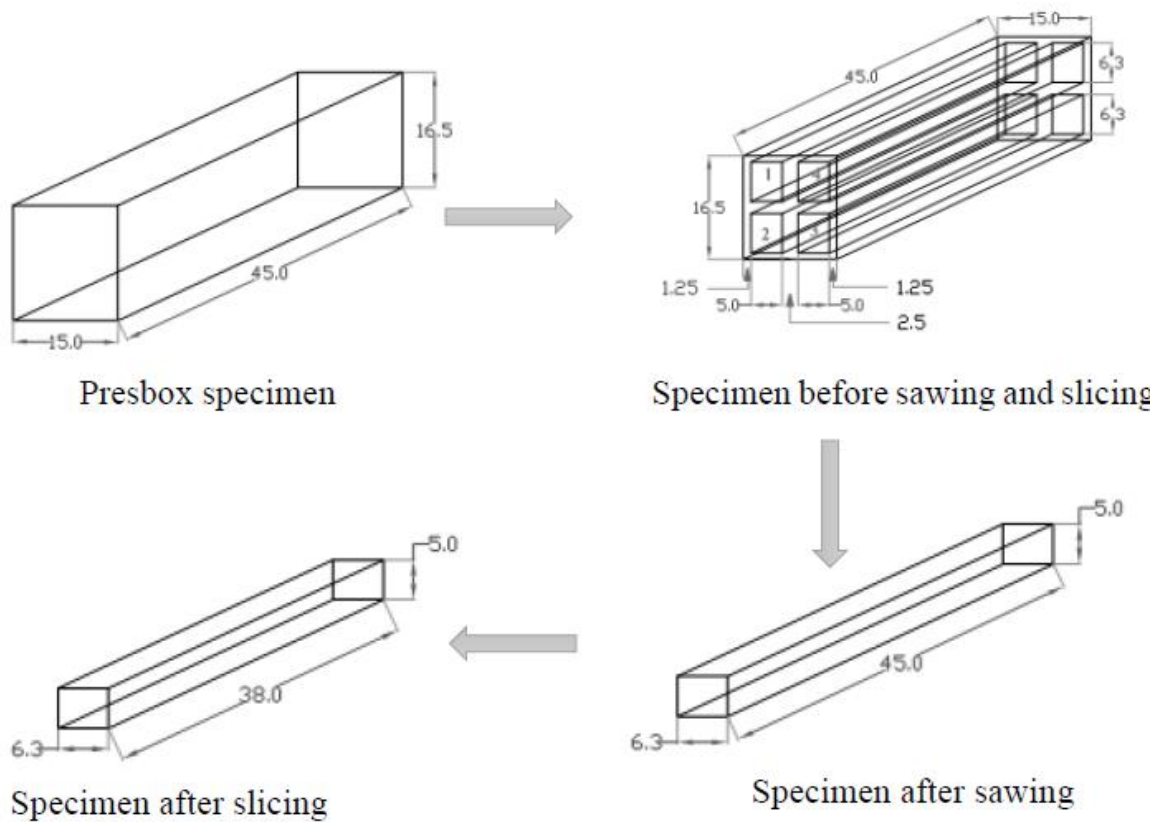


Samples produced using PReSBOX
(450x150x160 mm)



Sliced beams with 4% air voids
(380x63x50 mm)

Figure 3.7: Samples produced using shear box beam



(All dimensions are in centimeters)

Figure 3.8: Slicing process (Krishnan, J M and Veeraragavan, A, 2013)

A total of 16 beam samples were cast using the PReSBOX compactor during the course of the study. From each beam sample, 4 beams were sliced.

3.3 Sample Preparation for Surface Free Energy Measurement

Five different probe liquids namely water, diiodomethane, ethylene glycol, glycerol and formamide were used for measuring surface free energy of asphalt binders and aggregate.

3.3.1 Asphalt Binder

For the preparation of the specimen, a canister with the binder in it is placed in the oven at a temperature of 165 °C for a duration of 1 hour. A standard microscopic glass slide is first dipped and then left out several times from the melted binder, until a flat, smooth binder surface is obtained. The specimen was kept in a desiccator for 24 hours at a temperature of 25 °C. Two glass slides were prepared for each probe liquid and a total of six measurements were performed (three measurements per slide). This procedure has been replicated for all five probe liquids. The average contact angle for each probe liquid was then used for determining the surface energy components.



Figure 3.9

3.3.2 Aggregates

A coring tool was used to extract cylindrical cores of approx. 2 inches diameter from the specified large rocks for the contact angle measurement. Then the rock core was cut into circular disks using a tile saw that enables water-cooled cutting. The aggregate surface was then washed with distilled water followed by ethanol. Samples were then kept in a 100°C oven for 30 minutes, and then kept in a 24-hour desiccator at 20°C. Two circular rock disks were prepared for each liquid probe and a total of six measurements were performed (three measurements per circular rock disks).

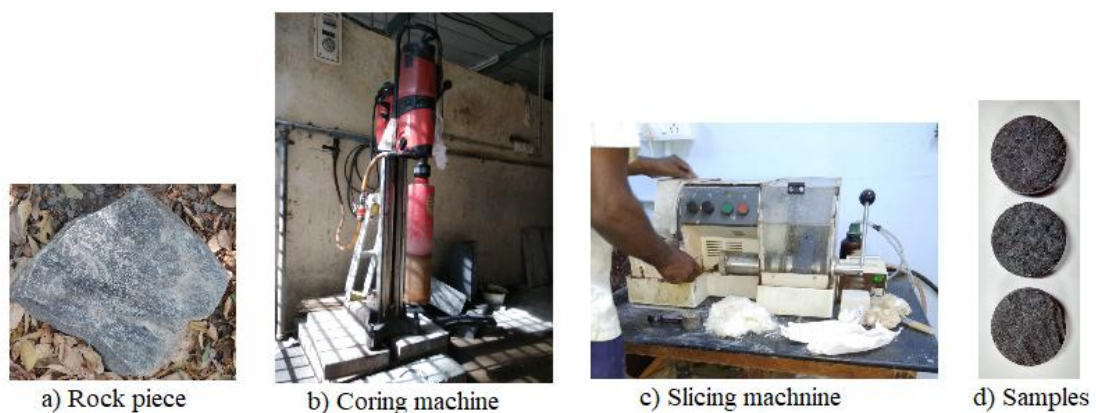


Figure 3.10

3.4 Preconditioning of Beam Specimens

The basic purpose of the preconditioning process is to cause a certain extent or level of moisture-damage in beam samples. This is typically achieved by saturating the beams with moisture and then placing these beams in a warm water bath to exacerbate the damage.

A new setup was fabricated to saturate the beams to the desired degree of saturation. A schematic diagram of the experimental setup is shown in Figure 3.11. This setup consists of a cylindrical desiccator, a vacuum pump, a non-return valve, a calibrated vacuum dial gauge, a vacuum controller, a moisture trap and connection tubes.

- *Desiccator*: A cylindrical desiccator having an inner diameter of 100 mm with a 5 mm thickness and a height of 550 mm with a glass flange on the top.
- *Vacuum Pump*: A vacuum pump which is capable of applying vacuum pressure up to 760 mm-Hg.

- *Non-return Valve*: A non-return valve to ensure there is no leakage of air from the vacuum pump and any of the joint.
- *Vacuum Dial Gauge*: A vacuum dial gauge to measure the applied vacuum.
- *Vacuum Controller*: A vacuum controller to maintain the desired level of vacuum (740 mm-Hg) in the desiccator. It helps the vacuum pump to restarts automatically, if vacuum falls below the specified range (700 mm-Hg).
- *Moisture Trap*: A moisture trap to prevent the moisture from infiltrating the vacuum pump during the process of saturation.

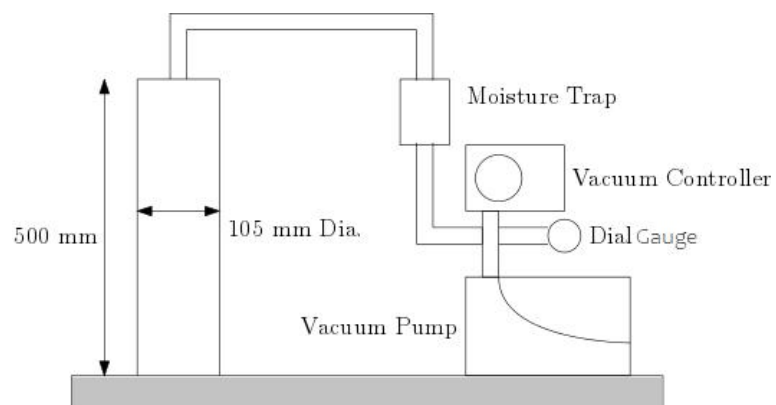


Figure 3.11: Schematic drawing of saturation of beams

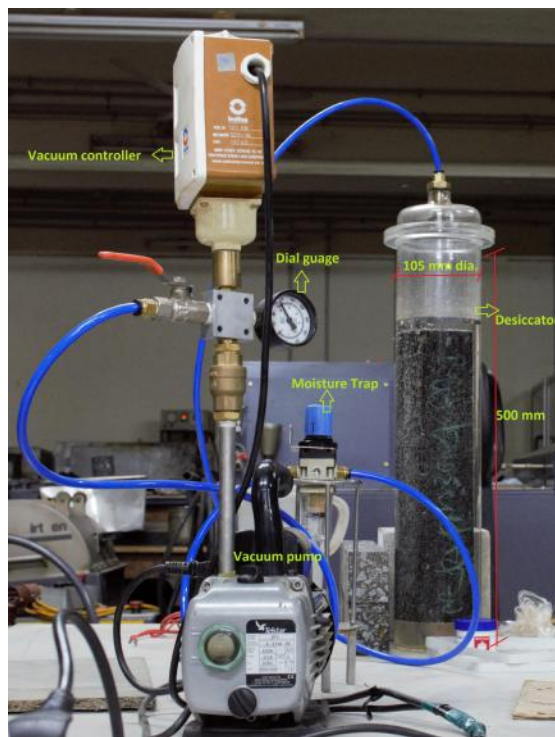


Figure 3.12: Setup for moisture-conditioning

To moisture-condition the beam specimens, they were first placed inside the airtight cylindrical glass desiccator and submerged completely with portable water at room temperature. The water level was adjusted such that the beam specimen has at least 25 mm of water above the top surface. A vacuum of 740 mm-Hg pressure was then applied for a duration of 3 hours. Following the vacuum application, the beam specimen was then allowed to remain submerged in water for 10 minutes after the release of the vacuum. The degree of saturation is then calculated using the difference in the air weight of the beam specimen before and after saturation as shown in Equation 3.1.

$$S = \frac{100 \times (W_{sat} - W_d)}{V_{air}}, \quad (3.1)$$

$$V_{air} = \frac{V_a \times V_{beam}}{100}, \quad (3.2)$$

where S - degree of saturation (%), W_{sat} - saturated surface dry weight of beam specimen after saturation (g), W_d - weight of dry beam in air (g), V_{air} - volume of air voids (cm^3), V_a - air voids (%), V_{beam} - volume of beam (cm^3). The beam specimen was then placed in a 60 ± 1 °C water bath for 24 ± 1 hours. After preconditioning, the specimen was cooled to room temperature by placing the beam specimen inside water for 30 ± 10 minutes and then wrapped with an impermeable plastic sheet, to retain the internal moisture. Then the beam samples were placed inside an environmental chamber at 20 ± 1 °C for 2 hours prior to testing as per [AASHTO:T321 \(2017\)](#).

From the sliced beams, 45 beam samples were selected for testing. Initially, multiple trials were carried out with different saturation duration to check the duration of saturation which was adequate to achieve a desired level of saturation. As a result, each specimen was kept in the desiccator for a duration of 3 hours. The final data set include the test results of 32 beams (16 moisture-conditioned beam and 16 unconditioned beams). The details of the degree of saturation for moisture-conditioned samples are given in Annexure B.

3.5 Experimental Investigation

3.5.1 4PB Fatigue Test Equipment

Fatigue tests were performed using an IPC EN standards testing equipment (Figure 3.14) with a four-point bending jig (Figure 3.13). The jig is fixed inside an environmental chamber.



Figure 3.13: Jig



Figure 3.14: Four point beam bending equipment

Fatigue tests were carried out at four different strain levels for both BC-VG10 and BC-VG30 mixtures. A test frequency of 10 Hz was selected with a continuous sinusoidal loading waveform. The tests were conducted at a temperature of 20 °C. The strain levels were selected as per [AASHTO:T321 \(2017\)](#) and [ASTM:D7460 \(2010\)](#). The test parameters selected for the study are given in Table 3.5.

Table 3.5: Test matrix

Mixture Type	Asphalt Concrete Grade II
Binder Type	VG 10 and VG 30
Temperature °C	20
Amplitude ($\mu\epsilon$)	200, 400, 600 and 800
Frequency (Hz)	10
Waveform	Sinusoidal
Saturation Level (%)	55 - 80
Conditioning Temperature °C	60 \pm 1
Conditioning Duration	24 \pm 1
Termination criteria	1 \times 10 ⁶ cycles or 80% reduction in stiffness

3.5.2 Test Procedure for 4PB Fatigue Beam

The beam samples sliced from the PReSBOX compacted sample with an air void content of $4 \pm 0.5\%$ were selected for the fatigue testing. The dimensions of the sliced beam samples were measured along the middle 100 mm length of the specimen. A minimum of 3 measurements was taken and the average of the three dimensions was considered for the test. The beams were conditioned in an environmental chamber at 20 °C for two hours prior to testing as per [AASHTO:T321 \(2017\)](#). After conditioning, the sample was placed into the loading frame and clamped as per [ASTM:D7460 \(2010\)](#). To reduce the variability in the results, two beams from the same PReSBOX sample were chosen. One was subjected to moisture-conditioning and another was kept dry. The LVDT was placed on top of the sample at the mid-span and the initial value was set to zero. The initial stiffness was computed at the 50th load cycle and the test was either terminated at a stiffness reduction of 80 percent or after 1 million cycles, whichever occurred first.

3.5.3 Integrity of the Waveform

PID tuning was carried out to ensure that the waveform of the applied strain is as close to sinusoidal as possible. The tuning parameter panel contains the tuning controls of proportional gain, integral gain and derivative gain collectively called the PID tuning parameters (IPC Global,2011). Proportional gain is adjusted for actuator response and stability depending upon loading waveform and amplitude. Integral gain specifies the time within which the actual amplitude error should reduce to zero following a level change. Derivative gain adjusts the transient or step response of the control system and is used to compensate for the different mass of platens, load cells and grippers (IPC Global, 2011).

Table 3.6: RMSE value of loading waveform for different strain levels and cycles

Strain ($\mu\epsilon$)	VG 10			VG 30		
	200 th	600 th	1000 th	200 th	600 th	1000 th
200	0.00328	0.00380	0.00398	0.00152	0.00152	0.00153
400	0.00661	0.00693	0.00723	0.00396	0.00378	0.00385
600	0.01113	0.01109	0.00934	0.00518	0.00521	0.00523
800	0.01180	0.01120	0.01098	0.00653	0.00707	0.00773

3.5.4 Sessile Drop Testing Equipment

In this study, contact angles were determined using the sessile drop (SD) technique with a drop shape analysis system (Kyowa DMs - 401). A probe liquid drop on the sample surface placed inside an environmental chamber was captured using a charge-coupled device (CCD) camera. The captured image was then analyzed using an application developed by Kyowa Interface Science Co, Ltd. for determining the contact angle at the edge of the drop. Then, the average of 6 measurements of contact angle for each probe liquid was used to calculate the components of surface free energy. All measurements of the contact angle were carried out at 20°C.

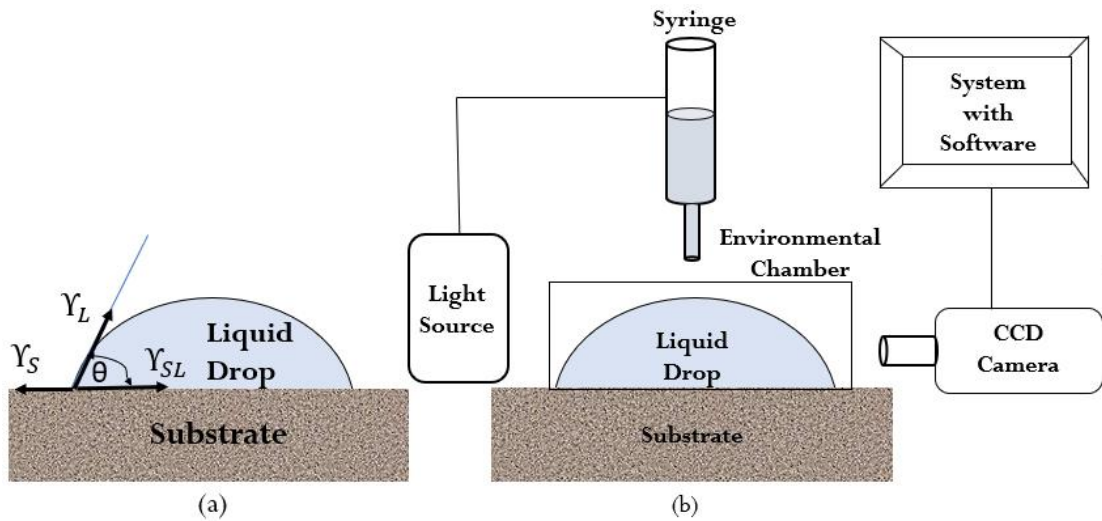


Figure 3.15: (a) Contact angle between a liquid drop and substrate; (b) Sessile drop method

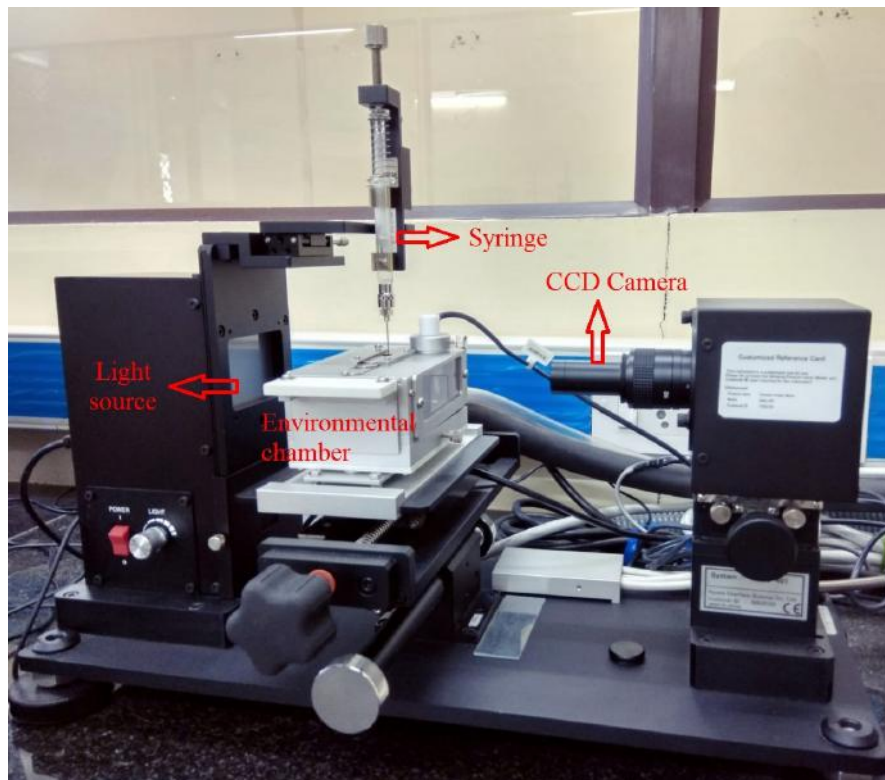


Figure 3.16: Experimental setup of sessile drop

The SD technique was introduced to measure the contact angles between different probe liquids and asphalt binders / aggregates from which the asphalt binder and aggregate surface-free energies were calculated using the Young-Dupre equation, which is commonly used to calculate the surface free energy components of solid materials by

means of contact angle measurements (van Oss, 2002):

$$(1 + \cos\theta)\gamma_L = 2 \left[\sqrt{\gamma_L^{LW}\gamma_S^{LW}} + \sqrt{\gamma_L^+\gamma_S^-} + \sqrt{\gamma_L^-\gamma_S^+} \right] \quad (3.3)$$

There are three unknowns in Eq.(3.3) (i.e. γ^{SLW} ; γ^{S+} ; γ^S). To determine the sample (aggregate or binder) SFE, contact angles with three separate probe liquids must be determined. Table 3.7 lists the surface energy components of the used probe liquids.

Table 3.7: Surface Energy Components of Liquid Probes

Probe Liquid	γ^{Total} (mJ/m ²)	γ^{LW} (mJ/m ²)	γ^{AB} (mJ/m ²)	γ^- (mJ/m ²)	γ^+ (mJ/m ²)
Water (W)	72.80	21.80	51.00	25.50	25.50
Diiodomethane (D)	50.80	50.80	0.00	0.00	0.00
Ethylene glycol (E)	47.9	29.00	18.90	47	1.90
Glycerol (G)	64	34.00	30	57.40	3.92
Formamide (F)	58.1	39.00	19.10	39.6	2.30

The test parameters selected for the study are as follows:

Table 3.8: Test matrix

Binder Type	VG10 and VG30
Aggregate Type	Blue Granite
Testing Temperature (°C)	20
Conditioning Temperature (°C)	20
Conditioning Duration (hours)	24
Probe Liquids	Water (W), Diiodomethane (D), Ethylene Glycol (E), Glycerol (G), Formamide (F)

CHAPTER 4

ANALYSIS AND DISCUSSION

4.1 4PB Fatigue Test Methods

Depends upon the type of loading (constant load or constant displacement), loading mode, frequency and temperature during testing, different test methods may be used to quantify the fatigue life.

The three most popular test methods available for determining and analyzing the fatigue life of compacted AC mixture subjected to repeated flexural bending are given in American Association of State Highway and Transportation Officials ([AASHTO:T321 \(2017\)](#)), American Society for Testing and Materials ([ASTM:D7460 \(2010\)](#)) and European Union Standard (EN 12697-04 (2004)). Test parameters for different standards are shown in Table 4.1.

Table 4.1: Fatigue Test Parameters

Test parameter	ASTM:D7460 (2010)	AASHTO:T321 (2017)	EN: 12697 (2004)
Loading waveform	Haversine	Sinusoidal	Sinusoidal
Test temperature	20 °C	-10 to 25 °C	0 and 20 °C
Frequency	5 to 10 Hz	5 to 10 Hz	0 to 60 Hz
Sample size (mm)	380 × 63 × 50	380 × 63 × 50	380 × 63 × 50
Conditioning time	2 hrs	2 hrs	2 hrs for 0 °C, 1 hr for 20 °C
Initial stiffness	50th cycle	50th cycle	100th cycle
Strain levels	50 to 3000 $\mu\epsilon$	250 to 750 $\mu\epsilon$	not less than 50 $\mu\epsilon$
Minimum number of cycles	10000	10000	10000

4.1.1 Post-Processing of Fatigue Test Data

Two methods were used for post-processing the fatigue data and quantify the fatigue life and they are listed as follows:

- 50% reduction in stiffness as per [AASHTO:T321 \(2017\)](#)
- Normalised modulus as per [ASTM:D7460 \(2010\)](#)

The [AASHTO:T321 \(2017\)](#) method describes fatigue failure as the number of cycles in which the initial stiffness of the material decreases by 50%. The initial stiffness is considered here as the stiffness module which corresponds to the 50th cycle. In cases where the experimental data obtained does not achieve a 50% reduction in stiffness during the period of the experiment, [AASHTO:T321 \(2017\)](#) suggests using an exponential function of the form $S = ae^{bx}$ to fit the experimental data. Though, the same relationship was not considered for the experimental data obtained, as the initial data sets did not follow the trend. Hence Equation 4.1 was used in this analysis.

$$S = ae^{bx} + ce^{dx}, \quad (4.1)$$

where S = stiffness (MPa); x = number of cycles; a , b , c and d are regression constants. The initial stiffness is calculated for $x = 50$. The exponential function for S was fit to the experimental data to obtain the regression constants, and the constants were then used in Equation 4.1 to determine the number of cycles to 50% reduction in stiffness.

The [ASTM:D7460 \(2010\)](#) method is based on the Miner's equation of cumulative damage. The normalized modulus is calculated in this method, and the peak point is considered as the failure point in the normalized modulus versus cycle plot. The determination of the normalized modulus is performed using the Equation 4.2. As per this equation, the product of stiffness modulus and the number of cycles are normalized with respect to the reference cycle and stiffness modulus at the reference cycle.

$$NM_i = \frac{S_i}{S_o} \times \frac{N_i}{N_o}, \quad (4.2)$$

where NM_i = normalised modulus at the i^{th} cycle; S_i = flexural beam stiffness at cycle i (Pa); $N_i = i^{th}$ cycle; S_o = initial flexural beam stiffness at 50th cycle (Pa); N_o = number of cycles where the initial stiffness is estimated. In the cases where the normalized

modulus curve does not achieve the peak value during the test duration, the failure point can be determined by fitting a Weibull distribution to the data set.

Equation 4.3 represents the Weibull function used for extrapolation of the fatigue life (Tsai et al., 2002).

$$\text{Ln}(-\text{Ln}(SR)) = \gamma \times \text{Ln}(N) + \text{Ln}(\lambda), \quad (4.3)$$

where $\text{Ln}(-\text{Ln}(SR))$ = natural logarithm of the negative of the natural logarithm of SR; SR = flexural beam stiffness ratio, beam stiffness at cycle i /initial beam stiffness; N = number of cycles; γ is the slope of the linear regression of the $\text{Ln}(-\text{Ln}(SR))$ versus $\text{Ln}(N)$; $\text{Ln}(\lambda)$ is the intercept of the linear regression of the $\text{Ln}(-\text{Ln}(SR))$ versus $\text{Ln}(N)$. The failure point is estimated by solving for N where $SR = 0.5$.

4.2 Analysis of Fatigue Test Data

Analysis of the test results is carried out as per the above standards to determine the fatigue life of AC materials at different strain amplitudes. From the raw data, parameters such as stiffness modulus, normalized modulus, phase lag and dissipated energy per cycle were calculated as per the standards for the analysis. These are presented below.

4.2.1 Initial Stiffness Modulus

Figures 4.1 to 4.6 show the variation of stiffness modulus at different strain level as a function of moisture-conditioning for both BC-VG30 and BC-VG10 samples. The moisture-conditioned samples were subjected to a lesser number of cycles to reach 80% reduction in initial stiffness modulus than dry samples at each strain level. It can be seen that the moisture-conditioned samples generally have lower initial stiffness than dry samples, and the stiffness of moisture-conditioned samples typically decrease at a larger rate than dry samples. It can also be seen that the tests are reasonably repeatable. The deviation between two trials is reasonably small both the mixtures at all the loading conditions.

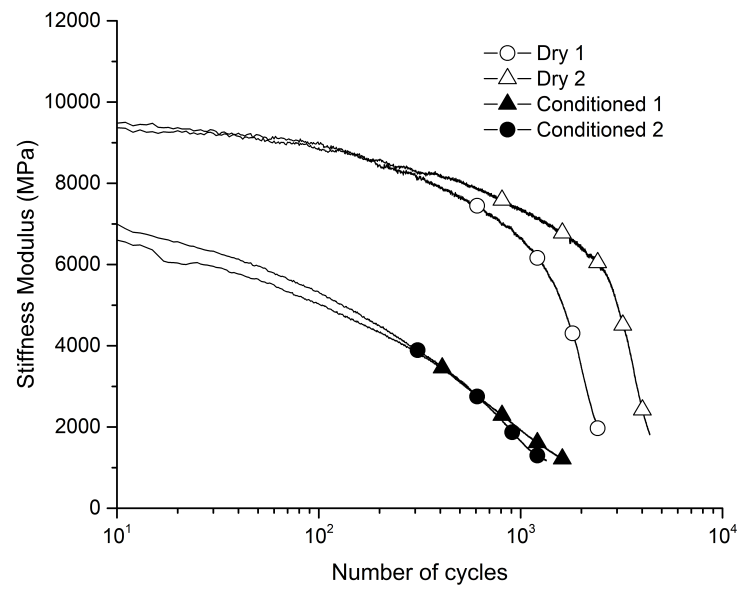


Figure 4.1: Variation of stiffness modulus for BC-VG30 samples at $800\mu\epsilon$

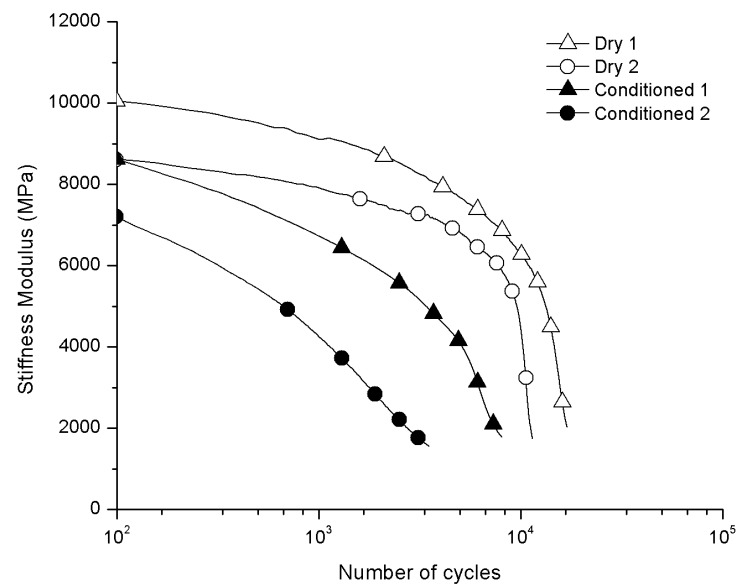


Figure 4.2: Variation of stiffness modulus for BC-VG30 samples at $600\mu\epsilon$

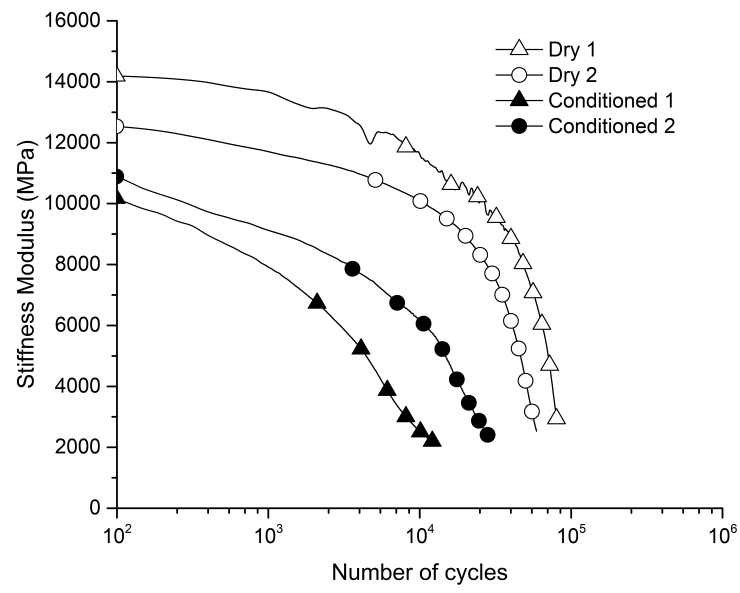


Figure 4.3: Variation of stiffness modulus for BC-VG30 samples at $400\mu\epsilon$

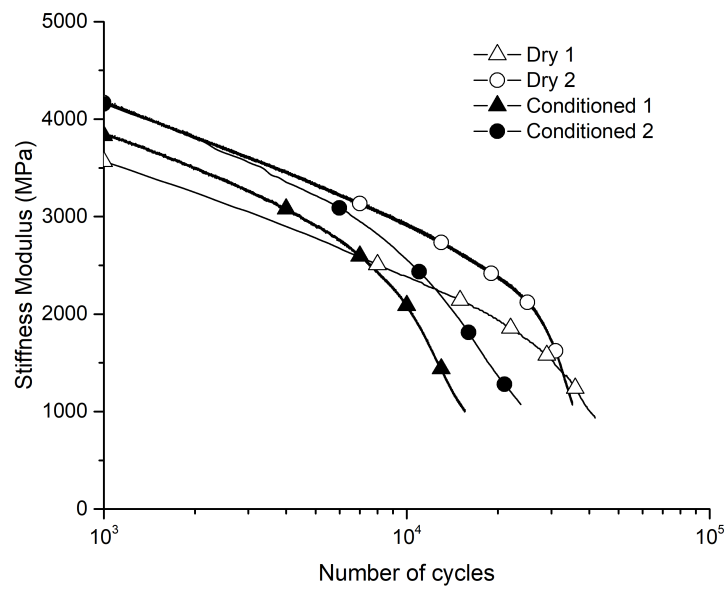


Figure 4.4: Variation of stiffness modulus for BC-VG10 samples at $800\mu\epsilon$

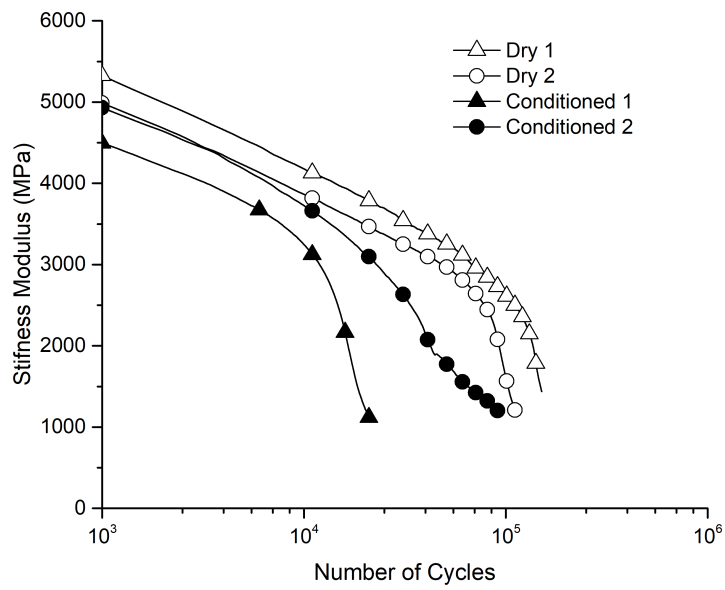


Figure 4.5: Variation of stiffness modulus for BC-VG10 samples at $600\mu\epsilon$

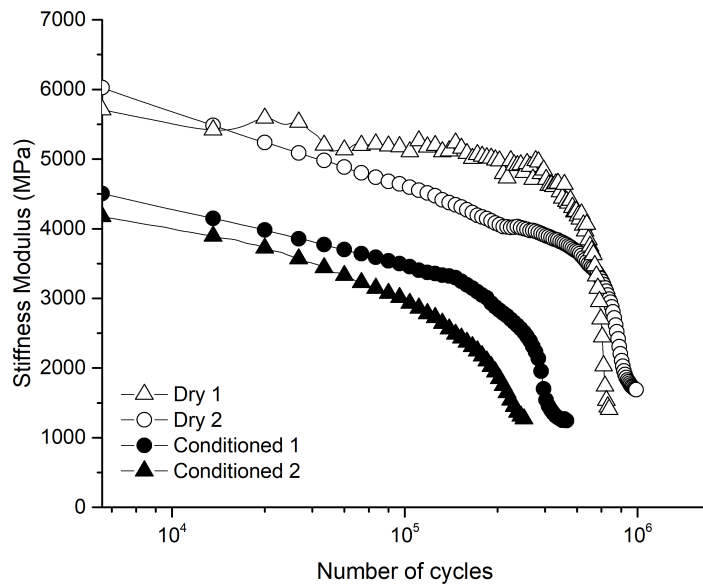


Figure 4.6: Variation of stiffness modulus for BC-VG10 samples at $400\mu\epsilon$

Figures 4.7 and 4.8 presents the initial stiffness modulus of moisture-conditioned samples and dry samples at different strain levels for BC-VG10 an BC-VG30. These values were obtained by taking the average of two trials conducted at each strain level. It can be seen that the moisture-conditioned samples generally have lower stiffness

compared to the dry samples, except for BC-VG10 at $800\mu\epsilon$. This is because of the moisture-conditioning and the associated damage (Shatnawi *et al.*, 1995) and (Lu, 2005). It was also observed that the initial stiffness modulus of BC-VG10 samples was considerably lower than that of BC-VG30 samples at any particular strain level. This is because of the low viscosity for the VG10 binder than that of the VG30 binder. Table 4.2 shows the initial stiffness ratio (ISR) defined as the ratio of initial stiffness modulus of moisture-conditioned samples to dry samples. A higher value of the ISR signifies less susceptibility to moisture damage (Shatnawi *et al.*, 1995) and (Lu, 2005). This indicates that the BC-VG10 mixtures are less susceptible to moisture damage as compared to BC-VG30 mixtures. The initial stiffness modulus was significantly affected by the binder type and moisture-conditioning.

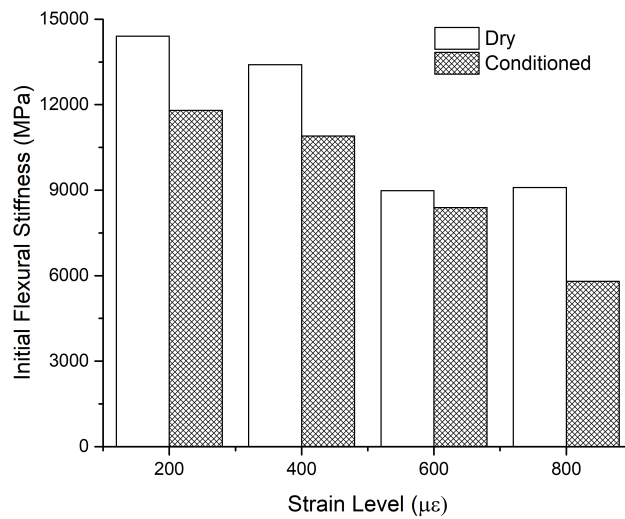


Figure 4.7: Initial Stiffness for BC-VG30 samples

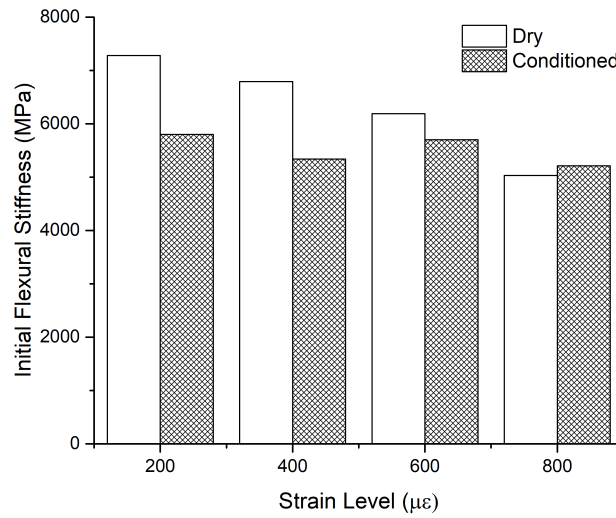


Figure 4.8: Initial Stiffness for BC-VG10 samples

Table 4.2: Initial Stiffness Ratio (ISR)

Mixture Type	Initial Stiffness Ratio (ISR)				
	200 $\mu\epsilon$	400 $\mu\epsilon$	600 $\mu\epsilon$	800 $\mu\epsilon$	Average
BC-VG10	0.80	0.79	0.92	1.03	0.89
BC-VG30	0.82	0.82	0.93	0.64	0.80

4.2.2 Fatigue life using AASHTO T321-17 (2017)

It was seen that the termination criteria (i.e., 50% of the initial stiffness modulus) for dry samples was within the test duration at 400, 600 and 800 $\mu\epsilon$ for both BC-VG10 and BC-VG30 samples. However, at 200 $\mu\epsilon$, BC-VG10 samples, both dry and moisture-conditioned and dry BC-VG30 samples did not reach a 50% reduction in stiffness modulus. Hence an exponential fit was carried out for such data.

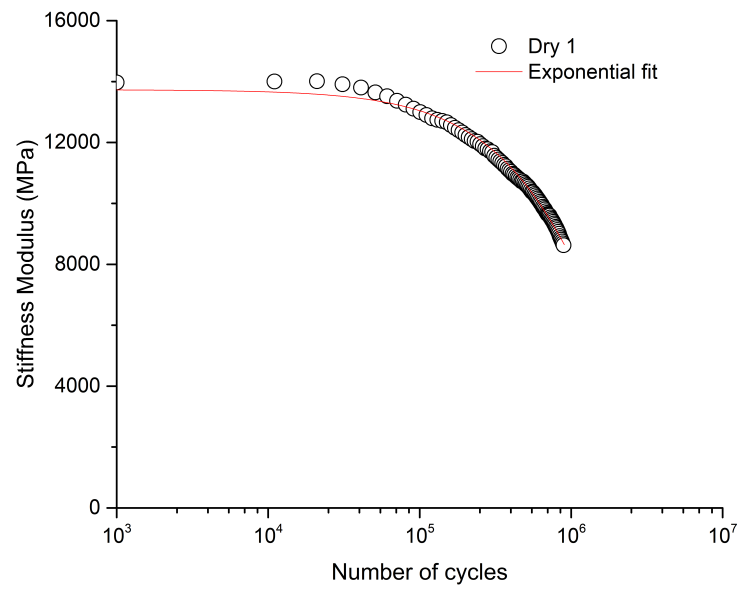


Figure 4.9: Exponential fit, BC-VG30 at $200\mu\epsilon$

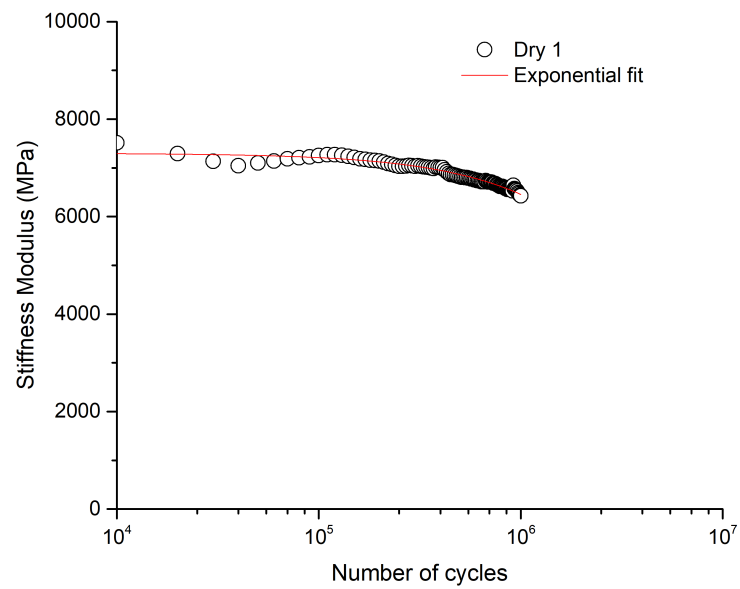


Figure 4.10: Exponential fit, BC-VG10 at $200\mu\epsilon$

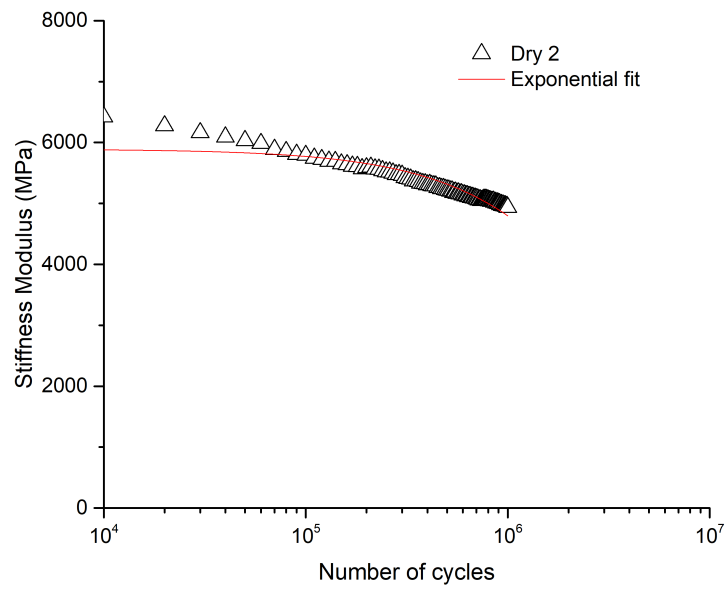


Figure 4.11: Exponential fit, BC-VG10 at $200\mu\epsilon$

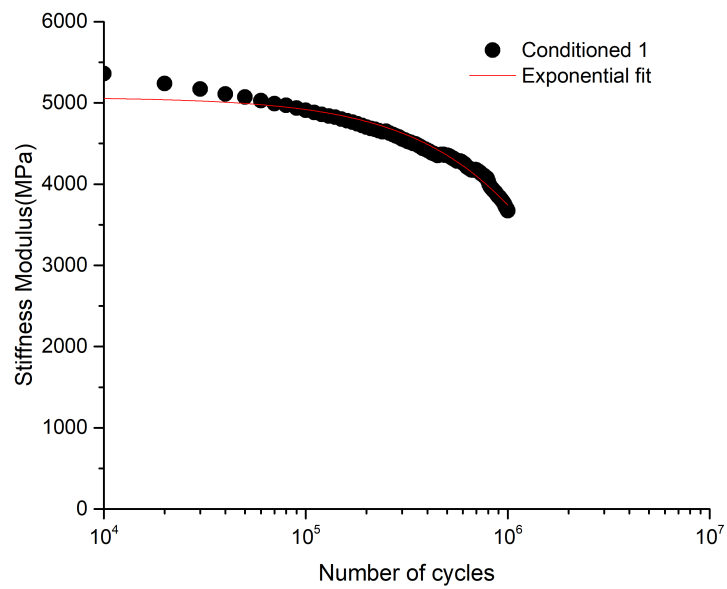


Figure 4.12: Exponential fit, BC-VG10 at $200\mu\epsilon$

Table 4.3: Parameters obtained from exponential fit

Sample	Condition	Parameters			
		a	b	c	d
BC-VG10					
200 $\mu\epsilon$	Dry 1	7303	-1.41E-07	5163	-2.21E-06
200 $\mu\epsilon$	Dry 2	1041	-4.15E-06	5216	-5.29E-08
200 $\mu\epsilon$	Conditioned 1	353.5	-3.79E-06	4827	-2.45E-07
200 $\mu\epsilon$	Conditioned 2	490.3	-1.19E-05	5347	-8.69E-08
VG 30					
200 $\mu\epsilon$	Dry 1	830.5	-1.09E-05	13400	-4.72E-07

The parameters obtained for both dry and moisture-conditioned samples at 200 $\mu\epsilon$ are shown in Table 4.3. Using the constants listed in Table 4.3 and Equation 4.1, the fatigue life was calculated and summarised in Table 4.4. It was observed that moisture-conditioned samples of both BC-VG10 and BC-VG30 showed lower the fatigue life when compared to dry samples at each strain-level.

Table 4.4: Fatigue life as per AASHTO T321-17

Strain Level ($\mu\epsilon$)	Fatigue Life			
	BC-VG10		BC-VG30	
	Dry	Conditioned	Dry	Conditioned
200	6.81E+06*	2.81E+06*	1.05E+06*	2.09E+05
400	5.82E+05	2.04E+05	4.75E+04	8.32E+03
600	4.95E+04	1.82E+04	1.17E+04	2.74E+03
800	1.20E+04	8.20E+03	2.46E+03	5.66E+02

* values estimated from exponential fit

4.2.3 Fatigue life using ASTM D7460-10 (2010)

Figures 4.13 to 4.19 show the variation of normalised modulus at different strain level as a function of moisture-conditioning for both BC-VG10 and BC-VG30 samples. It

was observed that the normalized modulus curve attained peak values at strain levels of 400, 600 and 800 $\mu\epsilon$ for both moisture-conditioned and dry samples of BC-VG10 and BC-VG30. The number of cycles corresponding to the peak value was considered as fatigue life.

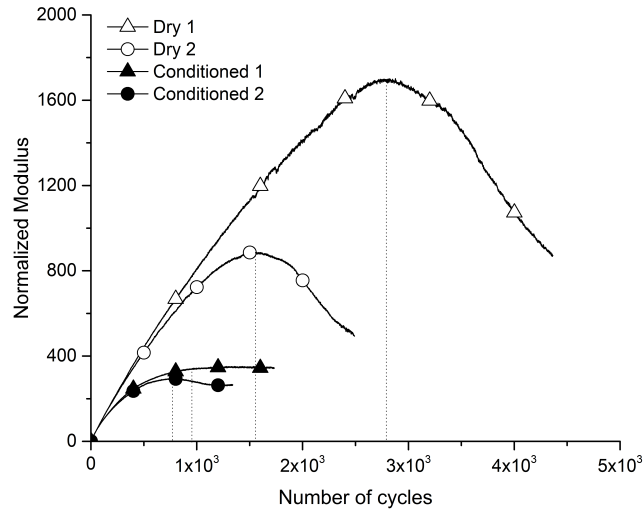


Figure 4.13: Normalized modulus curve for BC-VG30 samples at 800 $\mu\epsilon$

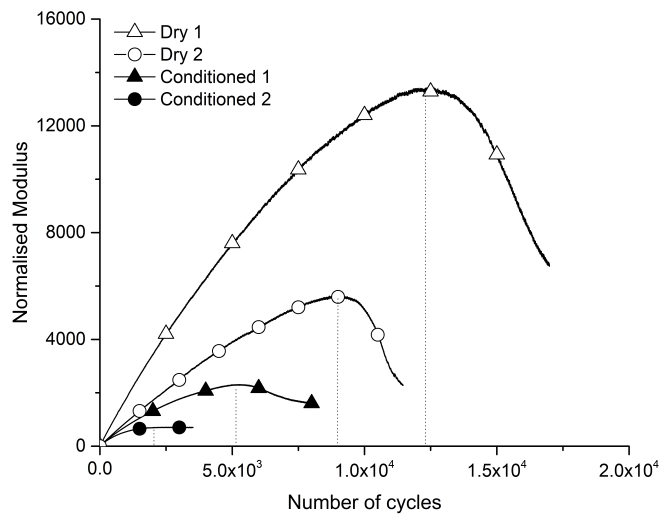


Figure 4.14: Normalized modulus curve for BC-VG30 samples at 600 $\mu\epsilon$

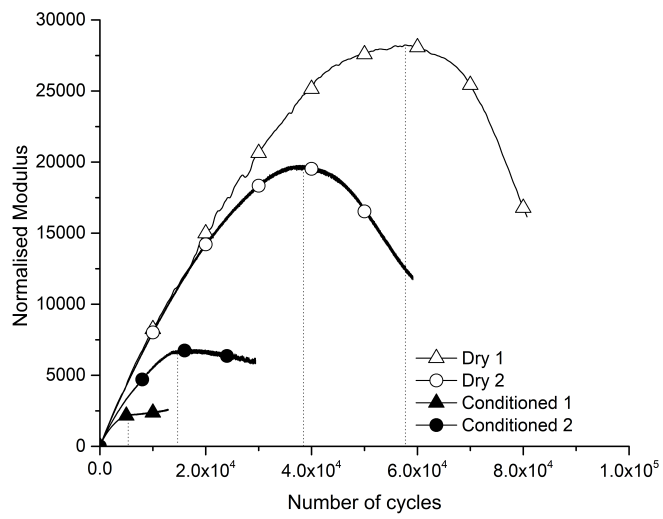


Figure 4.15: Normalized modulus curve for BC-VG30 at $400\mu\epsilon$

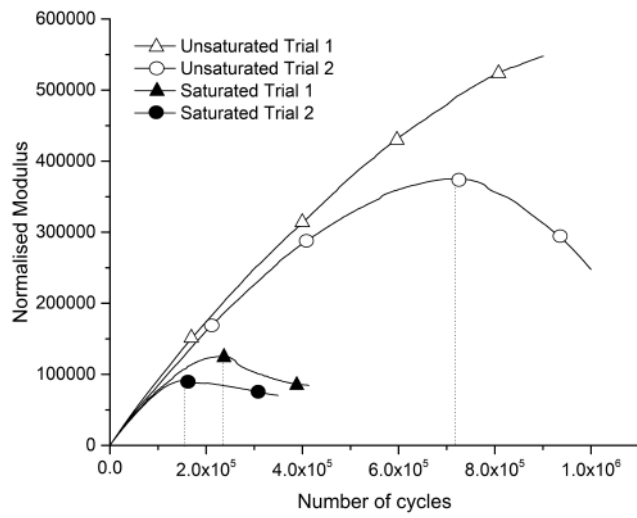


Figure 4.16: Normalized modulus curve for BC-VG30 at $200\mu\epsilon$

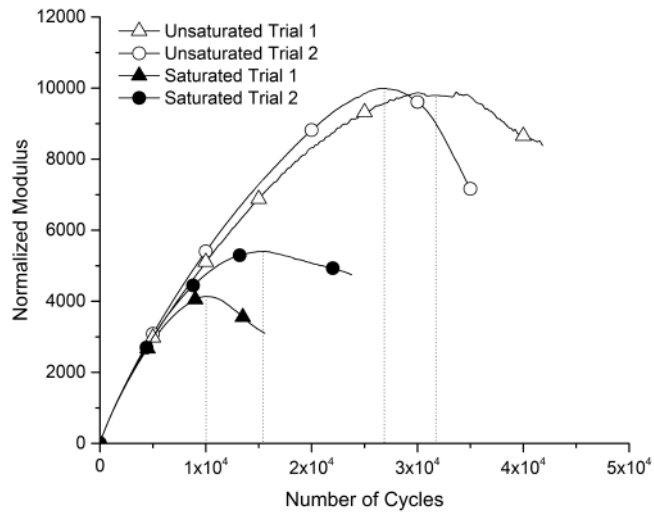


Figure 4.17: Normalized modulus curve for BC-VG10 at $800\mu\epsilon$

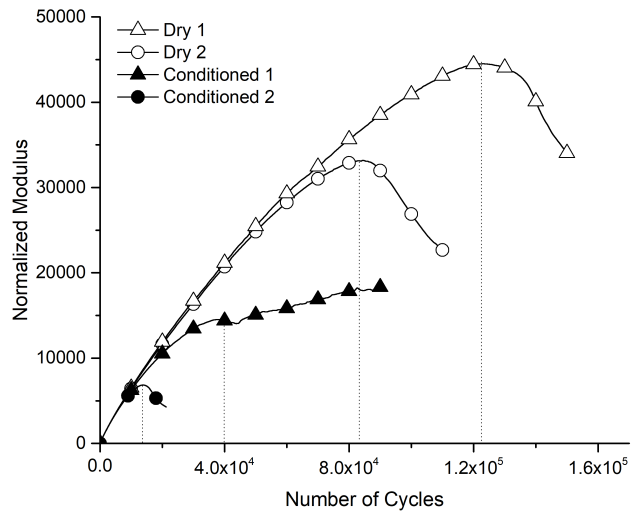


Figure 4.18: Normalized modulus curve for BC-VG10 at $600\mu\epsilon$

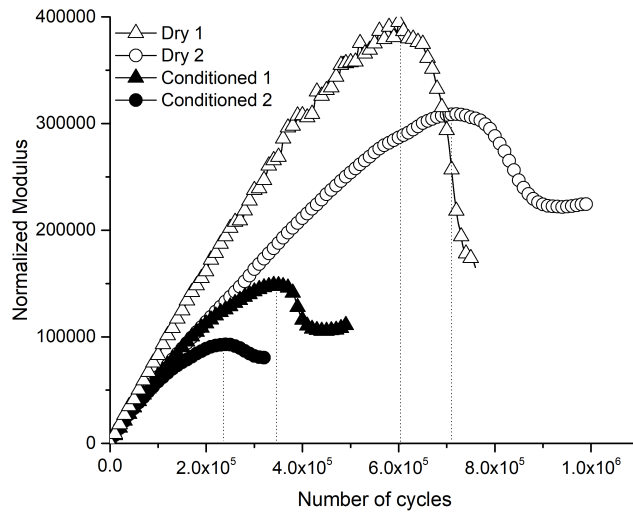


Figure 4.19: Normalized modulus curve for BC-VG10 at $400\mu\epsilon$

At $200\mu\epsilon$ for both moisture-conditioned and a dry sample of BC-VG10 and one dry sample of BC-VG30, the normalized modulus did not attain a peak value. Hence the peak value for the Normalized modulus was determined by fitting a Weibull distribution function in these cases. Figure 4.21 to 4.23 show the Weibull curve for the same.

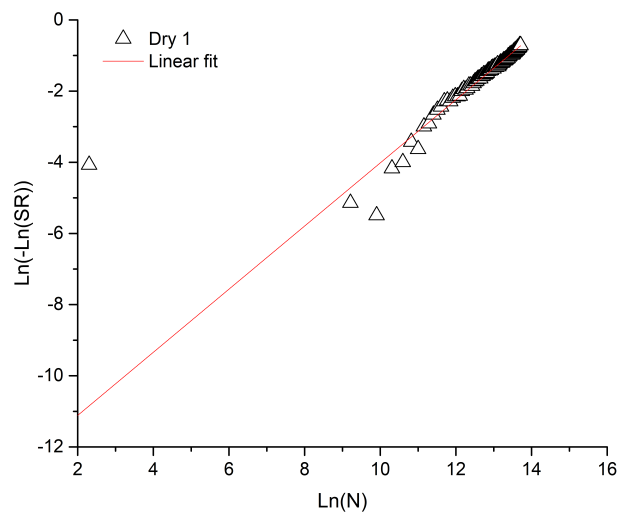


Figure 4.20: Weibull curve for BC-VG30 (dry) at $200\mu\epsilon$

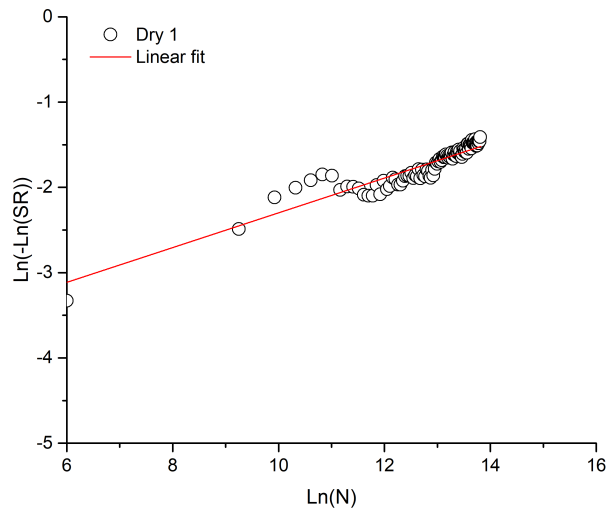


Figure 4.21: Weibull curve for BC-VG10 (conditioned) at $200\mu\epsilon$

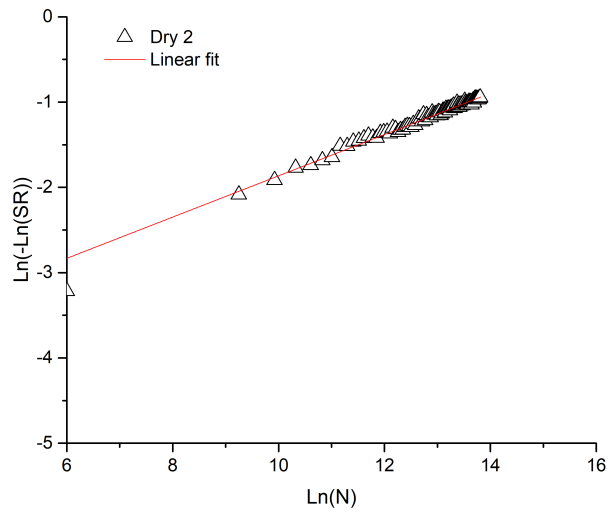


Figure 4.22: Weibull curve for BC-VG10 (dry) at $200\mu\epsilon$

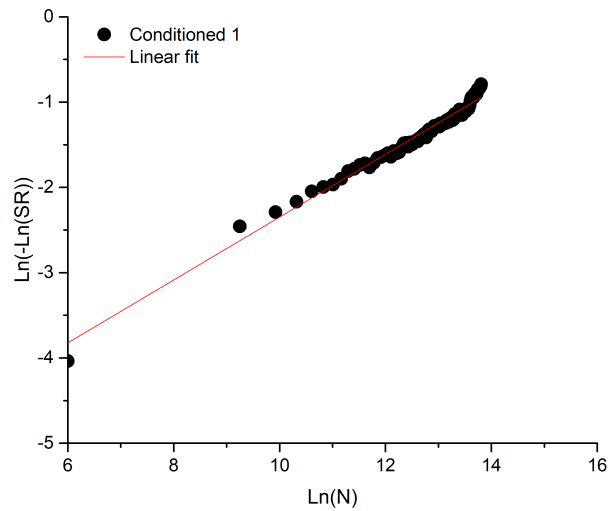


Figure 4.23: Weibull curve for BC-VG10 (conditioned) at $200\mu\epsilon$

Table 4.5: Parameters obtained from linear fit

Sample	Condition	Parameters	
		Slope	Intercept
BC-VG10			
200 $\mu\epsilon$	Dry 1	0.204	-4.337
200 $\mu\epsilon$	Dry 2	0.242	-4.284
200 $\mu\epsilon$	Conditioned 1	0.369	-6.037
200 $\mu\epsilon$	Conditioned 2	0.241	-4.283
BC-VG30			
200 $\mu\epsilon$	Dry 1	0.886	-12.887

The parameters obtained from the linear fit are presented in table 4.5. Using the parameters listed in table 4.5 and equation 4.3, the fatigue life was calculated and summarised in Table 4.6. It was observed that moisture-conditioned samples of both BC-VG10 and BC-VG30 showed significantly lower fatigue life when compared to dry samples at all strain levels Shatnawi *et al.* (1995) and Lu (2005). Table 4.7 and 4.8 show the average fatigue life ratio (FLR), the ratio of the fatigue life of moisture-conditioned samples to that of dry samples, for the mixtures BC-VG10 and BC-VG30, respectively.

Table 4.6: Fatigue life as per ASTM D7460-10

Strain Level ($\mu\epsilon$)	Fatigue Life			
	BC-VG10		BC-VG30	
	Dry	Conditioned	Dry	Conditioned
200	1.07E+07*	4.76E+06*	1.03E+06*	1.92E+05
400	6.60E+05	2.93E+05	4.73E+04	9.77E+03
600	1.04E+04	2.61E+04	1.06E+04	3.71E+03
800	2.92E+04	1.27E+04	2.71E+03	8.92E+02

* values estimated from linear fit

Table 4.7: FLR AASHTO T321-17

Mixture Type	Fatigue Life Ratio (FLR)				
	200 $\mu\epsilon$	400 $\mu\epsilon$	600 $\mu\epsilon$	800 $\mu\epsilon$	Average
VG 10	0.41	0.35	0.37	0.68	0.45
VG 30	0.20	0.18	0.23	0.23	0.21

Table 4.8: FLR ASTM D7460-10

Mixture Type	Fatigue Life Ratio (FLR)				
	200 $\mu\epsilon$	400 $\mu\epsilon$	600 $\mu\epsilon$	800 $\mu\epsilon$	Average
VG 10	0.44	0.44	0.25	0.44	0.39
VG 30	0.19	0.21	0.35	0.40	0.29

4.2.4 Reduction in the Fatigue Life after Moisture-Conditioning

Table 4.9 shows the percentage reduction in fatigue life after moisture-conditioning at the different strain levels for both BC-VG10 and BC-VG30 samples. It can be observed that the percentage reduction in the fatigue life for BC-VG30 samples is more than that of samples with BC-VG10. Furthermore, it was also observed that the percentage reduction in stiffness after moisture-conditioning is significantly affected by the post-processing method used for calculating the fatigue life.

Table 4.9: Effect of conditioning on the fatigue life

Strain Level ($\mu\epsilon$)	% Reduction in the Fatigue Life after Conditioning			
	VG 10		VG 30	
	AASHTO	ASTM	AASHTO	ASTM
200	59%	56%	80%	81%
400	65%	56%	82%	79%
600	63%	75%	77%	65%
800	32%	56%	77%	60%

4.2.5 Total Dissipated Energy per Cycle

Asphalt concrete dissipates energy when subjected to repeated loading due to the viscous friction within the material and the fatigue damage of the material. In this study, the change in the dissipation characteristics of the material with moisture-conditioning was investigated by determining the total dissipated energy per cycle during the fatigue tests. The energy dissipated per cycle will decrease with the number of cycles as the stress required to maintain the strain amplitude will reduce with the progress of the fatigue test. Work done or energy dissipated over a cycle is calculated as a cyclic integral of the product of stress and strain rate (Wineman and Rajagopal, 2000),

$$W = \oint \sigma \dot{\epsilon} dt$$

which results in the expression

$$W = \pi \sigma_o \epsilon_o \sin \delta$$

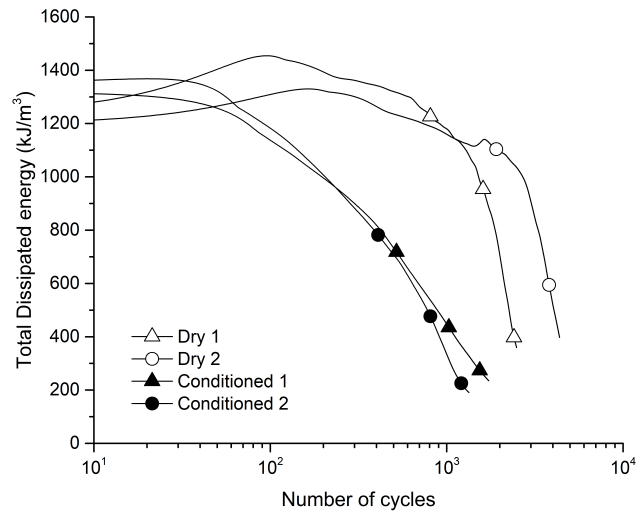


Figure 4.24: Dissipated energy per cycle for BC-VG30 at $800\mu\epsilon$

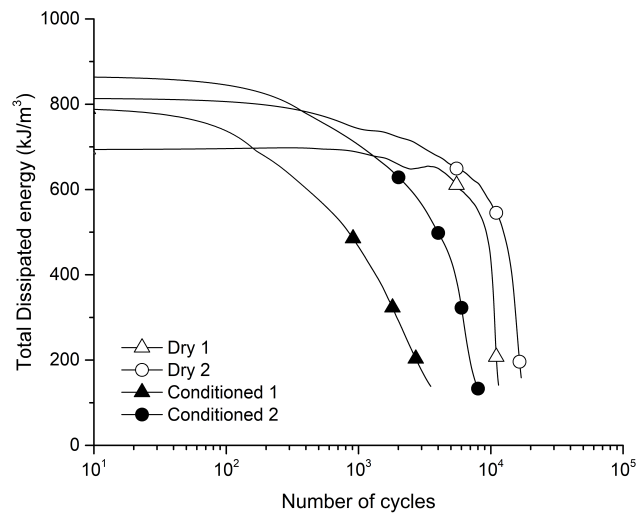


Figure 4.25: Dissipated energy per cycle for BC-VG30 at $600\mu\epsilon$

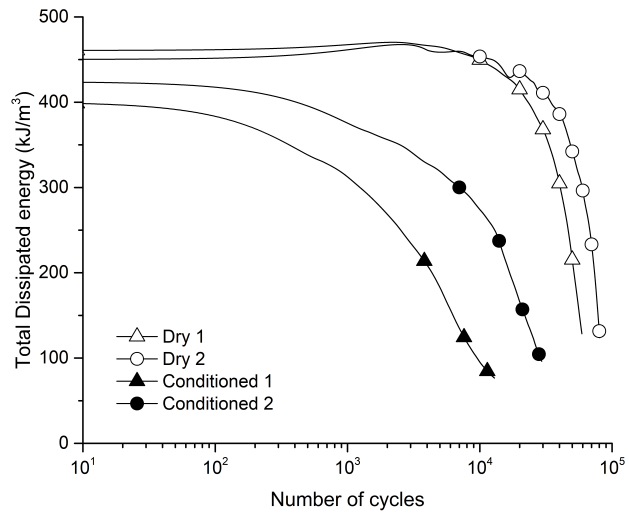


Figure 4.26: Dissipated energy per cycle for BC-VG30 at $400\mu\epsilon$

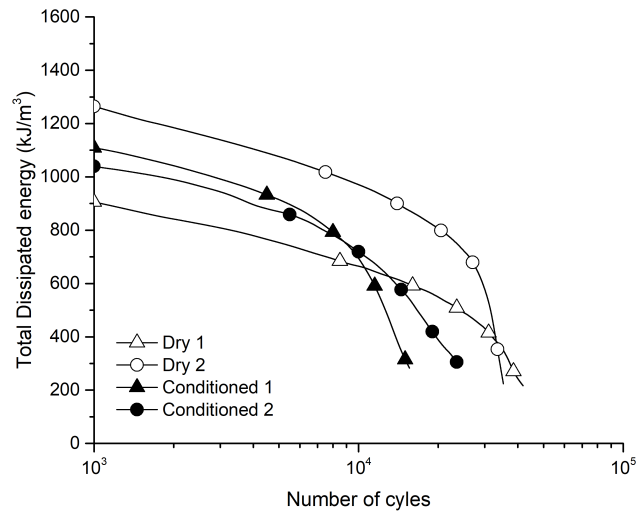


Figure 4.27: Dissipated energy per cycle for BC-VG10 at $800\mu\epsilon$

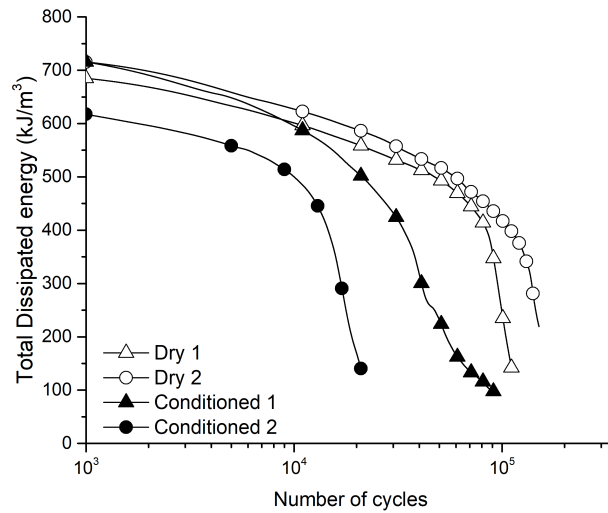


Figure 4.28: Dissipated energy per cycle for BC-VG10 at $600\mu\epsilon$

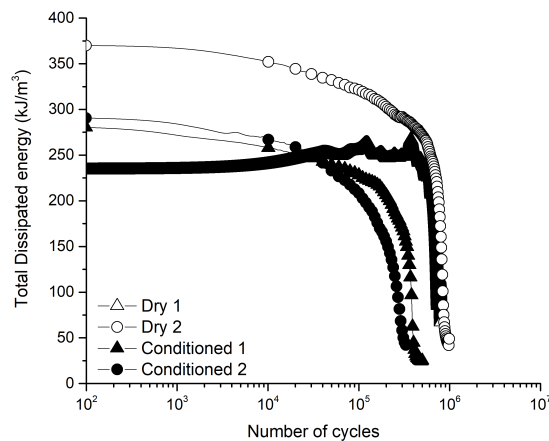


Figure 4.29: Dissipated energy per cycle for BC-VG10 at $400\mu\epsilon$

It was observed from the Figures 4.24 to 4.29 that the dissipated energy per cycle for moisture-conditioned samples was nearly the same as that of dry samples in the initial cycles. The dissipation in the initial cycles is usually attributed fully to viscous friction. Thus, the results essentially show that the viscous dissipation characteristics of moisture-conditioned samples are the same as that of dry samples. However, the rate at which dissipation energy per cycle reduced with repeated loading is significantly higher for moisture-conditioned samples, in comparison to the dry samples. This shows that moisture-conditioned samples are more susceptible to failure by fatigue.

4.2.6 Lissajous Plots

The variation of stress with strain within a cycle of repeated loading is called a Lissajous plot. For a viscoelastic material subjected to sinusoidal loading, the Lissajous plot is expected to be elliptical in shape. If the material is elastic in nature, the Lissajous plot will be a straight line and circle for a purely viscous material.

Figures 4.30 to 4.37 show Lissajous plots for moisture-conditioned and dry samples at different cycles of repeated loading at different strain levels for BC-VG30 and BC-VG10 samples.

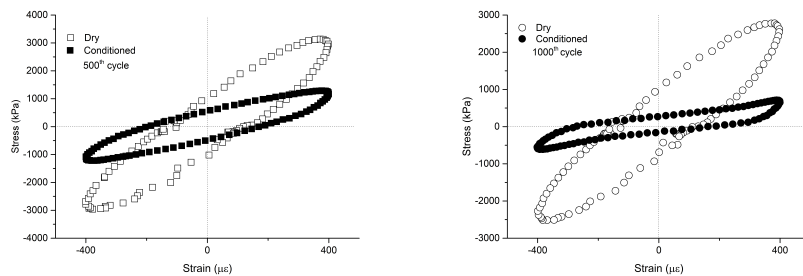


Figure 4.30: Variation of stress-strain curve with the loading cycles for BC-VG30 at $800\mu\epsilon$

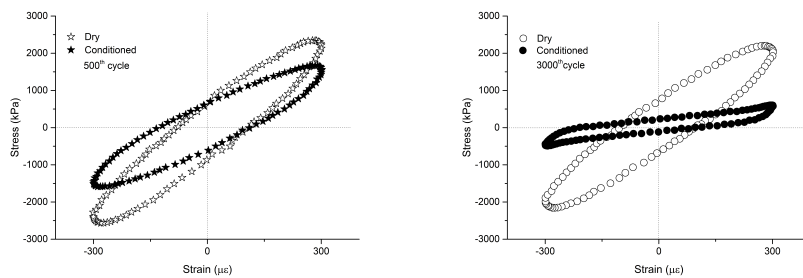


Figure 4.31: Variation of stress-strain curve with the loading cycles for BC-VG30 at $600\mu\epsilon$

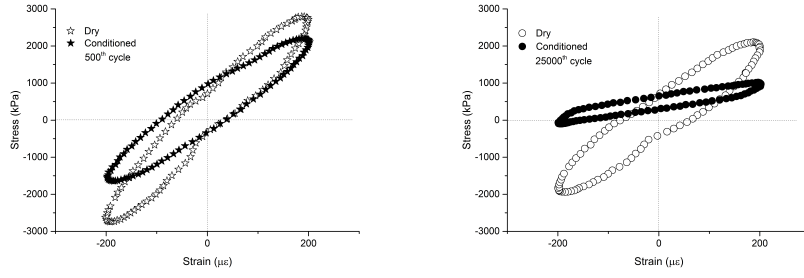


Figure 4.32: Variation of stress-strain curve with the loading cycles for BC-VG30 at $400\mu\epsilon$

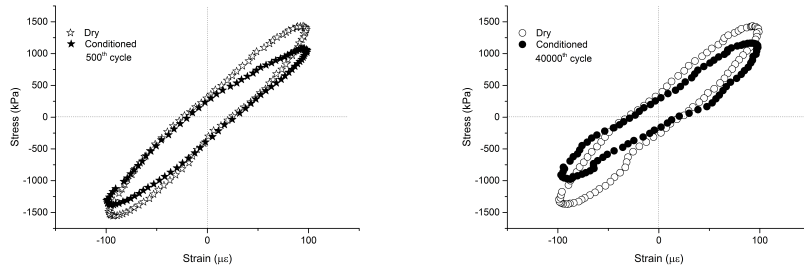


Figure 4.33: Variation of stress-strain curve with the loading cycles for BC-VG30 at $200\mu\epsilon$

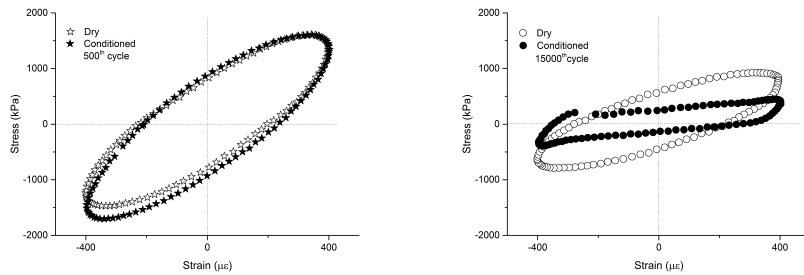


Figure 4.34: Variation of stress-strain curve with the loading cycles for BC-VG10 at $800\mu\epsilon$

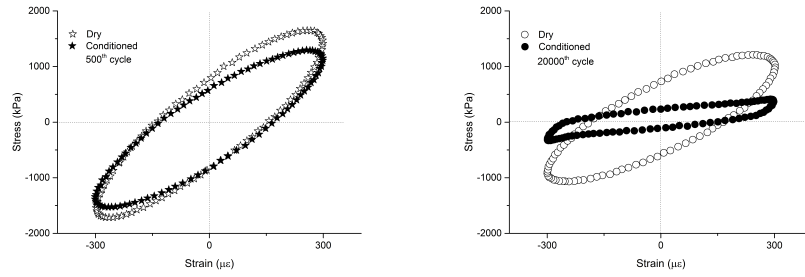


Figure 4.35: Variation of stress-strain curve with the loading cycles for BC-VG10 at $600\mu\epsilon$

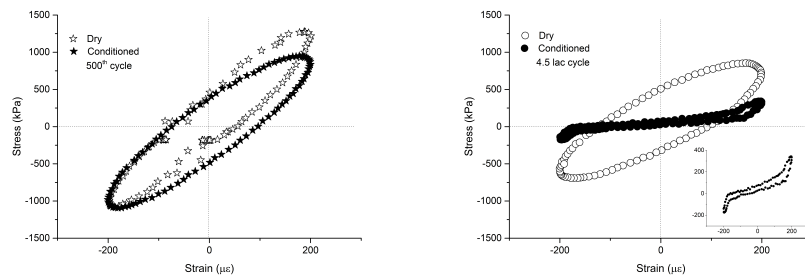


Figure 4.36: Variation of stress-strain curve with the loading cycles for BC-VG10 at $400\mu\epsilon$

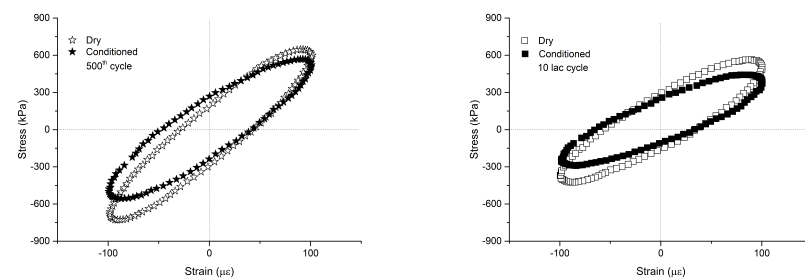


Figure 4.37: Variation of stress-strain curve with the loading cycles for BC-VG10 at $200\mu\epsilon$

During the initial cycles of loading, the Lissajous plot for both moisture-conditioned and dry samples is elliptical and this is expected because of the viscoelastic nature of the material (Lakes and Lakes, 2009). With the progress of the test, the mixtures are observed to lose their integrity and the stress-strain curve is distorted from its elliptical shape. It was found that the distortion of the Lissajous plot occurs earlier for moisture-conditioned should be hyphenated. This is an indication of the accelerated damage of

the material in the presence of moisture. It can also be observed that the Lissajous plot for 200 microstrains is elliptical for both moisture-conditioned and dry samples even up to 2 million cycles.

4.2.7 Phase Angle

The variation of phase angle with loading cycles for moisture-conditioned and dry samples at different strain levels for BC-VG10 and BC-VG30 binders are presented in Figures 4.38 to 4.43. The phase angle for moisture-conditioned samples is seen to be of comparable magnitude to that of dry samples in the initial cycles. But the drop in phase angle, which is associated with fatigue failure by some researchers, occurs markedly earlier for moisture-conditioned samples compared to dry samples.

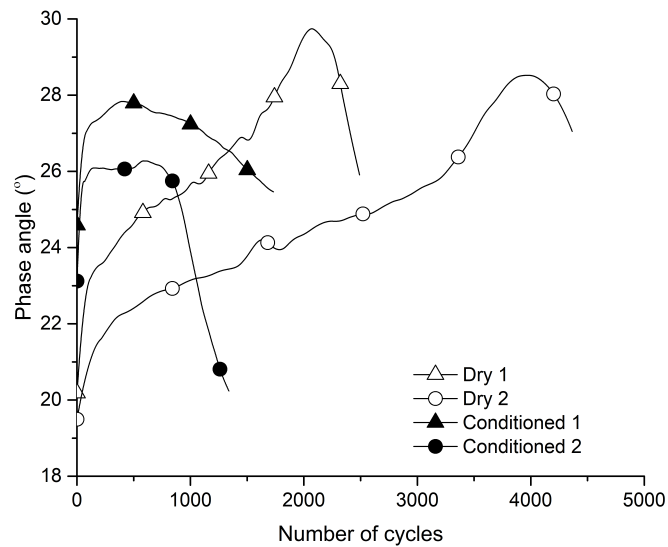


Figure 4.38: Variation of phase angle with the loading cycles for BC-VG30 at $800\mu\epsilon$

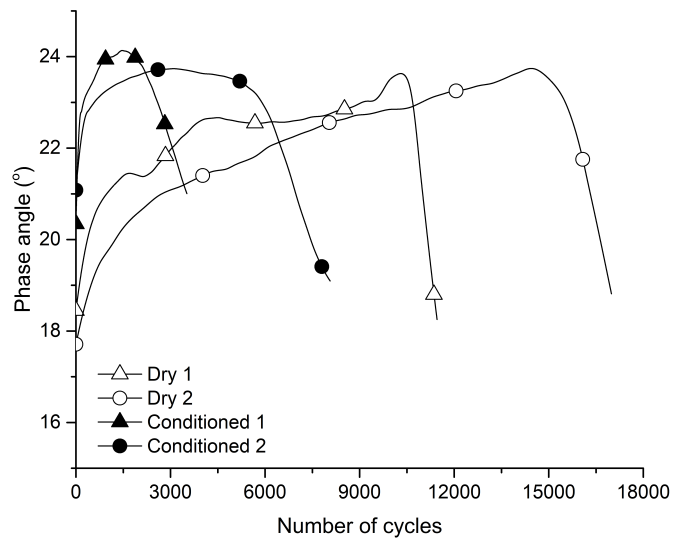


Figure 4.39: Variation of phase angle with the loading cycles for BC-VG30 at $600\mu\epsilon$

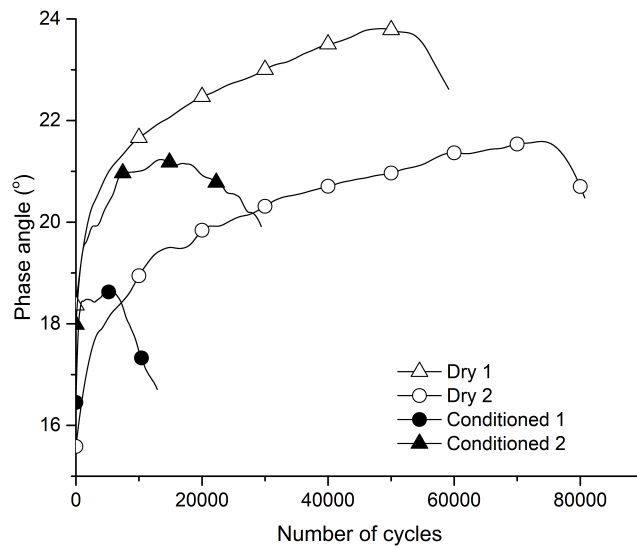


Figure 4.40: Variation of phase angle with the loading cycles for BC-VG30 at $400\mu\epsilon$

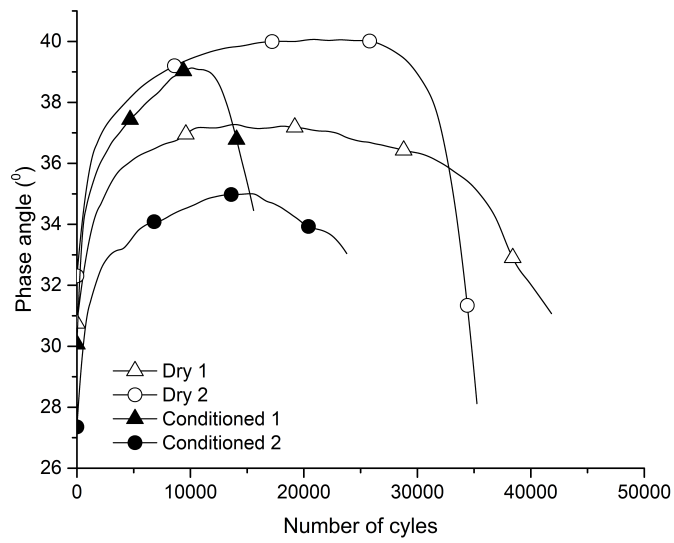


Figure 4.41: Variation of phase angle with the loading cycles for BC-VG10 at 800 $\mu\epsilon$

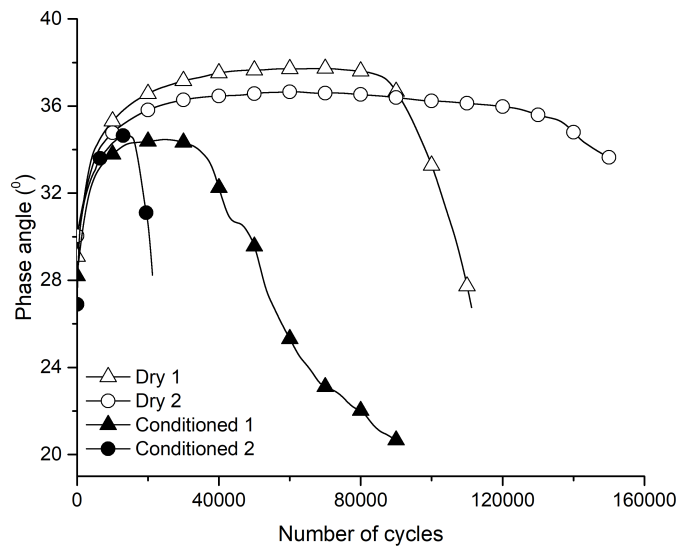


Figure 4.42: Variation of phase angle with the loading cycles for BC-VG10 at 600 $\mu\epsilon$

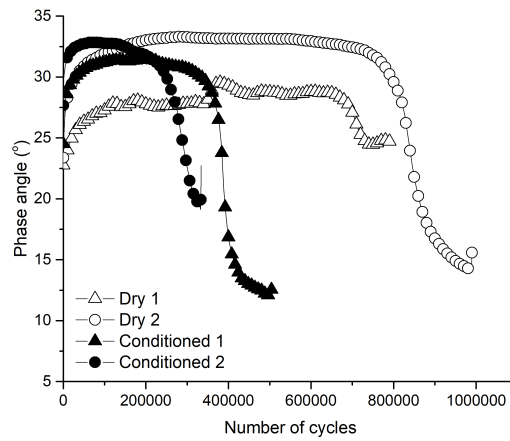


Figure 4.43: Variation of phase angle with the loading cycles for BC-VG10 at $400\mu\epsilon$

4.3 S-N Plot

The variation of fatigue life with the strain level is usually presented in a log-log scale and is referred to as an S-N plot. The fatigue test was carried out at four different strain levels (200, 400, 600 and $800\mu\epsilon$) at a temperature of 20°C on both moisture-conditioned and dry samples, as mentioned previously. In Table ?? and ??, the number of cycles to achieve a 50% reduction in stiffness against the corresponding strain amplitude was reported. The variation of the fatigue life with strain level was plotted on a log-log scale.

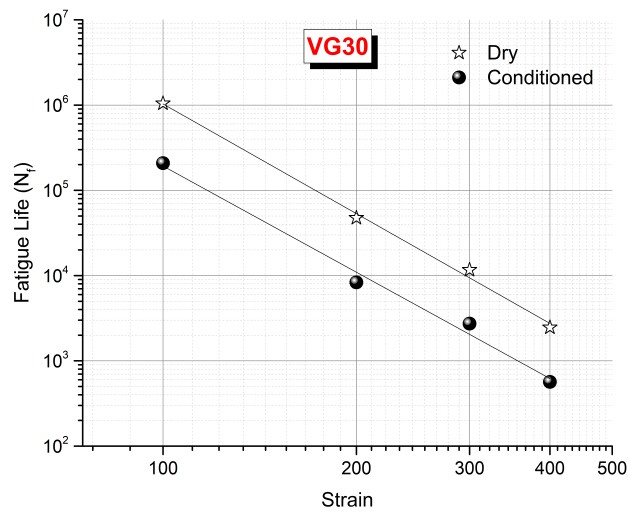


Figure 4.44: S-N plot for BC-VG30 samples using AASHTO T321-07

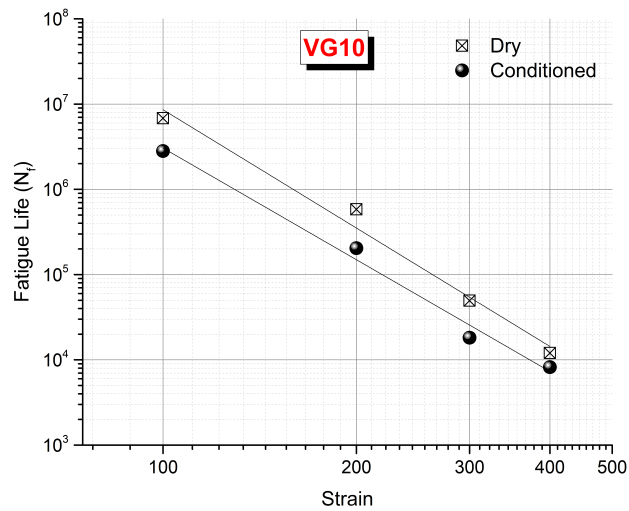


Figure 4.45: S-N plot for BC-VG10 samples using AASHTO T321-07

Figures 4.44 and 4.45 show the S-N plots for moisture-conditioned and dry samples of both BC-VG30 and BC-VG10 mixtures for the fatigue life determined by using AASHTO T321-07 method. It was observed that the difference in the fatigue life for moisture-conditioned and dry samples at different strain levels was more for BC-VG30 samples than that of BC-VG10 samples. This shows that BC-VG30 samples were more susceptible to moisture-induced damage.

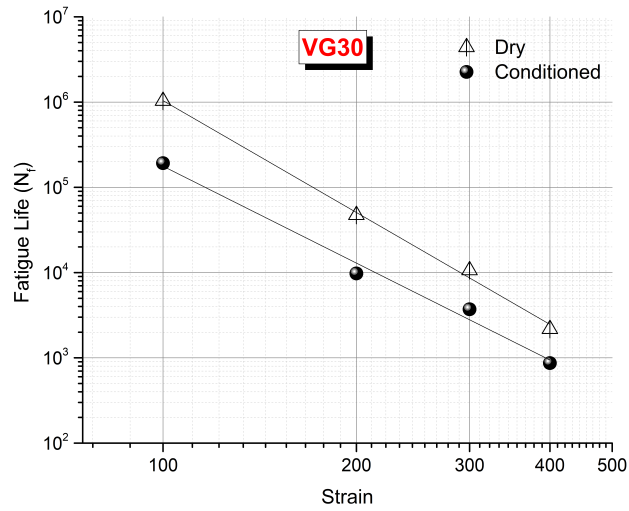


Figure 4.46: S-N plot for BC-VG30 samples using ASTM D7460-10

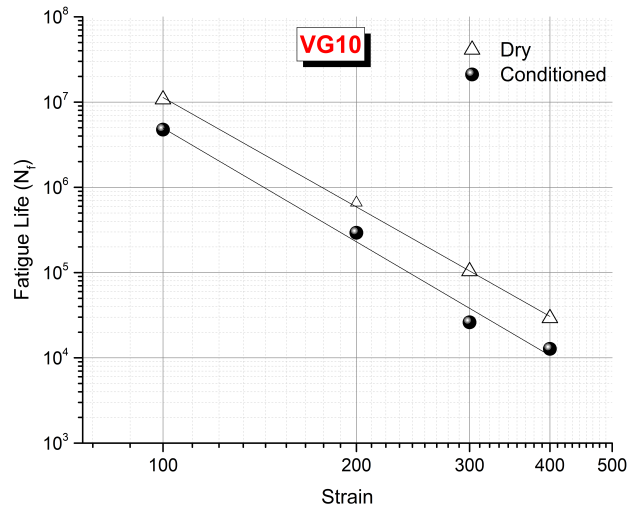


Figure 4.47: S-N plot for BC-VG10 samples using ASTM D7460-10

Figures 4.46 and 4.47 show the S-N plots for moisture-conditioned and dry samples of both BC-VG30 and BC-VG10 mixtures for the fatigue life determined by using ASTM:D7460 (2010) method. Here again, it was seen that the separation between the S-N plots of moisture-conditioned and dry samples was higher for BC-VG30 mixtures than BC-VG10 mixtures.

4.3.1 Incorporation of of Moisture Effect in Pavement Design

Using a performance-based test to assess the moisture effect helps us to incorporate the moisture effect into pavement design. This section provides a simple example showing a possible method for considering the effect of MID in pavement design.

The fatigue life obtained as a function of the applied strain level was fit with a power law model of the form Eq. 4.4 (Huang, 1993):

$$N_f = \alpha(\epsilon_t)^\beta, \quad (4.4)$$

in which N_f is the number of repetitions to failure, ϵ_t is the tensile strain, α and β are model parameters. The parameters for Eq. 4.4 are estimated by linear regression and are shown in Table 4.10 and 4.11.

Table 4.10: Estimated parameters as per AASHTO T321-07

Mixture	State	Ln(α)	β	R^2
BC-VG10	Dry	17.55	-4.61	0.978
	Conditioned	16.50	-4.35	0.983
BC-VG30	Dry	15.85	-4.28	0.995
	Conditioned	14.81	-4.14	0.985

Table 4.11: Estimated parameters as per ASTM D7460-10

Mixture	State	Ln(α)	β	R^2
BC-VG10	Dry	16.87	-4.26	0.999
	Conditioned	16.89	-4.43	0.983
BC-VG30	Dry	16.05	-4.36	0.995
	Conditioned	13.94	-3.78	0.985

From the fits shown in Figure 4.44 to 4.47, and the corresponding R^2 value shown in Tables 4.10 and 4.11, it is clear that the power-law model fits the SN curves reasonably well. The R^2 goodness of fit measure for the fits was at least 0.98 for all the mixtures

and test conditions. It can also be observed that the exponent β is nearly the same for all the mixtures. It does not change significantly with moisture-conditioning. The coefficient α , however, changes significantly from dry to moisture-conditioned samples. Since the exponent, beta, is nearly similar for all S-N plots, the ratio of the fatigue life of moisture-conditioned samples to that of dry samples can be taken to be a constant independent of strain-level:

$$\frac{N_f^w}{N_f^d} = \left(\frac{\alpha^w}{\alpha^d} \right), \quad (4.5)$$

Thus, if Miner's hypothesis of linear damage is assumed, the damage per pass in moisture-conditioned AC to that in dry AC becomes:

$$\frac{D_f^w}{D_f^d} = \left(\frac{\alpha^d}{\alpha^w} \right), \quad (4.6)$$

$$D_f^w = \left(\frac{\alpha^d}{\alpha^w} \right) \times D_f^d, \quad (4.7)$$

Using the parameter from Table 4.10 for BC-VG10 and the Eq. 4.7, the damage per pass for moisture-conditioned BC-VG10 is related to the damage per pass for dry BC-VG10 through:

$$D_f^w = 2.86 \times D_f^d, \quad (4.8)$$

The damage of AC when wet is thus several times higher than when it is dry. Considering the wet season to be 4 months long during a year and no seasonal variation in the traffic loading, the cumulative damage after moisture-damage can be expressed as:

$$\frac{4}{12} \times 2.86 D_f^d + \frac{8}{12} \times D_f^d = 1.62 D_f^d, \quad (4.9)$$

Thus, the damage in a year would be about 1.6 times higher for BC-VG10 when moisture-induced damage is considered for design. Similarly, for BC-VG30 mixtures, the cumulative damage after moisture-damage can be expressed as:

$$\frac{4}{12} \times 8.25 D_f^d + \frac{8}{12} \times D_f^d = 3.41 D_f^d, \quad (4.10)$$

Thus, the damage in a year would be about 3.4 times higher when moisture-induced damage is considered for design. In this way, the findings of this study can be used for determining the effect of moisture on the fatigue life of pavements and designing pavements accordingly. Although other factors affecting fatigue life of pavement in the field, such as temperature variation, staggered movement of traffic, and overloading of the commercial vehicles have not been taken into account. However, the example above clearly shows how moisture-induced damage can be given consideration in pavement design.

4.4 Degree of Saturation

It can be observed from Figure 4.48 that the degree of saturation for BC-VG30 mixtures after 3 hours of vacuum saturation was between 70-80%. However, BC-VG10 samples achieved only 55-65% degree of saturation after 3 hours at similar air voids and vacuum pressure. This shows that the internal microstructure, and specifically the interconnectivity of voids, can vary from one mixture to another, even if the air-void content is the same for both mixtures. It can also be inferred that the higher susceptibility of BC-VG30 to moisture-induced damage could be due to the higher degree of saturation of the BC-VG30 specimens.

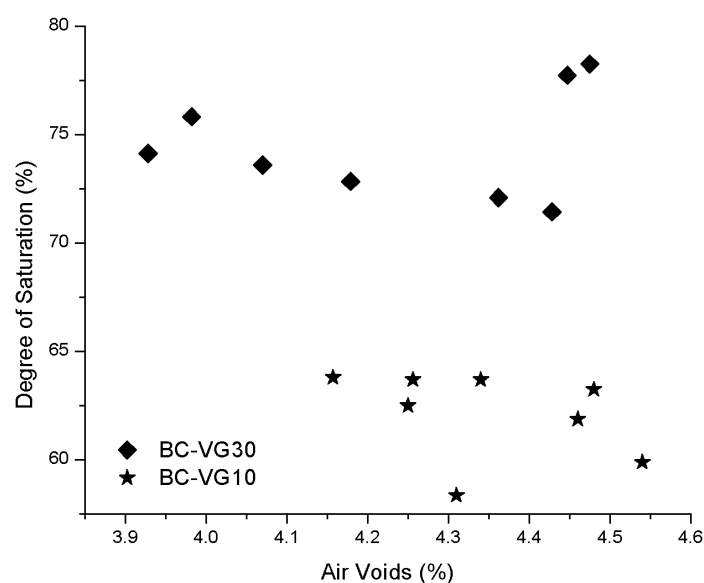


Figure 4.48: Degree of saturation for BC-VG10 and BC-VG30 moisture-conditioned samples

4.5 Analysis for Surface Free Energy Measurement

4.5.1 Contact Angle Measurement

Contact angles on the surface of binders and aggregates were determined using the Sessile drop technique with a drop shape analysis system. Figure 4.49 shows a probe liquid drop on the sample surface that was recorded using a charge-coupled device (CCD) camera. From the obtained image, a software automatically calculates the contact angle. All contact angle measurements were conducted at 20°C. Table 4.12 shows the average value of six measurements of the contact angles along with their coefficient of variation (COV) for two binders and one aggregate type. It can be seen from Table 4.12 that for binders, the COVs are in the range from 0.38% to 1.4%. In comparison, the COV values for the contact angle of probe liquid on aggregates ranged from 0.64 to 2.61%. This variation could be due to the roughness of the aggregate surface.

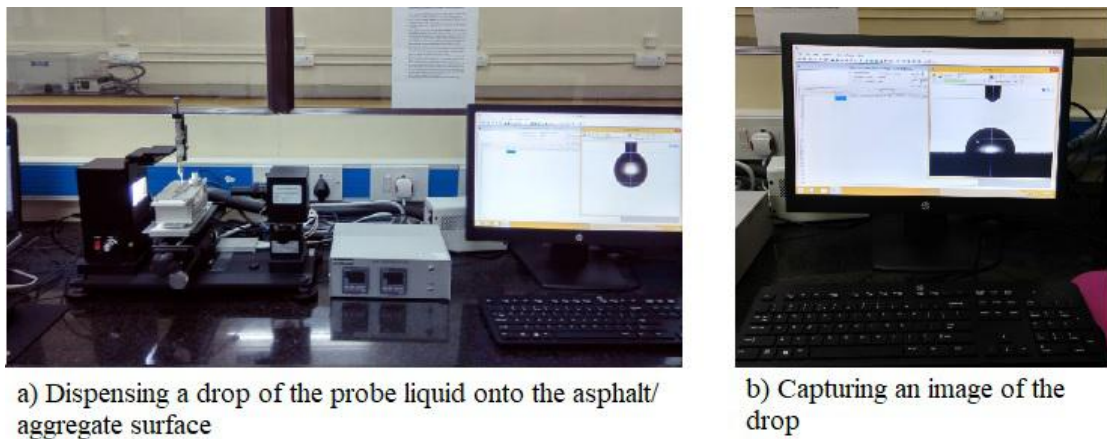


Figure 4.49: Procedure for measuring contact angles

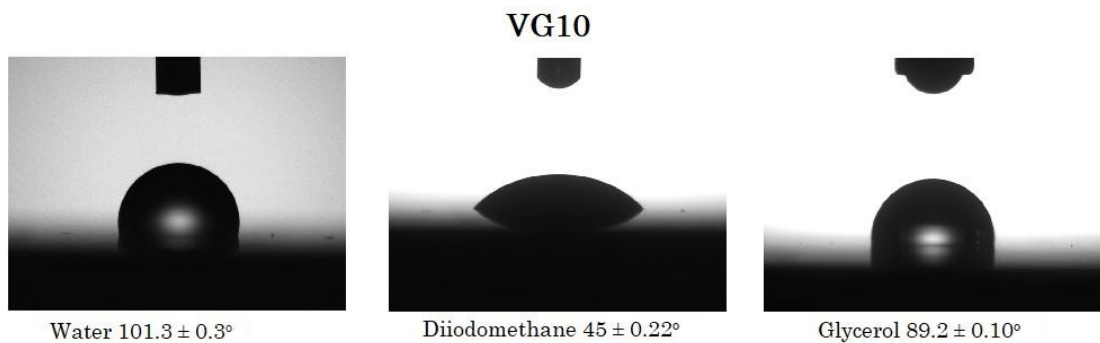


Figure 4.50: Sessile drop on the surface of VG10 binder

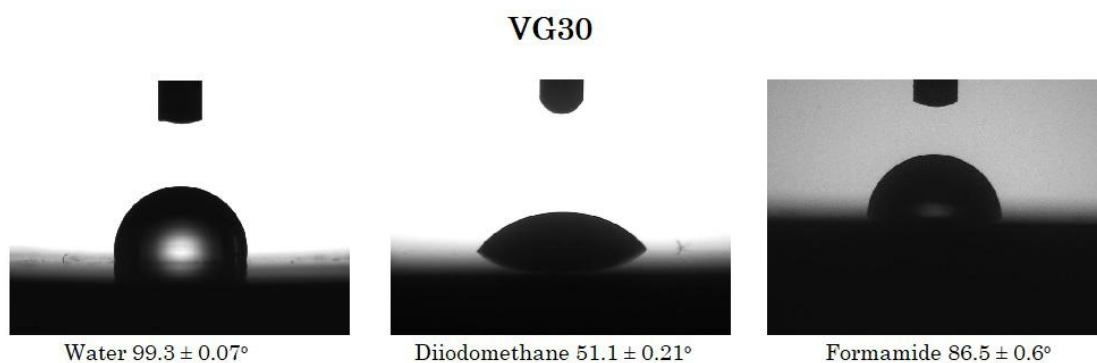


Figure 4.51: Sessile drop on the surface of VG30 binder

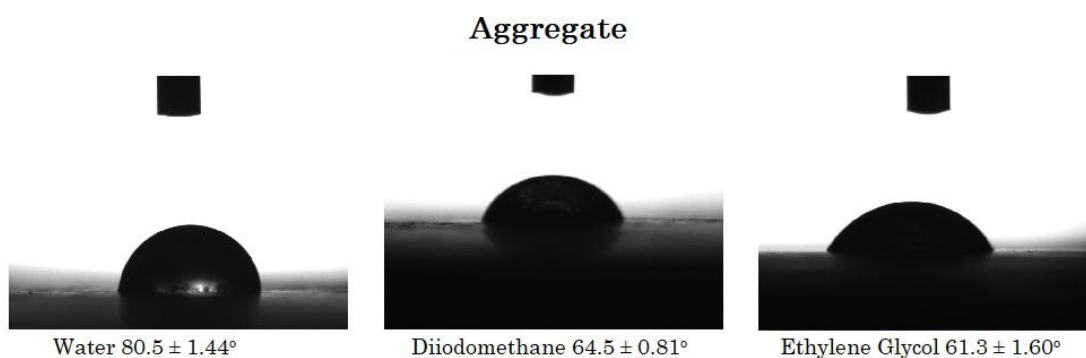


Figure 4.52: Sessile drop on the surface of aggregate

Table 4.12: Average contact angle and COV for two binders and aggregate at 20°C

Liquid probe	Contact Angle ($^\circ$)					
	VG10		VG30		Aggregate	
	Average	COV%	Average	COV%	Average	COV%
Water (W)	101.3	0.38	99.3	0.69	80.53	1.79
Diiodomethane(D)	45.0	0.68	51.1	1.4	64.48	1.26
Ethyleneglycol (E)	78.0	0.73	75.2	0.91	63.3	2.61
Glycerol (G)	89.2	0.49	111.7	0.71	100.23	0.63
Formamide (F)	86.0	0.44	86.5	0.88	66.18	0.93

4.5.2 Selection of Probe Liquids

Two approaches were adopted for the selection of appropriate probe liquids. In the first approach, the selection was made using the condition number (CN). A value of $CN < 10$ has been recommended, because higher values are very prone to errors in SFE calculation. The CN is measured using a matrix of SFE components of the chosen probe

liquids (Little and Bhasin, 2006). In the second approach, $\gamma_L \cos\theta$ was plotted against γ_L . Kwok and Neumann (1999) suggested that the combination of probe liquids with the best linear fit between $\gamma_L \cos\theta$ versus γ_L should be chosen for the analysis.

A combination of three probe liquids was then obtained based on the two aforementioned approaches for each of the two different binders and aggregate. The CN and Coefficient of determination (R^2) values of $\gamma_L \cos\theta$ versus γ_L are presented in Table 4.13. The R-squared values for the chosen combination of probe liquids are reasonably good for all the materials. The combination of probe liquids is different for each binder and aggregate. For the aggregate, the R^2 is found to be 0.999, which signifies that contact angle results meet Kwok's criteria.

Table 4.13: Condition number and Coefficient of determination (R^2)

Combination of Probe Liquid	Condition Number (CN)	R^2
W-D-G (VG10)	4.90	0.988
W-D-F (VG30)	5.17	0.913
W-D-E (Aggregate)	4.47	0.999

4.5.3 Surface Energy Components

Surface free energy components of the two binders and aggregates were calculated using the fundamental Eq. (3.3) and the average contact angle value determined from each combination of three probe liquids. If the square roots of the three unknown surface energy components of the asphalt binder are represented as x_1 , x_2 and x_3 ; Eq. (3.3) can be rewritten as follows:

$$(1 + \cos\theta)\gamma_L^{Tot} = 2 \left[(\sqrt{\gamma_L^{LW}})x_1 + (\sqrt{\gamma_L^+})x_2 + (\sqrt{\gamma_L^-})x_3 \right] \quad (4.11)$$

For evaluating the values of 3 unknowns: x_1 , x_2 and x_3 , a set of three linear equations has been derived by substituting the contact angle determined for asphalt binder using three probe liquids and SFE components of the similar probe liquids in Eq.(4.11). Hence, for m number of probe liquids Eq. (4.11) can be written as a matrix.

$$\begin{bmatrix} \sqrt{\gamma_{L1}^{LW}} & \sqrt{\gamma_{L1}^+} & \sqrt{\gamma_{L1}^-} \\ \sqrt{\gamma_{L2}^{LW}} & \sqrt{\gamma_{L2}^+} & \sqrt{\gamma_{L2}^-} \\ \vdots & \vdots & \vdots \\ \sqrt{\gamma_{Lm}^{LW}} & \sqrt{\gamma_{Lm}^+} & \sqrt{\gamma_{Lm}^-} \end{bmatrix}_{m \times 3} \begin{bmatrix} x_1 \\ x_2 \\ x_3 \end{bmatrix} = \frac{1}{2} \begin{bmatrix} \gamma_{L1}^{Tot}(1 + \cos \theta_1) \\ \gamma_{L2}^{Tot}(1 + \cos \theta_2) \\ \vdots \\ \gamma_{Lm}^{Tot}(1 + \cos \theta_m) \end{bmatrix}_{m \times 1}$$

Table 4.14: Surface Energies Calculated from Contact Angle Data

Solid	Combination of liquids	γ^{Total}	γ^{LW}	γ^{AB}	γ^-	γ^+
		(mJ/m ²)				
VG10	W-D-G	37.95	37.02	0.93	0.36	0.59
VG30	W-D-F	39.19	33.65	5.54	4.17	1.84
Aggregate	W-D-E	29.40	25.88	3.56	9.85	0.32

Table 4.15: Comparison of Surface Energy Components

Asphalt	γ^{Total}	γ^{LW}	γ^{AB}	γ^-	γ^+
	(mJ/m ²)				
VG10	38.35	37.02	1.33	0.82	0.54
VG30	34.45	33.65	0.80	1.13	0.14
PG64 – 22 ¹	36.53	35.38	1.15	2.82	0.12
PG64 – 22 ²	30.07	29.95	0.05	1.02	0.01
PG64 – 22 ³	38.80	38.38	0.38	3.52	0.01

where, superscript 1 - [Koc and Bulut \(2013\)](#) using Sessile drop; 2 - [Lytton et al. \(2005\)](#) using Wilhelmy plate; 3 - [Bhasin et al. \(2006\)](#) using Wilhelmy plate.

From Table 4.14 it can be seen that the Lifshitz-van der Waals component is the primary contribution to total surface energy for binders. This signifies that the asphalt binders are primarily nonpolar. Table 4.15 presents the comparison of surface energy components measurements of the PG 64-22 grade binder in the literature. It can be observed that the components of the SFE were susceptible to the measured methodology.

4.5.4 Work of Adhesion and Cohesion

The work of adhesion between the binder and aggregate at their interface in the dry and wet conditions is given by Eq. 2.12 and 2.14. A ratio of the work of adhesion under the wet condition to the work of adhesion under dry condition ($\Delta W_a^{wet} / \Delta W_a^{dry}$), was used to rank the mixtures (Lytton *et al.*, 2005). A higher ratio value would be ideal. Table 4.16 presents the ratio of work of adhesion in the wet conditions to the work of adhesion in dry conditions. It was observed that mixture with VG10 binder has more resistance to moisture in the context of adhesive bonding. Table 4.17 presents the ratio of the work of cohesion in the wet condition to the work of cohesion in dry conditions. It was observed that the VG30 binder has more resistance to moisture in the context of cohesive bond energy.

Table 4.16: Work of adhesion in dry and wet condition

Asphalt Binder	Work of Adhesion	Work of Adhesion	Ratio ($\Delta W_a^{wet} / \Delta W_a^{dry}$)
	ΔW_a^{dry} (mJ/m^2)	ΔW_a^{wet} (mJ/m^2)	
VG10	67.44	57.41	0.85
VG30	69.84	42.04	0.60

Table 4.17: Work of cohesion in dry and wet condition

Asphalt Binder	Work of Cohesion	Work of Cohesion	Ratio ($\Delta W_c^{wet} / \Delta W_c^{dry}$)
	ΔW_c^{dry} (mJ/m^2)	ΔW_c^{wet} (mJ/m^2)	
VG10	75.90	70.69	0.93
VG30	78.38	88.47	1.13

4.6 Comparison of 4PB and SFE Test Results

Table 4.18 shows the comparison of results from the 4PB fatigue and sessile drop tests. It was observed that the ISR and FLR ratios from the 4PB test are correlated well with

the ratio of the work of adhesion in wet to dry conditions. The higher values of ISR, FLR and the ratio of work of adhesion under the wet condition to the work of adhesion under dry condition ($\Delta W_a^{wet} / \Delta W_a^{dry}$) for VG10 binder shows that the mixtures with VG10 binder were less susceptible to moisture-damage as compared to mixtures with VG30 binder. Hence, it can be inferred from the test results that both the 4PB test and the Sessile drop test were sensitive to the effect of moisture on the AC mixture.

Table 4.18: Comparison between the test results

Mixture	Sessile Drop		4PB		
	Ratio of Work of Adhesion	Ratio of Work of Cohesion	ISR	FLR (AASHTO T321)	FLR (ASTM D7640)
VG10	0.85	0.93	0.89	0.45	0.39
VG30	0.60	1.13	0.81	0.21	0.29

CHAPTER 5

SUMMARY AND CONCLUSION

5.1 Summary

The changes in the fatigue characteristics of AC mixtures due to moisture was evaluated in this investigation by conducting four-point beam fatigue tests on dry and moisture-conditioned beam specimens at four different strain amplitudes. For this purpose, specimens were subjected to vacuum saturation by submerging completely in water and applying vacuum pressure to the system. Two parameters - the average initial flexural stiffness ratio (ISR) and the average fatigue life ratio (FLR) were used to express the change in the fatigue characteristics of AC mixtures after moisture-conditioning.

To evaluate the effect of moisture on the cohesive bond energy of asphalt mastic and the adhesive bond energy between asphalt and aggregates, the surface free energy of asphalt and aggregates were measured using a Sessile drop apparatus. A ratio of the work of adhesion in wet to dry condition was used to express the change in the bond energies in the presence of moisture. Furthermore, a relationship between the FLR and ISR with the ratio of work of adhesion wet to dry condition was also examined.

5.2 Conclusions and Recommendations

Based on the range of materials and the parameters tested in this investigation, the principal findings can be summarized:

- Moisture-conditioning decreases the initial flexural stiffness modulus possibly by reducing the strength of the cohesive and the adhesive bonding between mastic and aggregate. This may lead to the premature failure of AC pavements in the presence of moisture.
- Moisture-conditioning decreases the fatigue life by around 60% for BC-VG10 mixtures, while around 80% for BC-VG30 mixtures. When SN plots were constructed from the results of the fatigue tests, the S-N curve for moisture-conditioned AC mixtures was parallel and lower to the S-N curve for the dry AC mixtures,

which shows a reduction in the fatigue life after the moisture-conditioning. The S-N plots can be used to introduce a shift factor for the evaluation of reduction in the fatigue life in the presence of moisture, by considering the suitable number of the wet season during a year.

- The percentage reduction in fatigue life after moisture conditioning depends upon the adopted post-processing method.
- The rate at which flexural stiffness modulus and total dissipation energy decrease with cycles is higher for moisture-conditioned samples. This shows that moisture-conditioned samples are more susceptible to failure by fatigue.
- In view of variation in the degree of saturation between the two mixtures, it may be concluded that the degree of saturation is dependent on the type of binder. The internal microstructure, specifically the extent of the interconnectivity of air voids can be different from one binder to another.
- Surface free energy of asphalt binder and aggregates was measured using the Sessile Drop method. The ratio of the work of adhesion under the wet condition to the work of adhesion under dry condition ($\Delta W_a^{wet} / \Delta W_a^{dry}$) can be used to identify the combinations of aggregates and asphalt binder having good resistance to moisture-induced damage.
- Surface free energy measurement test results (i.e., the ratio of the work of adhesion under the wet condition to the work of adhesion under dry condition) are consistent with the fatigue test results (i.e., fatigue life ratio). The higher values of FLR and ($\Delta W_a^{wet} / \Delta W_a^{dry}$) for VG10 binder show that the mixtures with VG10 binder have good resistance to moisture-damage as compared to mixtures with VG30 binder.

5.3 Future Research

While conducting the laboratory testing and data analysis, the following issues are raised that suggested further research or improvement:

- The 4PB procedure may be used to differentiate mixtures with different sensitivity to moisture, and to rank the mixtures. However, further research on different binders and aggregates sources needs to be conducted. In addition, extensive field performance data must be obtained before this methodology can be applied for the calibration of the test results.
- In order to better determine the relationship between cohesive/adhesive bond energies and 4PB tests, the experimental and analytical methods used in this study need to be extended to a wide range of materials.

REFERENCES

1. **AASHTO:R30** (2002). Mixture conditioning of hot mix asphalt. standard specification for transportation materials and methods of sampling and testing. *R30-02 Part 1B, American Association of State Highway and Transportation Officials.*
2. **AASHTO:T321** (2017). Determining the fatigue life of compacted hot mix asphalt subject-ed to repeated flexural bending. *American Association of State Highways and Transportation Officials, Washington, D.C, USA..*
3. **Arambula, E., S. Caro, and E. Masad** (2009). Experimental measurement and numerical simulation of water vapor diffusion through asphalt pavement materials. *Journal of Materials in Civil Engineering*, **22**(6), 588–598.
4. **ASTM:D4402/D4402M** (2015). Standard test method for viscosity determination of asphalt at elevated temperatures using a rotational viscometer. *ASTM International, West Conshohocken, PA, USA.*
5. **ASTM:D6857/D6857M** (2011). Standard test method for maximum specific gravity and density of bituminous paving mixtures using automatic vacuum sealing method. *West Conshohocken, PA: American Society for Testing and Materials.*
6. **ASTM:D7460** (2010). Standard test method for determining fatigue failure of compacted asphalt concrete subjected to repeated flexural bending. *ASTM International, West Con-shohocken, Pennsylvania, USA.*
7. **ASTM:D7981** (2015). Standard practice for compacting of prismatic asphalt specimens by means of means of the shear box compactor. *ASTM International, West Conshohocken, Pennsylvania, USA.*
8. **Bhasin, A., D. Little, K. Vasconcelos, and E. Masad** (2007). Surface free energy to identify moisture sensitivity of materials for asphalt mixes. *Transportation Research Record: Journal of the Transportation Research Board*, (2001), 37–45.
9. **Bhasin, A., E. Masad, D. Little, and R. Lytton** (2006). Limits on adhesive bond energy for improved resistance of hot-mix asphalt to moisture damage. *Transportation research record: journal of the transportation research board*, (1970), 3–13.
10. **Birgisson, B., R. Roque, and G. C. Page** (2003). Evaluation of water damage using hot mix asphalt fracture mechanics (with discussion). *Journal of the association of asphalt paving technologists*, **72**.
11. **Caro, S., E. Masad, A. Bhasin, and D. N. Little** (2008). Moisture susceptibility of asphalt mixtures, part 1: mechanisms. *International Journal of Pavement Engineering*, **9**(2), 81–98.
12. **Chen, X. and B. Huang** (2008). Evaluation of moisture damage in hot mix asphalt using simple performance and superpave indirect tensile tests. *Construction and Building Materials*, **22**(9), 1950 – 1962.

13. **Cheng, D., D. Little, R. Lytton, and J. Holste** (2002). Surface energy measurement of asphalt and its application to predicting fatigue and healing in asphalt mixtures. *Transportation Research Record: Journal of the Transportation Research Board*, (1810), 44–53.
14. **Cheng, D., D. N. Little, R. L. Lytton, and J. C. Holste** (2003). Moisture damage evaluation of asphalt mixtures by considering both moisture diffusion and repeated-load conditions. *Transportation Research Record*, **1832**(1), 42–49.
15. **Cheng, D. X., D. N. Little, R. L. Lytton, and J. C. Holste**, Surface free energy measurement of aggregates and its application to adhesion and moisture damage of asphalt-aggregate systems. In *International Center for Aggregates Research 9th Annual Symposium: Aggregates-Concrete, Bases and Fines*, Final Draft. 2001.
16. **Fromm, H. J.** (1974). The mechanisms of asphalt stripping from aggregate surfaces.
17. **Hamed, G. H. and M. F. Nejad** (2015). Using energy parameters based on the surface free energy concept to evaluate the moisture susceptibility of hot mix asphalt. *Road Materials and Pavement Design*, **16**(2), 239–255.
18. **Harvey, J. and C. L. Monismith** (1993). Effects of laboratory asphalt concrete specimen preparation variables on fatigue and permanent deformation test results using strategic highway research program a-003a proposed testing equipment. *Transportation Research Record*, (1417).
19. **Hefer, A. W.** (2005). *Adhesion in bitumen-aggregate systems and quantification of the effect of water on the adhesive bond*. Ph.D. thesis, Texas A&M University.
20. **Hefer, A. W., A. Bhasin, and D. N. Little** (2006). Bitumen surface energy characterization using a contact angle approach. *Journal of Materials in Civil Engineering*, **18**(6), 759–767.
21. **Hicks, R.** (1991). Moisture damage in asphalt concrete. *Transportation Research Record*, **NCHRP Synthesis of Highway Practice 175**.
22. **Huang, Y.**, *Pavement Analysis and Design*. Englewood Cliffs, NJ: Prentice-Hall, Inc., 1993.
23. **IS:73** (2013). Specification for paving grade bitumen. *Bureau of Indian Standards*, New Delhi, India.
24. **Kandhal, P.** (1992). Moisture susceptibility of hma mixes: identification of problem and recommended solutions. *NCAT Report 92-1*.
25. **Kanitpong, K. and H. U. Bahia** (2008). Evaluation of hma moisture damage in wisconsin as it relates to pavement performance. *International Journal of Pavement Engineering*, **9**, 9.
26. **Kassem, E., E. Masad, R. Lytton, and R. Bulut** (2009). Measurements of the moisture diffusion coefficient of asphalt mixtures and its relationship to mixture composition. *International Journal of Pavement Engineering*, **10**(6), 389–399.
27. **Kiggundu, B. M. and F. L. Roberts** (1988). Stripping in hma mixtures: State-of-the-art and critical review of test methods (report 88-02).

28. **Koc, M. and R. Bulut** (2013). Assessment of a sessile drop device and a new testing approach measuring contact angles on aggregates and asphalt binders. *Journal of materials in civil engineering*, **26**(3), 391–398.
29. **Kringos, N., H. Azari, and A. Scarpas** (2009). Identification of parameters related to moisture conditioning that cause variability in modified lottman test. *Transportation Research Record*, **2127**(1), 1–11.
30. **Kringos, N. and A. Scarpas** (2005). Raveling of asphaltic mixes due to water damage: computational identification of controlling parameters. *Transportation research record*, **1929**(1), 79–87.
31. **Kringos, N. and A. Scarpas** (2008). Physical and mechanical moisture susceptibility of asphaltic mixtures. *International Journal of Solids and Structures*, **45**(9), 2671–2685.
32. **Kringos, N., T. Scarpas, C. Kasbergen, and P. Selvadurai** (2008). Modelling of combined physical–mechanical moisture-induced damage in asphaltic mixes, part 1: governing processes and formulations. *International Journal of Pavement Engineering*, **9**(2), 115–128.
33. **Kwok, D. Y. and A. W. Neumann** (1999). Contact angle measurement and contact angle interpretation. *Advances in colloid and interface science*, **81**(3), 167–249.
34. **Lakes, R. and R. S. Lakes**, *Viscoelastic materials*. Cambridge university press, 2009.
35. **Little, D. N. and A. Bhasin** (2006). Using surface energy measurements to select materials for asphalt pavement. Technical report.
36. **Little, D. N. and Jones**, Chemical and mechanical processes of moisture damage in hot-mix asphalt pavements. *In Moisture Sensitivity of Asphalt Pavements-A National Seminar* California Department of Transportation; Federal Highway Administration; National Asphalt Pavement Association; California Asphalt Pavement Alliance; and Transportation Research Board. 2003.
37. **Lu, Q.** (2005). Investigation of conditions for moisture damage in asphalt concrete and appropriate laboratory test methods. University of california transportation center, University of California Transportation Center.
38. **Lytton, R.** (2002). Mechanics and measurement of moisture damage. *Proceedings of moisture damage symposium*, WRI, Wyoming..
39. **Lytton, R. L., E. A. Masad, C. Zollinger, R. Bulut, and D. N. Little** (2005). Measurements of surface energy and its relationship to moisture damage. Technical report.
40. **Maher, A., N. Gucunski, W. Yanko, and F. Petsi** (2001). Evaluation of pothole patching materials. Technical report.
41. **Majidzadeh, K. and F. N. Brovold**, *State of the art: Effect of water on bitumen-aggregate mixtures*. Highway Research Board, National Research Council, 1968.
42. **Masad, E. A., C. Zollinger, R. Bulut, D. N. Little, and R. L. Lytton** (2006). Characterization of hma moisture damage using surface energy and fracture properties (with discussion). *Journal of the association of asphalt paving technologists*, **75**.

43. **Mehrara, A. and A. Khodaii** (2011). Evaluation of asphalt mixtures' moisture sensitivity by dynamic creep test. *Journal of Materials in Civil Engineering*, **23**(2), 212–219.
44. **Mehrara, A. and A. Khodaii** (2013). A review of state of the art on stripping phenomenon in asphalt concrete. *Construction and Building Materials*, **38**, 423–442.
45. **MoRTH** (2013). Specification for road & bridge works, fifth revision. *Ministry of Road Transport & Highways*, New Delhi, India.
46. **Shatnawi, S., M. Nagarajaiah, and J. T. Harvey** (1995). Moisture sensitivity evaluation of binder-aggregate mixtures. *Transportation research record*, **1492**, 71–84.
47. **Solaimanian, M., J. Harvey, M. Tahmoressi, and V. Tandon**, Test methods to predict moisture sensitivity of hot-mix asphalt pavements. *In Moisture Sensitivity of Asphalt Pavements-A National Seminar California Department of Transportation; Federal Highway Administration; National Asphalt Pavement Association; California Asphalt Pavement Alliance; and Transportation Research Board.*. 2003.
48. **Taylor, M. and N. Khosla** (1983). Stripping of asphalt pavements: state-of-the-art. *Transportation research record: journal of the transportation research board*, (911), 150–157.
49. **Terrel, R. L. and S. Al-Swailmi**, *Water sensitivity of asphalt-aggregate mixes: test selection*. SHRP-A-403. 1994.
50. **van Oss, C. J.** (2002). Use of the combined lifshitz-van der waals and lewis acid–base approaches in determining the apolar and polar contributions to surface and interfacial tensions and free energies. *Journal of Adhesion Science and Technology*, **16**(6), 669–677.
51. **Van Oss, C. J., M. K. Chaudhury, and R. J. Good** (1988). Interfacial lifshitz-van der waals and polar interactions in macroscopic systems. *Chemical Reviews*, **88**(6), 927–941.
52. **Varveri, A., S. Avgerinopoulos, and A. Scarpas** (2016). Experimental evaluation of long-and short-term moisture damage characteristics of asphalt mixtures. *Road Materials and Pavement Design*, **17**(1), 168–186.
53. **Wei, J. and Y. Zhang** (2012). Application of sessile drop method to determine surface free energy of asphalt and aggregate. *Journal of Testing and Evaluation*, **40**(5), 807–813.
54. **Wineman, A. S. and K. R. Rajagopal**, *Mechanical response of polymers: an introduction*. Cambridge university press, 2000.

LIST OF PAPERS BASED ON THESIS

PUBLICATIONS IN CONFERENCE PROCEEDINGS

1. Chauhan, M. and Narayan, A. Effect of Moisture on Fatigue Characteristics of Asphalt Concrete Mixtures *In: Pasetto M., Partl M., Tebaldi G. (eds) Proceedings of the 5th International Symposium on Asphalt Pavements & Environment (APE). ISAP APE 2019. Lecture Notes in Civil Engineering*, 48, 356-366, (2019).

ANNEXURE A

Volumetric Properties for Mixtures

BC Grade 2								
Nominal Aggregate Size		13.2 mm		Retained weight (gm.)				
IS Sieve (mm)	Cumulative % by weight of total aggregate passing	% Mean Passing	% Retained	Gmm Sample	VG 30		VG 10	
					PreSBOX Beam	1 Batch	PreSBOX Beam	1 Batch
19	100	100	0	0	0	0	0	0
13.2	90-100	95	5	100	1361	340	1356	339
9.5	70-88	79	16	320	4355	1089	4338	1084
4.75	53-71	62	17	340	4627	1157	4609	1152
2.36	42-58	50	12	240	3266	816	3253	813
1.18	34-48	41	9	180	2449	612	2440	610
0.6	26-38	32	9	180	2449	612	2440	610
0.3	18-28	23	9	180	2449	612	2440	610
0.15	12-20	16	7	140	1905	476	1898	474
0.075	4-10	7	9	180	2449	612	2440	610
Pan				140	1898	475	1894	474
Total				2000	27216	6802	27112	6777

Mixture with 5% BC	Total mix Wt. (gm)	Binder Wt. (gm.)	Aggregate Wt. (gm.)
Gmm	2105	105	2000
BC-VG30 (PreSBOX)	28648	1432	27216
BC-VG30 (Beam)	7162	358	6804
BC-VG10 (PreSBOX)	28539	1427	27112
BC-VG10 (Beam)	7135	357	6778

ANNEXURE B

Degree of Saturation for Moisture Conditioned Samples

BC-VG30								
Sample ID	Saturation Time (min)	Weight in air (gms)	SSD weight of sample (gms)	Weight of water (gms)	Sample volume (cm ³)	Sample Air Voids (%)	Volume of Air Voids (cm ³)	Degree of Saturation (%)
BVPM30-04_BR_Trial1_800	180	3096.32	3140.14	43.82	1267.63	4.45	56.37	77.73
BVPM30-04_BL_Trial2_800	180	3151.96	3197.13	45.17	1289.88	4.48	57.72	78.25
BVPM30-05_TR_Trial1_600	180	3103.77	3140.26	36.49	1253.21	3.93	49.23	74.13
BVPM30-09_BL_Trial2_600	180	3099.80	3137.85	38.05	1260.24	3.98	50.18	75.82
BVPM30-03_TL_Trial1_400	180	3119.55	3157.26	37.71	1259.00	4.07	51.24	73.59
BVPM30-12_TL_Trial2_400	180	3220.25	3261.06	40.81	1297.85	4.36	56.61	72.09
BVPM30-14_BR_T1_200	180	3130.44	3168.87	38.43	1262.51	4.18	52.76	72.84
BVPM30-13_BL_T2_200	180	3076.99	3116.65	39.66	1253.95	4.43	55.52	71.43
BC-VG10								
BVPM10-13_TL_800	180	3193.48	3228.83	35.35	1281.29	4.46	57.15	61.86
BVPM10-11_TL_800	180	2981.34	3015.75	34.41	1265.83	4.54	57.47	59.88
BVPM10-15_BL_600	180	3125.24	3159.02	33.78	1273.95	4.16	52.96	63.79
BVPM10-15_TL_600	180	3157.30	3189.32	32.02	1273.29	4.31	54.88	58.35
BVPM10_01_BR_400	180	3044.36	3078.16	33.80	1247.05	4.26	53.07	63.68
BVPM10-11_TR_400	180	2995.70	3030.90	35.20	1242.46	4.48	55.66	63.24
BVPM10-10_TR_200	180	3170.07	3204.82	34.75	1257.06	4.34	54.56	63.70
BVPM10-14_BL_200	180	3090.85	3124.06	33.21	1250.54	4.25	53.15	62.49

CURRICULUM VITAE

1. **NAME** : Mohit Chauhan

2. **DATE OF BIRTH** : 20 May 1992

3. **EDUCATIONAL QUALIFICATIONS**

2014 Bachelor of Technology (B. Tech.)

Institution : JB Institute of Technology Dehradun

Specialization : Civil Engineering

Master of Science (M.S.)

Institution : Indian Institute of Technology Madras

Specialization : Transportation Engineering

Registration Date : 14 July 2015

GENERAL TEST COMMITTEE

- CHAIRPERSON** : Dr. Manu Santhanam
Professor and Head
Department of Civil Engineering
- GUIDE(S)** : Dr. Atul Narayan
Assistant Professor
Department of Civil Engineering
- MEMBERS** : Dr. Subhadeep Banerjee
Associate Professor
Department of Civil Engineering
- Dr. Abhijit P. Deshpande
Professor
Department of Chemical Engineering